Interplate Earthquake Potential off Western Java, Indonesia, based on GPS data

(GPS データに基づく インドネシア、ジャワ島西部沖の プレート間地震発生ポテンシャル）

NURAINI RAHMA HANIFA

Doctor of Science

Graduate School of Environment Studies

Nagoya University

2014

Interplate Earthquake Potential off Western Java, Indonesia, based on GPS data

(GPS データに基づく　インドネシア、ジャワ島西部沖のプレート間地震発生ポテンシャル)

NURAINI RAHMA HANIFA

A Dissertation for the degree of Doctor of Science

Department of Earth and Environmental Sciences,
Graduate School of Environment Studies
Nagoya University

2014

When there is a will, there is a way

For my lovely family, and people of Indonesia.

Abstract

The Java Trench is a plate boundary where the Indo-Australian plate subducts beneath the Sunda plate and many megathrust earthquakes as well as tsunami earthquakes repeatedly occur. In contrast with the Java Trench off Sumatra, the trench off Java has much less historical seismicity during last 300 years. However, since Java is the most populated area of Indonesia and there occurred significant tsunami earthquakes in 1994 and 2006 (both were M_w7.8), it is of great importance to evaluate potential of megathrust earthquake south off Java.

We use three years data from 5 January 2008 to 31 December 2010, from 13 newly installed continuous GPS sites of the Indonesia Geospatial Agency (BIG) and Institute of Technology Bandung (ITB) located in western Java and southern Sumatra. First, we process the GPS data with data from the 7 International GNSS Service (IGS) sites to obtain daily coordinate time series of each site in the International Terrestrial Reference Frame 2008 (ITRF2008) by using Bernese GPS Software Version 5.0 (Dach et al., 2007). Daily repeatability of 2.5-3.2 mm for horizontal and 9.1-12.5 mm for vertical components was achieved except for a few sites around the Sunda Strait. Then we fit a linear trend to each time series to estimate displacement rate vector at each GPS site. The displacement rate error is estimated assuming a white noise and precision of the estimated velocities is about 0.2-0.9 mm/year for the horizontal components and 0.6-2.1 mm/year for the vertical component.

The estimated velocities are transformed into the Sunda block reference frame (Simons et al., 2007), but the result is not consistent with the previous study. It is possible that the postseismic effects of the 2006 M_w7.8 Java tsunami earthquake and the 2004 M_w9.1 Sumatra-Andaman earthquake may be responsible for the changes.

Since the old Sunda block reference frame is not directly applicable to our data, in order to avoid uncertainties regarding the reference frame, we use baseline length change rates for our analysis. On the other hand, we use the absolute vertical displacement rate in the ITRF2008 reference frame for our analysis.

We use the concept of interseismic deformation at subduction zones proposed by Savage (1983) to interpret the observed crustal movements in western Java. The observed surface deformation is attributed to distribution of fault slip deficit/excess with respect to a steady plate subduction on the plate boundary.

We presume a fault plane on the plate interface with a length of 500 km and a width of 225 km extending to the trench. We divide the fault plane into 720 subfaults with a uniform size of 12.5 km x 12.5 km. We assume the dip angle of the plate boundary based on model Slab 1.0 (Hayes et al., 2012). The fault rake angle is fixed to a value based on relative plate motion and the magnitude of slip deficit/excess is the only parameter to be estimated for each subfault. We apply a geodetic inversion method by Yabuki and Matsu'ura (1992) to estimate slip deficit/excess distribution with a prior constraint that the distribution of slip deficit/excess is spatially smooth. The optimum degree of smoothness is determined by the ABIC minimization principle (Akaike, 1980).

To test the reliability of the spatial resolution of the analysis, we conduct a checkerboard test. We invert a synthetic surface deformation data created from prescribed distribution of slip deficit/excess and compare the inversion result with the true distribution. The checkerboard test demonstrates that the slip deficit/excess rate is reasonably resolved up to ~100 km from the coast, corresponding to the slab depth of 20-30 km, within a fault size until 62.5 km x 62.5 km. The model cannot resolve patches smaller than 62.5 km x 62.5 km. Resolution for the shallow part (depth <

20km) and the resolving power for the periphery of the source region is very limited although we may be able to distinguish the existence of a slip deficit in the shallow part by enlarging the fault size.

The inversion result of the GPS data clearly shows a heterogeneous distribution of slip deficit/excess in both the strike and dip directions. We identify one slip excess patch and two significant slip deficit patches. The slip excess is located off Pangandaran near the rupture area of the 2006 M7.8 Java earthquake, in the depth range of 15~20 km, with a slip excess rate of 57-61 mm/yr. In depth range less than 20 km, the detailed slip distribution cannot be resolved by the on-land GPS. However, based on the resolution test, we assured that there is an ongoing afterslip of the 2006 M7.8 earthquake, 4.5 years after the main shock. The southward motion of CPMK and coastal extension is the supporting evidence of this inference. However, we cannot resolve whether the afterslip occurs inside the main shock rupture area or in the adjacent down-dip area. It is also possible that afterslip extend further to the east because of the absence of GPS data to the east of CPMK.

The first significant slip deficit patches is located off Ujung Kulon-Pelabuhan Ratu at 20 to 40 km depth, with a slip rate of 48 to 56 mm/yr, equivalent to 70-82% of the relative plate motion. We also obtain slip deficit to the shallow portion. Although our model cannot resolve detailed spatial distribution of slip deficit, we point out significant amount of slip deficit can exist in the shallow portion south off Java. Second, interplate coupling off Pangandaran at 37 to 45 km depth below the rupture area of the 2006 M7.8 earthquake with a slip rate of 48 to 55 mm/yr, equivalent to 75-80% of the relative plate motion. Existence of the slip deficit patch at depth is supported by the observed coastal uplift.

The absence of a megathrust earthquake for at least 300 years in this region implies seismic moment accumulation during this time period of 1.6×10^{22} Nm (~Mw 8.7) off Ujung Kulon-Pelabuhan Ratu, and 3.9×10^{21} Nm (~Mw 8.3) off Pangandaran, unless episodic slow slips release tectonic stress. Thus significant potential of megathrust earthquake exists in south off western Java.

Base on the inversion result, we propose two possible scenarios for future earthquake off western coast of Java. In the first scenario, earthquake nucleates from the slip-deficit patch at the intermediate depth, then propagates to the shallower portion of the plate boundary producing a large tsunami as the 2011 M9.0 Tohoku earthquake. In the second scenario, earthquake nucleates in the shallow part, generating a tsunami earthquake, and the down-dip portion will release stress by afterslip, as in the case of the 2006 M7.8 Java and 2010 M7.8 Mentawai tsunami earthquakes. In either case, there is a high potential of occurrence of interplate earthquake which rupture could propagate to the shallow part of the plate interface and generate a large tsunami.

Acknowledgments

In the name of Allah, the Beneficent, the Merciful.

I am grateful to many people who have been helping me during my completion of my thesis, directly and indirectly.

I would like to express my deepest gratitude to my advisors, Prof. Takeshi Sagiya and Prof. Fumiaki Kimata, for vast encouragement, knowledge sharing, support, patience and guidance throughout my study. I thank my committee members, Prof. Teruyuki Kato, Prof. Muneyoshi Furumoto, Prof. Koshun Yamaoka, Prof. Hiroyuki Kumagai, and Dr. Ito Takeo for fruitful discussions. I also thank other professors in the Dynamic group of the Earth and Planets Department, as well as members of crustal deformation group.

I benefited to meet many Professors and international researchers during years of JICA training course "Operating Management of Earthquake, Tsunami and Volcano Eruption Observation System" conducted in Nagoya University that enrich my knowledge. I thank to Prof. Hiroo Kanamori, from whom I first understand about the unusual phenomenon of the 2006 Java earthquake and who has teach me tsunami earthquake during my early stay in Nagoya University.

I thank Mr. Cecep Subarya and other collegues in BIG for collaboration in GPS data, and for professors and collegues in ITB for support. I thank Mrs. Kishiki Mizuno and Mrs. Kei Furuno for endless support and help. I am grateful to meet friendly and helpful friends in crustal deformation seminar and dynamics.

I wouldn`t have been able to accomplish this work without support from people who have helping me to take care of my children with their best, the nursery school teachers and my Indonesian friends.

Finally I thank my lovely family for endless love and support.

Table of Contents

List of Figures

List of Tables

Glossary of Abbreviations

ABIC	Akaike Bayesian information criterion
AUNP	ASEAN-EU University Network programme
BAKOSURTANAL	National Coordinating Agency for Surveying and Mapping of Indonesia
BIG	Geospatial Information Agency of Indonesia
BMKG	The Indonesia Agency for Meteorology, Climatology, and Geophysic
FES2004	Finite Element Solutions 2004
GEBCO	General Bathymetric Chart of the Oceans
GEODYSSEA	Geodynamic of South and Southeast Asia
GPS	Global Positioning System
GPS-GPS	Geodynamics Project in Sumatra by Global Positioning System
IGS	International Terrestrial Reference Frame
IPGSN	Indonesian Permanent GPS Station Network
ITB	Institute of Technology Bandung
ITRF	International Terrestrial Reference Frame
LIPI	Indonesian Institute of Sciences
NEIC	The United States National Earthquake Information Center
RINEX	Receiver Independent Exchange Format
SEAMERGE	South-East Asia Mastering Environmental Research with Geodetic Space techniques
SF	Sumatra Fault
SOPAC	Scripps Orbit and Permanent Array Center
SuGAr	Sumatran GPS Array
USGS	United States Geological Survey
VSI	Volcanological Survey of Indonesia

Chapter 1

Introduction

1.1. Background

Along subduction zone, interplate megathrust events and tsunami earthquakes may cause catastrophic tsunami. Recent megathrust event of the 2004 M9.3 Sumatra-Andaman earthquake and the 2011 M9.0 Tohoku-Oki earthquake have show that large destructive earthquakes could occur in a place where there were no historical earthquake of M>9. On the other hand, earthquakes of M7~ when occurred in shallow portion of the plate boundary may lead to generation of extremely large tsunami compare to its seismic magnitude, so called tsunami earthquake events (Kanamori, 1972).

Shallow near-trench part of the subduction megathrust has been considered to be aseismic and pose no tsunami threat (e.g. Scholz, 1998; Moore et al., 2007). However, rupture in the shallowest portion of the subduction sometimes exhibits exceptional seismic energy release aspect, such as low rupture velocity, low seismic radiation and low stress drop. These events could rupture up-dip to the accretionary prism in the shallowest portion of subduction and can generate exceptionally disproportionately devastating tsunamis (Polet and Kanamori, 2000, Hill et al, 2012). Kanamori (1972) named these events as tsunami earthquakes, whose tsunamis have much larger amplitudes then would be expected from their seismic magnitude. The low seismic radiation causes weak shaking, and as a consequence people may not be aware to take any preventive measure for early tsunami evacuation (e.g. Okal, 2012).

Occasional devastating events of M>9 megathrust events, such as the 2004 Mw9.0-9.3 Sumatra-Andaman Earthquake and the 2011 Mw9.0 Tohoku-Oki earthquake, could have much longer recurrence period than available in historical records. Many studies suggested that any subduction is apparently capable of generating such Mw>9 megathrust earthquakes, thus suggested the importance to re-evaluate possibility in other subduction zone (e.g. McCaffrey, 2008).

Among such subduction zone, there is the Java trench that curves along the islands of Java and Sumatra of Indonesia with a total length of more than 5600 km. In this region, the oceanic lithosphere of the Indo-Australian plate subducts beneath the Sunda block at the Java Trench in an almost perpendicular direction to the trench off the south coast of Java and at an oblique angle off the west coast of Sumatra (Figure 1.1). The subduction rate gradually decreases from 68 mm/yr off central Java to 60 mm/yr off central Sumatra (DeMets et al., 2010).

The Java trench has recent great megathrust earthquakes such as the 2004 M9.3 Sumatra-Andaman earthquake, the 2005 M8.5 Nias earthquake, the 2007 M8.7 Bengkulu earthquake, occurring off Sumatra, and 4 known tsunami earthquakes; the 1994 Mw 7.8 Java earthquake (Abercrombie et al., 2001; Polet and Kanamori, 2000), the 2006 Mw 7.8 Java earthquake (Kato et al., 2007; Ammon et al., 2006; Fujii and Satake, 2006), occurring off Java, and the 2010 Mw 7.8 Mentawai earthquake (e.g. Lay et al., 2012), and the 1907 Mw 7.7 Simuleue earthquake (Kanamori, 2010) occurring off Sumatra.

Based on seismological research (Newcomb and McCann, 1987) as well as global GPS studies (e.g. Bock et al., 2003; Simons et al., 2007), in contrast to Sumatra, the subduction process south off Java was considered to be mainly aseismic; in other words, plate coupling at the Java Trench is weak and the relative plate motion is accommodated by steady subduction without accumulating tectonic stress at the plate boundary. Megathrust earthquake of magnitude larger than 8 is absent in this region during the written history in at last 300 years (Newcomb and McCann, 1987, Okal et al., 2012). On the other hand, there have been two tsunami earthquakes in recent years; the 1994 M7.8 and 2006 M7.8 Java tsunami earthquakes. These earthquakes are considered to have occurred as a result of thrust faulting on the shallow plate interface near the Java Trench (e.g. Abercrombie et al., 2001; Ammon et al., 2006), indicating stress accumulation associated with the plate subduction along the shallow portion of the Java Trench.

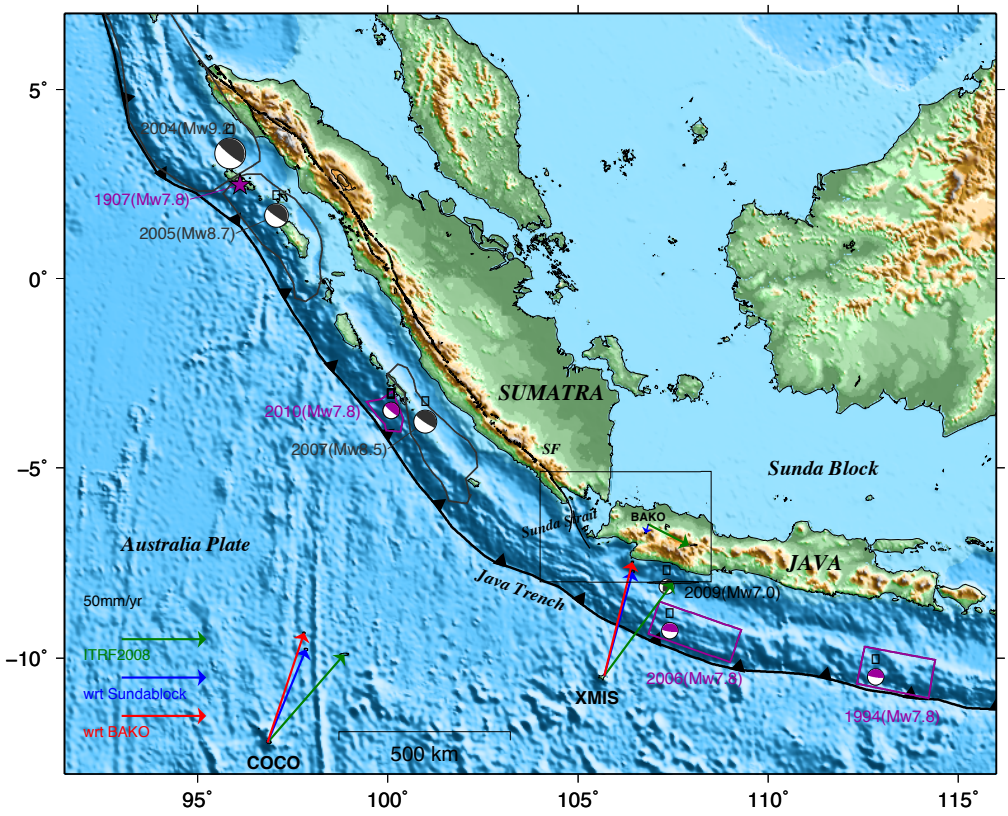

Figure 1.1. Tectonic setting of study area. Purple and black focal mechanisms indicate known tsunami earthquake events and significant megathrust earthquakes after 2004 (M>8) from NEIC epicenters, with the polygon line denote the source region of the ruptured area, redrawn from Bilek and Engdhal (2007), Hanifa et al. (2007), Chlieh et al. (2008), Newman et al. (2011), and Kanamori (2010). Gray focal mechanism shows an intraplate thrust event that might affect the GPS time series. Green, blue and red vectors are the observed horizontal displacement rates from 3 years GPS data in 2008 to 2010 in ITRF 2008, w.r.t. Sundablock, and fixed to BAKO, respectively. SF is Sumatra Fault (Sieh and Natawidjaja, 2000).

Occurrence of the 2006 M7.8 Java Tsunami Earthquake, the 2004 M9.3 Sumatra-Andaman and the 2011 M9.0 Tohoku Oki Earthquake 2011 motivate us to reassess the state of interplate coupling in particular off the south coast of western Java. In addition, with it`s dense population, Java is vulnerable to earthquake and tsunami hazard. Thus, it is crucial to investigate the potential occurrence of interplate earthquake in this particular region.

Global Positioning System (GPS) technology provides precise daily coordinates and has enables a precise measurements surface deformations caused by factors such as plate motion, interseismic, coseismic, postseismic, and slow transient deformation, including in subduction zones (e.g. Sagiya, 2004; Nishimura et al., 2004). GPS data provide a complement to seismological data in earthquake studies.

At the end of 2007, the Geospatial Information Agency of Indonesia established continuous GPS (cGPS) sites in Indonesia called the Indonesian Permanent GPS Station Network (IPGSN) (Subarya et al., 2010), including several sites in Java and Sumatra. This network brought an opportunity to understand the detailed crustal deformation and to reveal the interplate coupling thus the megathrust earthquake potential off western Java.

Thus, **t**his thesis addresses the question on possible interplate coupling off the south coast of western Java. For this purpose, we use GPS observation data from IPGSN, to obtain the crustal deformation rate in the western part of Java. Then we conduct some modeling to understand the interplate coupling off the south coast of western Java from the GPS observation. Finally we interpret the interplate coupling to assess the possibility of future earthquake occurrence along the Java trench.

1.2. Dissertation Outline

This thesis consists of 7 Chapters. Chapter 2 reviews the slip behavior at subduction zones in a global overview. We briefly explain the concept of interplate locking, coseismic, postseismic, tsunami earthquakes, and slow earthquakes. Chapter 3 reviews the tectonic background of Java trench, the historical earthquakes along Java trench, and tsunami earthquakes occurrence along Java Trench.

Chapter 4 explains the data and methodology done in this study; the GPS data and GPS analysis consisting of GPS processing procedure, GPS time series, and GPS velocities. Then we discussed interpretation from obtained surface deformation. Chapter 5 discusses the interplate coupling model by conducting GPS inversion to obtain the slip deficit on the plate interface. Then we interpret the obtained slip deficit/slip excess on the plate interface.

Combination of chapter 4, 5 and some part of chapter 7 as been accepted for publication in Earth and Planetary Science Letters (June 2014), entitle “Interplate coupling model off the southwestern coast of Java, Indonesia, based on continuous GPS data in 2008-2010”.

Chapter 6 describes the numerical modeling of the 2006 M7.7 Java tsunami earthquake which is done to fit the tsunami height, GPS, and tide gauge observation. This chapter was published in advances of geosciences (2009), entitled “Numerical modeling of the 2006 Java tsunami earthquake”.

Finally, Chapter 7 discusses the plausible scenario of future megathrust earthquake from off southwestern Java. Then we summarize the main results of this study.

Chapter 2

Slip Behavior at Subduction Zones

2.1. Seismogenic Zone in Subduction Zone

Subduction zone is a convergent plate boundary where oceanic-oceanic or oceanic-continental platetake place. Convergence at these boundaries is accommodated by underthrusting of one lithospheric plate beneath another. Typically, an oceanic plate is bent at 10° to 30° dip angle and dives below the overriding plate. This results in large contact interface between subducting and overriding plate on which frictional sliding take place, producing so called interplate earthquakes. This contact area is the seismogenic zone in subduction zone where thrust faulting occurs. Coseismic crustal deformation under the ocean can displace the ocean water and generate a large tsunami. Examples of such earthquakes are the 1960 M9.5 Chilean earthquake, 2004 M9.3 Sumatra Andaman earthquake, and 2011 M9.0 Tohoku-Oki earthquake. Majority of seismic energy release on the earth occurs in subduction zones (Figure 2.1)

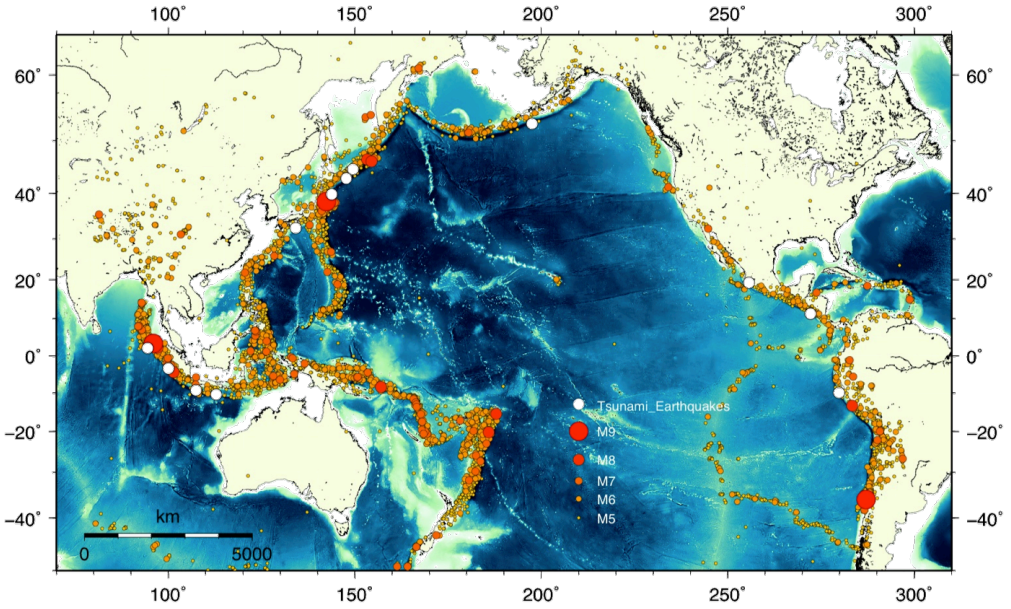

Figure 2.1. World map showing seismicity with M>5 NEIC catalogue for the time period of 1977–2010. Most earthquakes occur in subduction zones.

In the interseismic model, convergent motion in subduction zone is accommodated by a locked patch on the main thrust zone and steady aseismic slip on the rest of the plate interface (Savage, 1983). Conceptional plot is given in Figure 2.2.

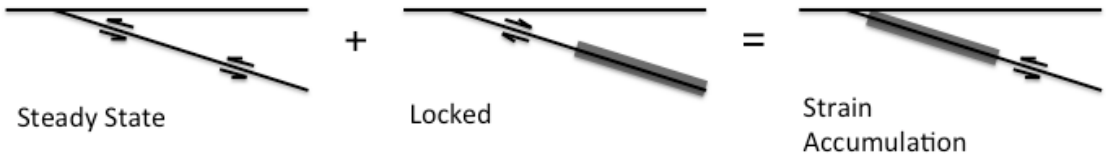

Figure 2.2. Conceptional plot of interseismic deformation at subduction zone by Savage (1983). A locked or no slip condition at an interface is indicated by thick gray line in the interface.

We adapt the definition describing kinematic fault behavior from Wang and Dixon, 2004. The term "locked" refer to a case of no or low slip. When a plate boundary fault is slipping more slowly than the plate convergence rate, it is "partially locked". In summary, Wang and Dixon (2004) explain terms describing kinematical fault behavior as shown in Table 2.1.

Table 2.1 Terms describing kinematical fault behavior (Wang and Dixon, 2004)

Simple Expressions	*Comments*	*Alternate Expressions*
Locked	Not slipping, regardless of fault property or stress	Coupled; fully coupled; strongly coupled; Coupling ratio=1
Slip at plate convergence rate	Regardless of fault property or stress	Decoupled; free slip; creeping; Coupling ratio=0
Slip more slowly than plate convergence rate	Regardless of fault property or stress	Creeping; partially coupled; weakly coupled; coupling ratio between 0 and 1
Slip faster than plate convergence	Regardless of fault property or stress	Coupling ratio < 0
Slip backward	Represents a normal fault, likely unphysical	Coupling ratio > 1

The strength of coupling on the fault is governed by the product of the area of contact and the average breaking stress of the asperities, with strong coupling resulting from large asperity area and high friction coefficient (Lay et al., 1982). Asperity is a patch(es) or

region(s) within the overall area of rupture in a specific great earthquake that has a large coseismic displacement (e.g. Hyndman, 2007; Lay and Kanamori, 1981; Lay et al., 1982). Asperities are often inferred to be "stronger" than the surrounding region of the thrust and therefore they accommodate most of the plate convergence seismically, whereas adjacent areas have more aseismic slip. Asperities are usually mapped though aftershock distribution, seismic waveform modeling, tsunami waveform and geodetic data modeling.

Dark gray regions in Figure 2.3 represents the asperities with strong coupling, light gray represent the conditionally stable area, that is sliding is stable or aseismically under quasi-static loading, but can become unstable or seismic under dynamic loading if there is a rapid change of velocity. White regions represent the aseismic area.

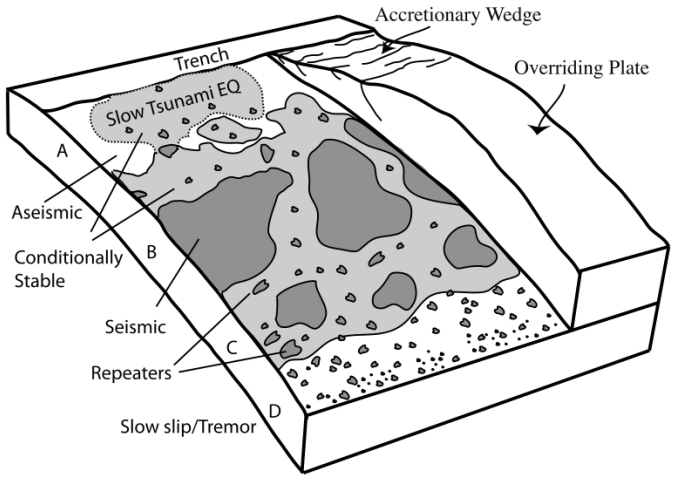

Figure 2.3. Ilustration of asperity model (Lay et al., 2012)

2.2. Interseismic, Coseismic, and Postseismic Slip

Earthquake cycle consists of interseismic, coseismic and postseismic slip. Interseismic period reflects the physical process of strain energy accumulation due to a fault locking. This accumulated strain will likely be released by earthquakes and slow slip events (Sagiya, 2004). Coseismic slip refers a slip that occurs at the moment of the earthquake. Postseismic slip attributes to slip following an earthquake as a stress relaxation of the rock medium in

response to previous earthquakes and ongoing loading. Postseismic slip tends to decays back to the steady interseismic slip.

Slip on the plate interface influences the surface deformation. This surface deformation can be detected by geodetic observations such as GPS (Figure 2.4 and 2.5). When the plate interface is locked, the subducting oceanic plate will drags the overriding plate so that the surface displacement on the overriding plate typically shows a displacement parallel to the plate convergence, resulting coastal shortening and an uplift (Figure 2.6). Conversely, when the plate interface is creeping, such surface displacement pattern is not found.

When earthquake occurs, surface deformation shows a trenchward motion directing to the earthquake epicenter. Then in case of large earthquakes, trenchward postseismic deformation continues for months to decades (e.g. Feigl and Tatcher, 2006). Example of surface deformation pattern in interseismic, coseismic and postseismic period of the 2011 Tohoku-Oki Earthquake Northeast Japan is given in Figure 2.7.

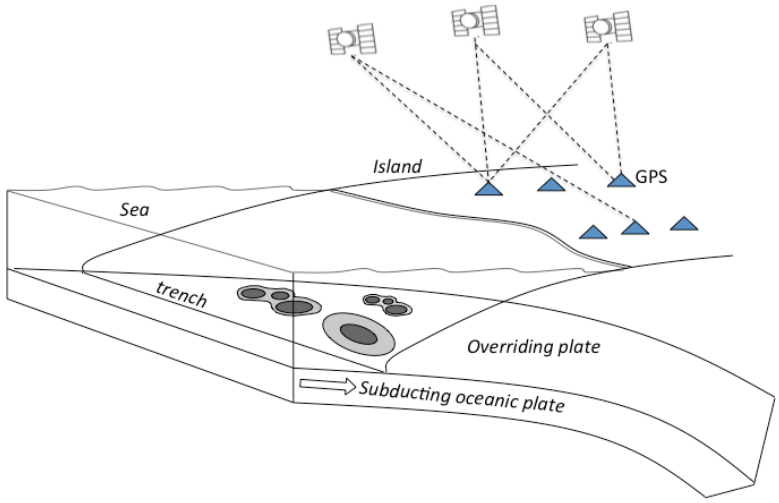

Figure 2.4. Ilustration of GPS data to observed crustal deformation in subduction zone (re-draw with modification from Wang et al., 2012)

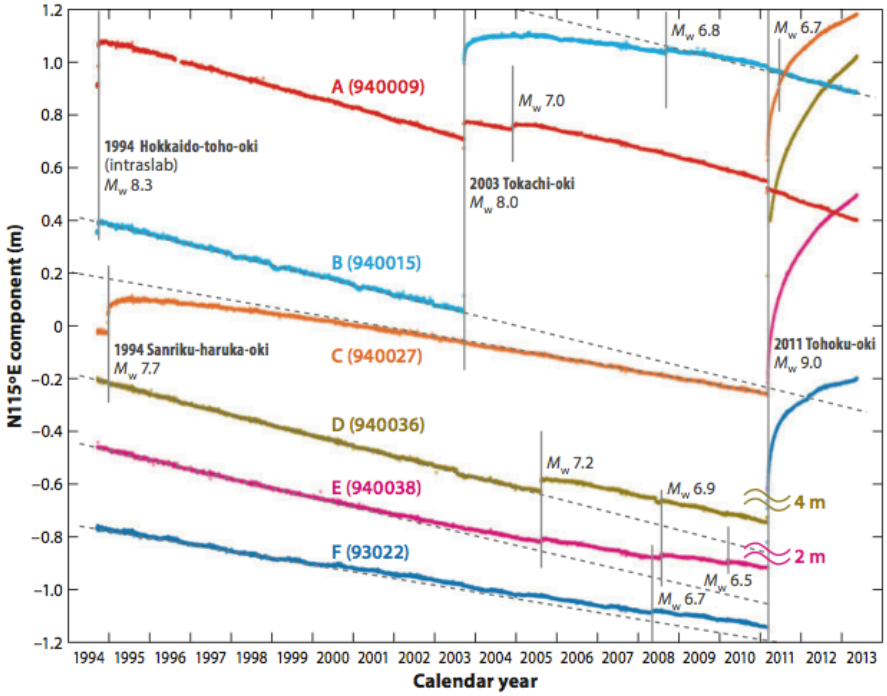

Figure 2.5. Example of time series in Japan, showing the interseismic, coseismic offset, and postseismic slip, which is usually logarithmic just after earthquake (Nishimura et al., 2014). For location refer to Figure 2.7-left.

From geodetic surface displacement, one can model slip distribution on the plate interface to find slip-deficit or back-slip, and slip-excess. Slip deficit or back slip is the difference between the long-term plate convergence rate and the actual relative displacement rate of the plate interface. Slip deficit is a measure of stress accumulation on a fault plane in the plate interface. If slip deficit is zero, it usually means there is no interplate locking. If the slip deficit is as large as the plate convergence rate, then it means the region is fully locked. Slip excess represents coseismic, afterslip or slowslip.

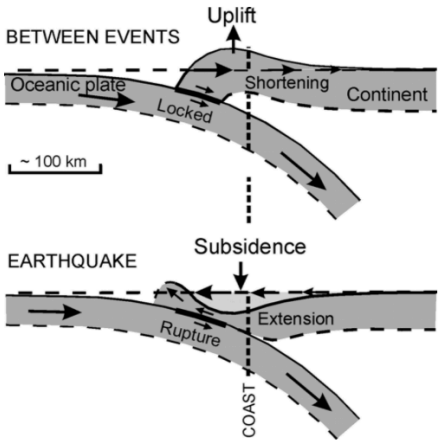

Figure 2.6. Ilustration of correlation between locking, rupture and surface displacement (Leonard et al., 2004)

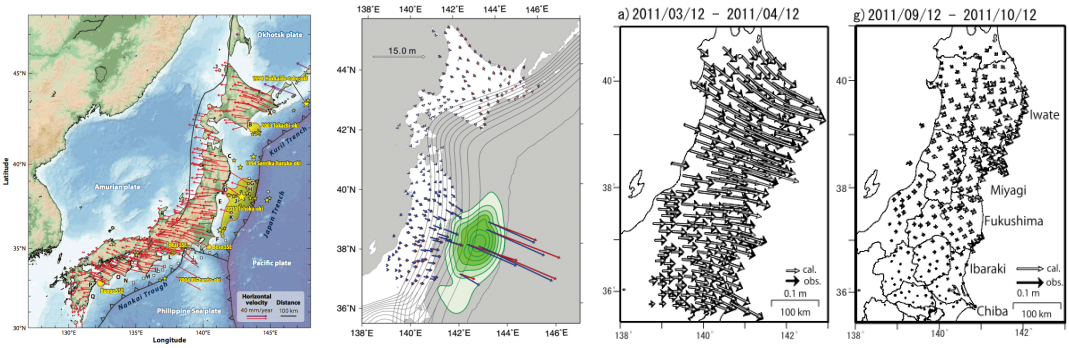

Figure 2.7. (Left) Horizontal velocity at onshore and offshore GPS in Japan w.r.t to Eurasia plate in interseismic period from September 2007 to Februari 2011, prior the 2011 M9.0 Tohoku-Oki earthquake (Nishimura et al., 2014). (Middle) Trenchward coseismic displacement (Hashimoto et al., 2012). (Right) Trenchward postseismic deformation after the 2011 Tohoku earthquake, magnitude of slip decay by time (Ozawa et al., 2012)

Within these two decades of GPS observation, it is found that there is a close spatial correlation between slip-deficit of interseismic period distribution with coseismic slip distribution. For example in Sumatra (e.g. Konca et al., 2008), Northeast Japan (e.g. Simons et al., 2011, Hashimoto et al., 2012), and Chile (e.g. Moreno et al., 2011) as shown in Figure 2.8-2.10.

In Sumatra, Chlieh et al. (2008) has estimated the interseismic slip deficit from GPS data and coral data along western coast off Sumatra, consist of locked and creep patches (Figure 2.8). Konca et al. (2008) infer that the 2007 M8.4 and M7.9 Bengkulu earthquake nucleate in the edge of a locked patch and ruptured in a highly locked area (Figure 2.8). The 2007 coseismic rupture a part of patches from previous earthquake in 1797 (M8.7-8.9) and 1833 (M8.9-9.1). They suggest that the same portion in the plate interface can rupture in different patterns depending on whether the earthquake break one isolated asperity or several asperities at once producing larger rupture.

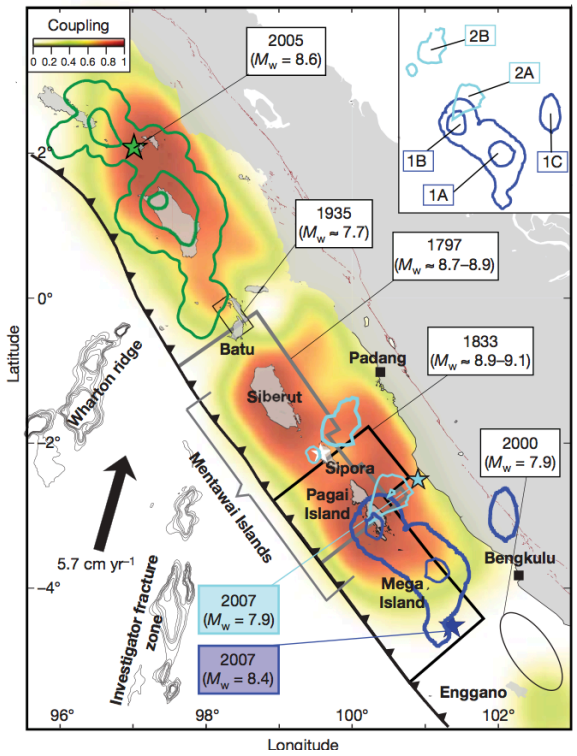

Figure 2.8. Spatial correlation between slip deficit distribution in interseismic period with coseismic slip distribution in Sumatra. Yellow to red indicate degree of coupling estimated from coral and GPS data. Green, blue, navy star and line indicate epicenter and rupture area of recent 2005 M8.5 Nias, 2007 M8.4 and 7.9 Bengkulu earthquakes, respectively (Konca et al., 2008).

In northeast Japan, the 2011 M9.0 Tohoku-Oki earthquake occurred in area which is determined as highly locked (Figure 2.9) (e.g. Ito et al, 2000; Hashimoto et al., 2009; Simons et al., 2011). However most study did not estimate slip deficit equivalent to M ≥ 9 neither

estimated high lock in the shallow part that could accommodate rupture to shallow portion. Coseismic rupture several highly locked portion and several asperities, including area that was thought to be creeping. Hashimoto et al. (2012) suggested that the earthquake rupture a large basement asperity underlying much smaller-scale local asperities.

In Chile (Moreno et al, 2010; 2011), the 2010 Maule earthquake nucleate in the full locked patches estimated by GPS inversion (Figure 2.10). That segment was inferred to have not been ruptured by any earthquake with M>8.5 since 1835, and by seismic and geodetic estimated was considered to have been undergoing strain accumulation. The 2010 is estimated to have release most of the accumulated stresses in the area since 1835.

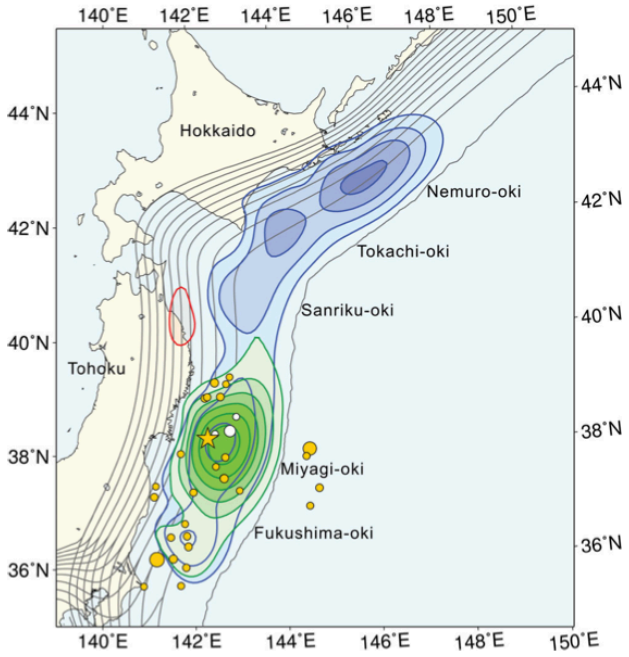

Figure 2.9. Spatial correlation between slip deficit distribution in interseismic period with coseismic slip distribution in Northeast Japan. Blue and green contour indicate the slip-deficit distribution prior 2011 M9.0 Tohoku earthquake and its coseismic slip (Hashimoto et al., 2012).

Although the theory that slip decifit in interseismic period correlate with coseismic rupture is not well established, but recent events as mention above shows the importance to monitor the slip deficit distribution for prediction of large earthquakes.

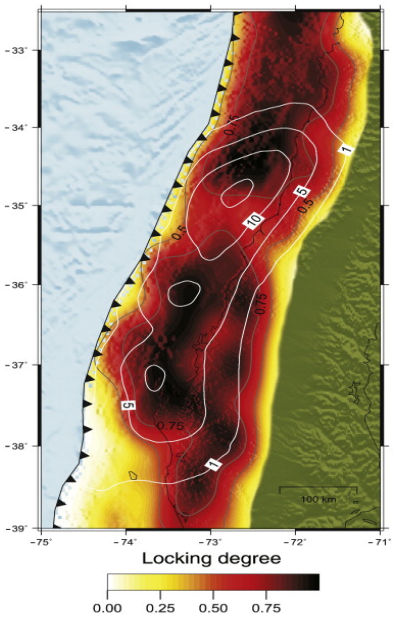

Figure 2.9c. Spatial correlation between slip deficit distribution in interseismic period with coseismic slip distribution in Chile. Yellow to red indicate degree of coupling estimated from GPS data. White contours indicate the coseismic rupture area of the 2010 M8.8 Maule earthquake (Moreno et al., 2011).

Postseismic deformation is caused by several mechanism; afterslip (e.g. Hsu *et al.* 2006; Ozawa et al., 2012), viscoelastic relaxation (e.g. Pollitz *et al.* 2000), poroelastic rebound (e.g. Fialko 2004), and their combination (e.g. Barbot and Fialko, 2010; Gunawan et al., 2014). Afterslip is a slow slip that follows an earthquake, located on or adjacent to the coseismic fault plane (Figure 2.11). Afterslip duration is from days to years with a rapid initial rate of slip followed by a logarithmic decay (Figure 2.5). Sometimes afterslips have cumulative values that approach or exceed 50% of the average coseismic slip (Schwarts and Rokosky, 2007).

Viscoelastic relaxation is response of the mantle or the lower crust to abrupt stress change due to an earthquake. Viscoelastic relaxation usually continues over much longer time from years to decades with an exponential decay. Poroelastic rebound is crustal response to coseismic changes in pore fluid pressure in the crust. Pore-fluid-pressure causes fluid flow and poroelastic deformation.

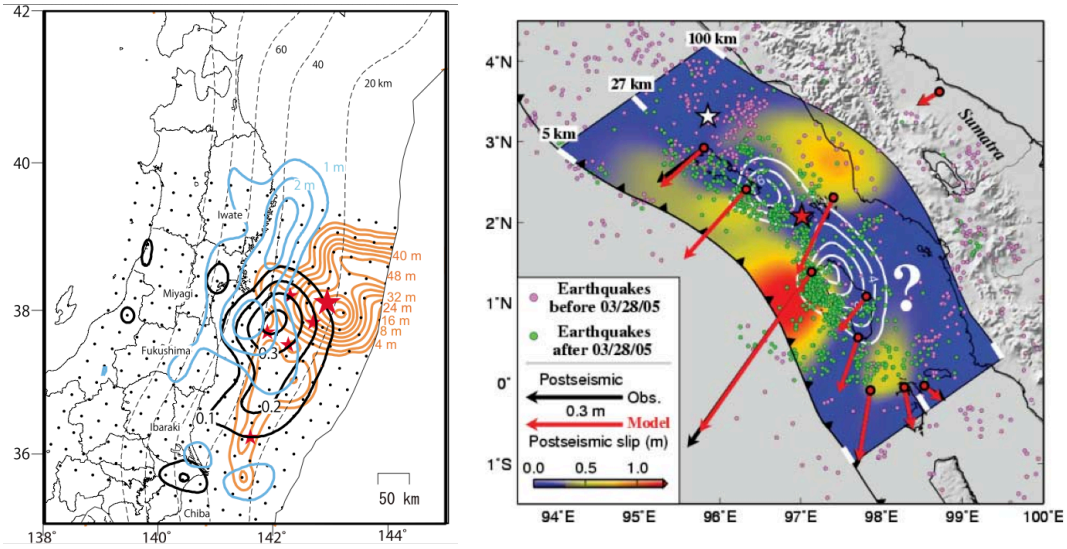

Figure 2.11. Example of spatial correlation between coseismic slip and afterslip. (Left) In the 2011 M9.0 Tohoku-Oki earthquake, afterslip (blue contours) is located in downdip of the rupture area coseismic (red contours) (Ozawa et al. 2012). (Right) In the 2005 M8.5 Nias earthquake, afterslip (color scale) is located updip of the coseismic area (white contours) (Hsu et al., 2006).

Other slip phenomenon in subduction zone is slow slip. Slow slip event (SSE) is an episodic slow fault slip without radiating seismic waves (e.g. Nishimura et al., 2014). SSEs have been reported at subduction zones in Japan (e.g. Heki et al., 1997; Hirose et al., 1999; Sagiya, 2000; Ozawa et al., 2014), Mexico (e.g. Lowry et al., 2001; Kostglodov et al., 2003), Costa Rica (e.g. Outerbridge et al., 2010), Kamchatka (e.g. Burgmann et al., 2001), Alaska (e.g. Freymuller et al., 2002), New Zealand (e.g. Douglas et al., 2005), and Cascadia (e.g. Dragert et al., 2001). Slow slip usually occur downdip of seismogenic zone, place of transition zone from seismic to aseismic, within a period of days to years.

2.3. Tsunami Earthquakes

Tsunami earthquake is attributed to earthquake that generates extraordinarily larger tsunami amplitude than expected from their seismic waves (Kanamori, 1972). In case of a tsunami earthquake, usually no or very weak shaking is felt but a large tsunami attacks later. In general, tsunami earthquake are characterize as having slow velocity with long rupture

duration, rupture in shallow portion of the subduction near the trench within a weak mechanical property such as the soft sediment of accretionary wedge (e.g. Fukao, 1979, Polet and Kanamori, 2000; Ammon et al., 2006; Lay and Bilek, 2007; Newman et al., 2011; Okal, 2012). Examples are the 1989 Sanriku, the 1992 Nicaragua, the 1996 Peru, the 1994 and 2006 Java, and the 2010 Mentawai tsunami earthquakes.

There is also tsunami triggered by a landslide, which is also categorized as tsunami earthquakes, such as the 1992 Flores and the 1998 New Guinea earthquakes. Locations of tsunami earthquake events are shown in white circle in Figure 2.1. Tsunami earthquake poses a threat in disaster mitigation since it is not accompanied by strong shaking there is no natural warning for the people to evacuate. However the generated tsunami can be catastrophic in populated coastal areas.

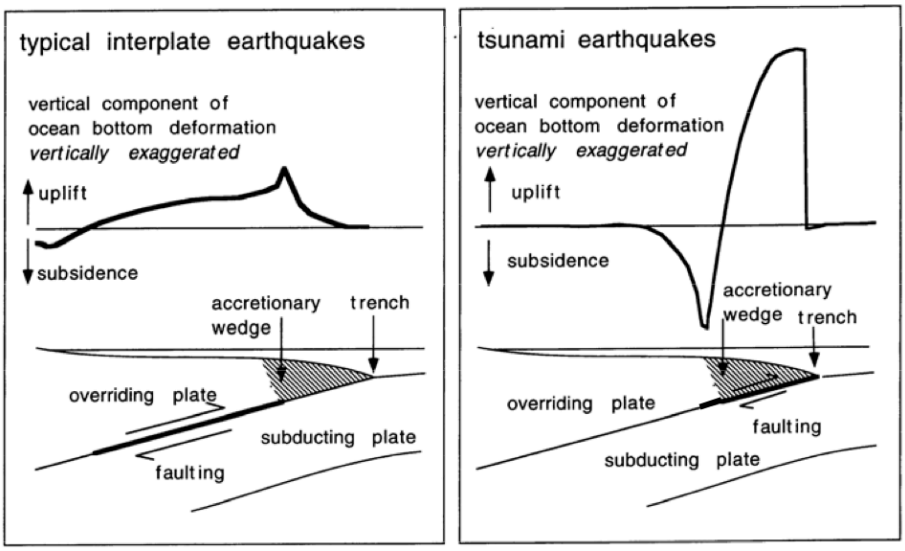

Figure 2.12. Illustration of tsunami earthquake (redraw from Satake and Tanioka, 1999)

Chapter 3

Tectonic Background of Java Trench

2.1. Tectonics

The Sunda Arc curves along the islands of Sumatra and Java with a total length of more than 5600 km. The trench is either named Sunda Trench or Java Trench. In this study, for consistency we use the term “Java Trench”. The Sunda Arc consists of the Java Trench, fore-arc ridge, fore-arc basin, active volcanic arc and Cenozoic foreland in northeast Sumatra and northern Java (Hamilton, 1979; Susilohadi et al., 2005). Some part of the fore-arc ridge off Sumatra rise above sea-level forming small islands, while south off Java lie below sea level (Susilohadi et al., 2005).

In this region, the Indo-Australian plate subducts beneath the Sunda Block at the Java Trench in an almost perpendicular direction to the trench off the south coast of Java Island and at an oblique angle off the west coast of Sumatra Island, Indonesia (Figure 3.1). The subduction system here was commenced in Cretaceous and become very active during the Paleocene, with subduction rate greater than 15 cm/yr (Susilohadi et al., 2005). In Middle Eocene, the Indian continent started to collide with Eurasia and the convergence rate slowed down to 3cm/yr (Susilohadi et al., 2005). Then in the late Eocene-early Oligocene the Indian Ocean began to spread, increasing the subduction rate to 5-6 cm/yr. Currently, the subduction rate gradually decreases from 68 mm/yr off central Java to 60 mm/yr off central Sumatra (DeMets et al., 2010). The collision of India and Eurasia caused massive amount of sediments to be formed into the Indian Ocean and the Java Trench, rapidly accreted and creates large accretionary prism (Susilohadi et al., 2005).

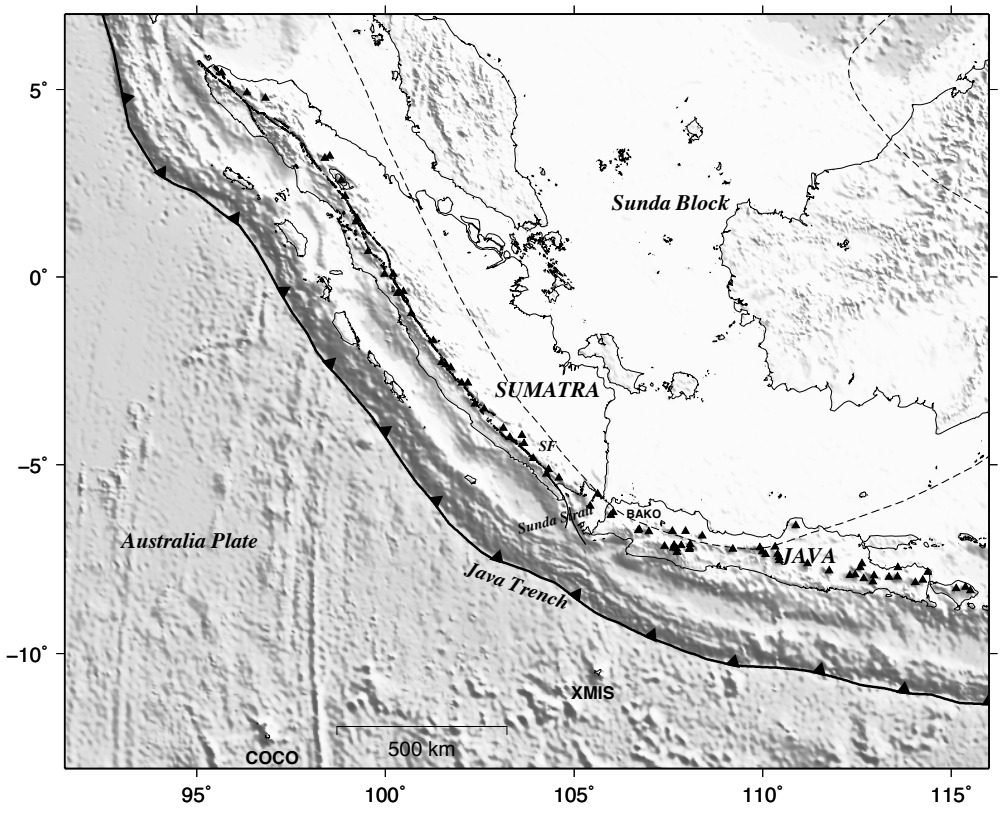

Figure 3.1. Tectonic setting of western Indonesia.

The main tectonic feature of Sumatra is the Sumatra Fault, accommodating the oblique motion of the subduction (SF in Figure 3.1). The Sumatra Fault is a right-lateral strike slip fault with a length about 1600 km extending along Sumatra from North to South. (e.g. Zen, 1983). The formation of the right lateral movement is though to have started during the Mid Miocene. Along SF, there also exist chain of volcanoes (Figure 3.1), which produced large quantities of acid volcanic in the Cenozoic time (Zen, 1983). The SF continues to Sunda Strait and terminates there on a North-South structure, thus manifest normal faulting (Zen, 1983). Sunda strait separate Sumatra from Java and is considered to be the transition between Java and Sumatra (e.g. Zen, 1983). Volcanologically, Sunda Strait and westernmost part of Java show more similarity to Sumatra than to Java. In Java, the volcanic activity started in Early Miocene, and produce andesitic-rocks (Zen, 1983).

Sumatra and Java is assigned to be part of Sunda block, with Java located on it`s south boundary (Figure 3.2 and 3.3) (e.g. Bemmelen, 1948; Hall, 2009). The Sundaland is formed during the Pleistocene. It mainly comprises Thailand, Malaysia, Indochina, Borneo, Java, Sumatra, and interjacent shallow seas with a number of smaller islands (Bemmelen, 1948; Hall, 2009). Seismicity and GPS measurements (e.g. Bock et al., 2003; Simons et al., 2007) indicate that Sunda block is currently moving slowly relative to the Eurasian plate. Sunda block is widely regarded as a stable area (e.g. Hall, 2009, Simons et al., 2007).

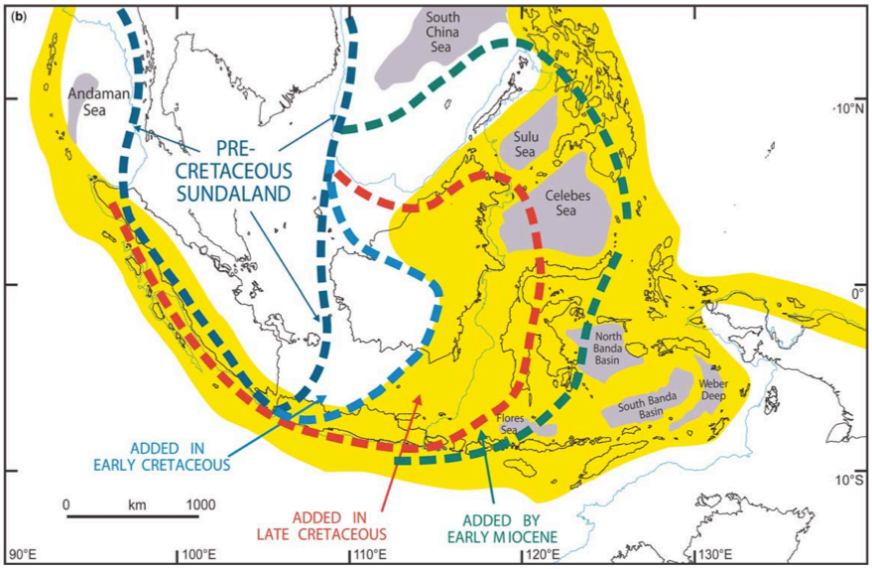

Figure 3.2. Formation of Sundaland (Hall, 2009)

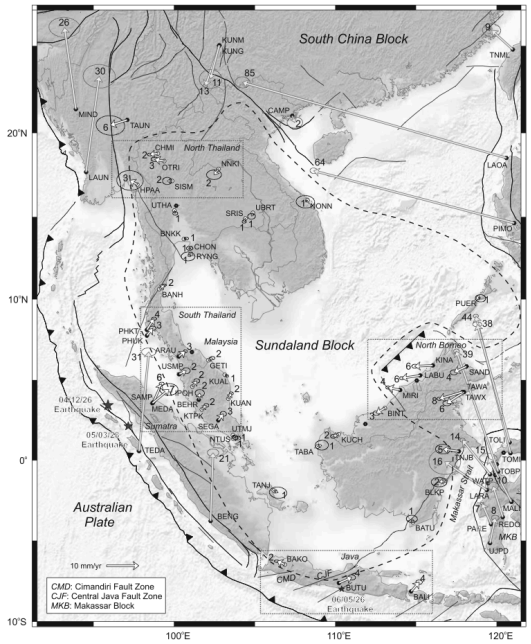

Figure 3.3. Sunda block inferred from GPS measurement (Simons et al., 2007)

Java has an area of 127.000 km^2, with length about 1000 km in the E-W direction. According to Bemmelen (1949), the main structural elements of the island are the geanticline, a broad uplift of regional extend, in south Java extending along the southern half of the island, and the geosynclinals basin of north Java occupying its northern half. The southern flank of the Java-geanticline is formed by the southern mountains. The southern mountains consist of volcanic deposits of the old-andesites formed in the Miocene age. These are crustal blocks, tilted towards the Indian Ocean. In the middle part of Java, the southern mountains have disappeared below sea level, so that here the median depression is bordered by the Indian Ocean (Figure 3.4).

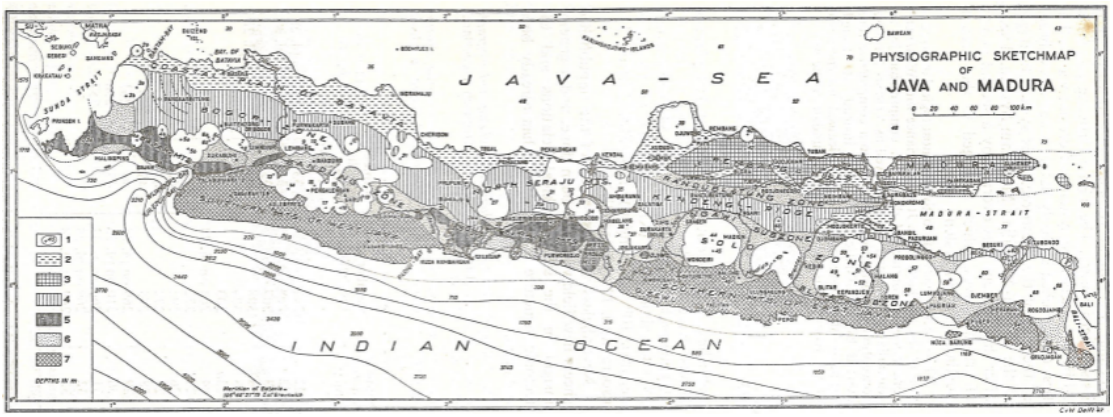

Figure 3.4. Physiography sketch map of Java (Bemmelen, 1949).

Java Island is currently the most populated island in Indonesia, houses big cities in the country including the capital of Jakarta.

2.2. Seismicity along Java Trench

Seismic data along the Java Trench show a lower seismic activity than in Sumatra (Figure 3.5). This was also suggested by Newcomb and McCann who reviewed 300 years of the seismic history of the Sunda arc from the late 1600`s through the early 1900`s (Figure 3.6).

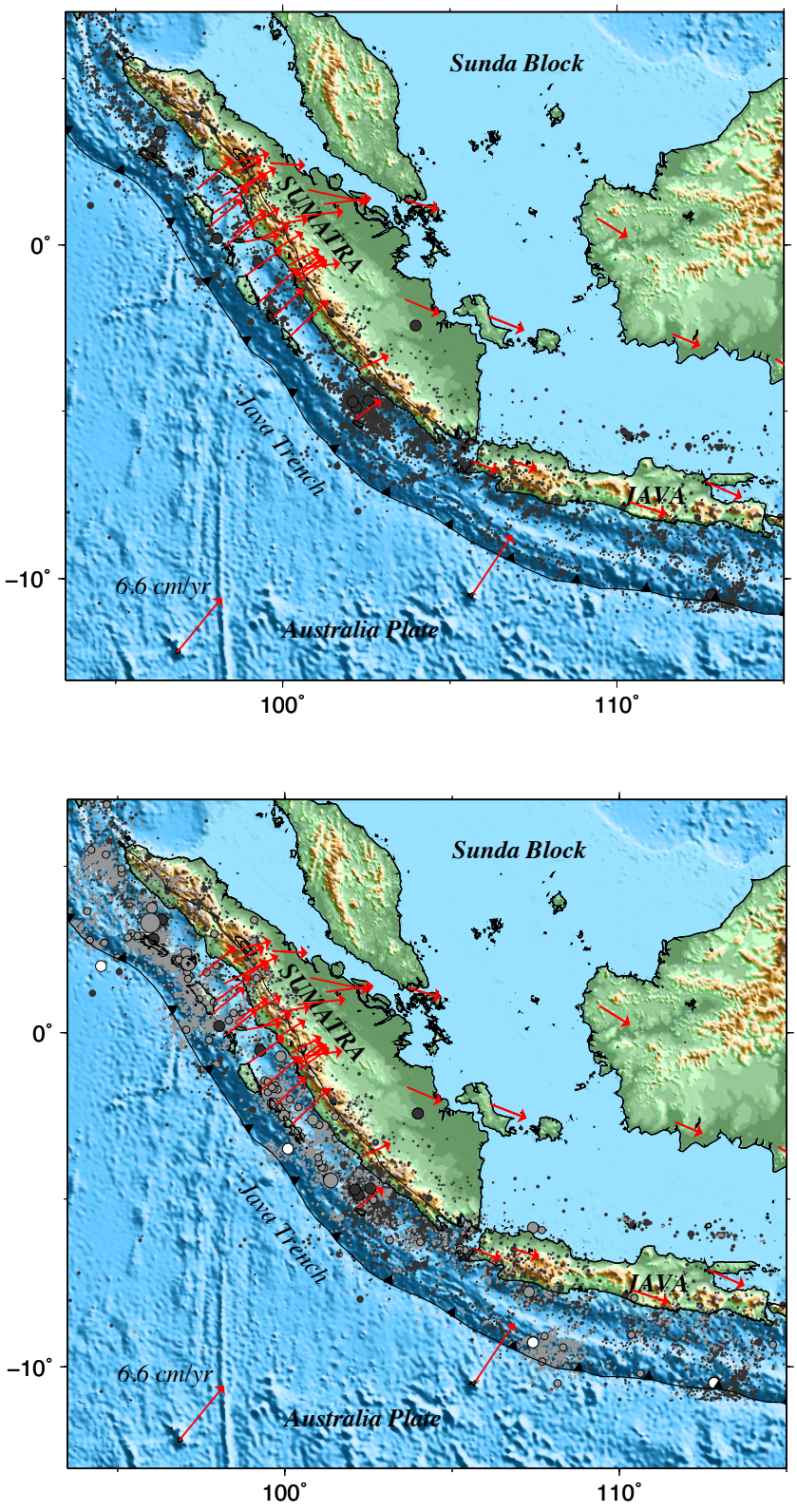

Figure 3.5. Seismicity along the Java trench prior (up) and after (down) the 2004 M9.3 Sumatra-Andaman earthquake. Red arrows are GPS vector from Bock (2003) in the ITRF2000 reference frame. Epicenter data from USGS catalogue from 1973 to 2010.

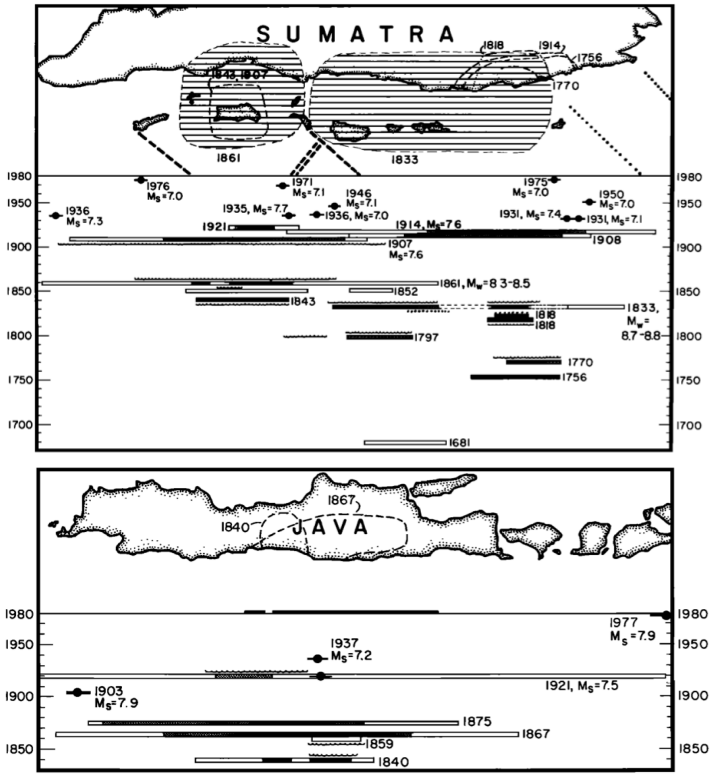

Figure 3.6. Historical reoccurrence of earthquakes in Java and Sumatra from 17th century to mid 1900 (Newcomb and McCann, 1987)

Historical megathrust earthquakes along the Sumatra segments occurred in 1797 (M=8.4), and 1833 (M~9.0) in Central-Southern Sumatra, and in 1861 (M~8.5) in Northern Sumatra (Figure 3.6 and magenta line in Figure 3.7). These earthquakes also were reported to caused large tsunamis. The 2005 M8.5 Nias earthquake ruptured the same region as the 1861 and the 1907 earthquakes. And the 2007 M8.7 Bengkulu earthquake rupture in partial region of the 1979 and 1833 events. Before the 2004 M9.3 Sumatra-Andaman earthquake, there was no historical record of an M>9 in that area. However, recenty Meltzner et al. (2010) found coral evidence for earthquake recurrence of an A.D. 1390-1455 at the south of the 2004 Suamtra-Andaman rupture area. Historical interplate event prior to the 1994 earthquake also has not been found off Java (Newcomb and McCann, 1987; Okal, 2012).

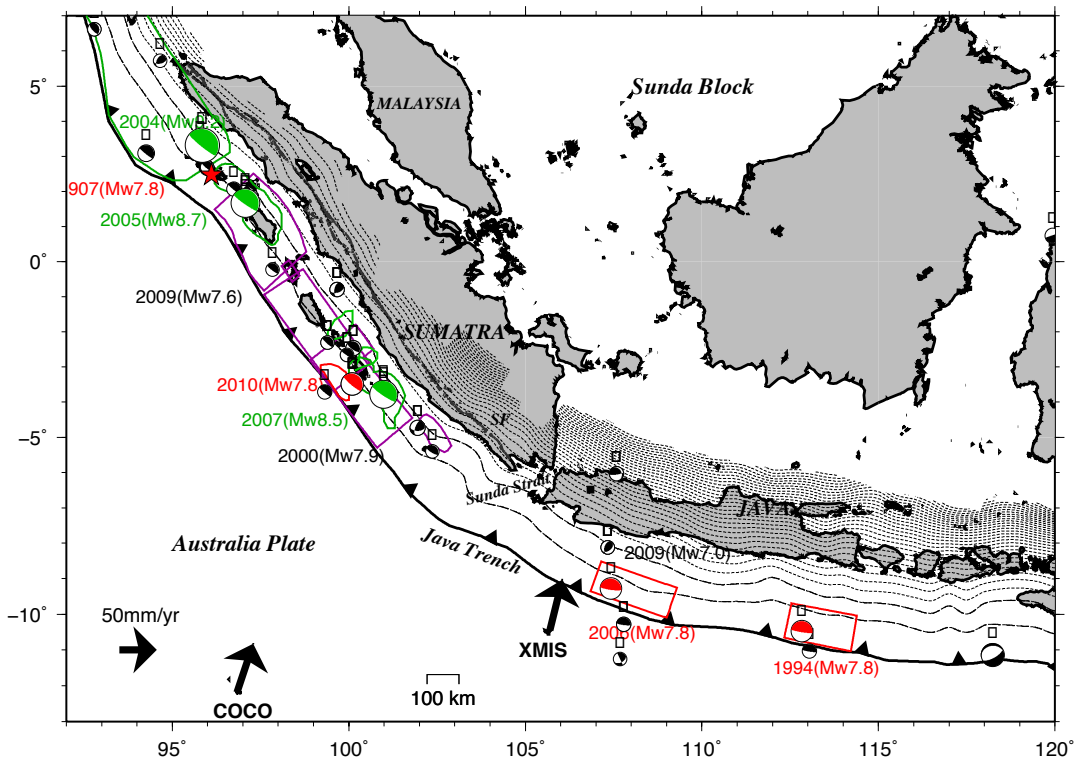

Figure 3.7. Historical interplate event along Java Trench. Magenta, green and red color indicate events before and after 1900, and tsunami earthquakes, respectively.

In Java, in general there are four types of earthquakes (Figure 3.8 and 3.9). First is shallow crustal earthquake. Recent example is the 2006 M6.3 Yogyakarta earthquake. The earthquake was due to strike slip fault of Opak Fault. There was strong shaking along the fault, which causes casualty of 5800 and many structural damage. Second is intraslab earthquake. Recent example is the 2009 M7.0 Tasik earthquake in the depth of 50 km. The shaking was felt across the Java Island, causing casualty of 80 mainly due to landslide. Third is deep earthquake. Recent example is the 2007 M7.5 Indramayu earthquake occurring in depth of 600 km. This earthquake gave medium shaking around western Java without causing any report of casualty. Fourth is tsunami earthquake. Recent examples are the 1994 and 2006 M7.8 Java tsunami earthquakes.

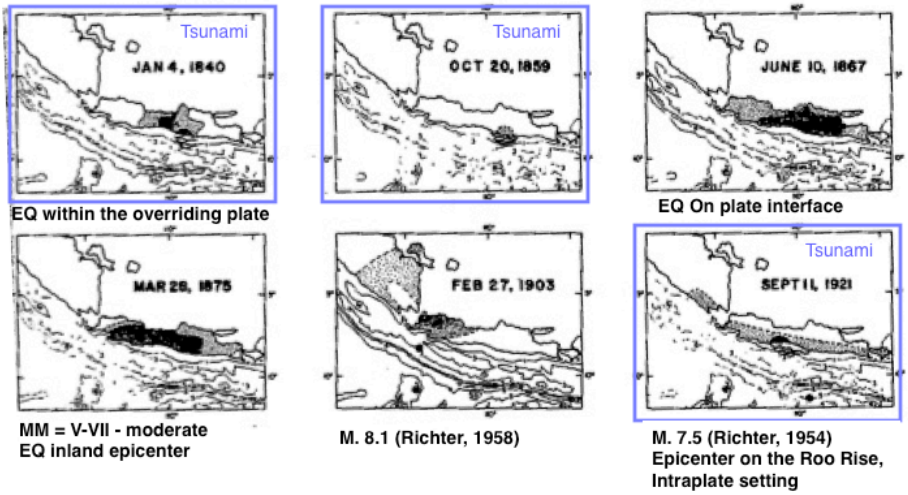

Figure 3.8. Java seismicity in late 1600 to mid 1900 (Newcomb and McCann, 1987).

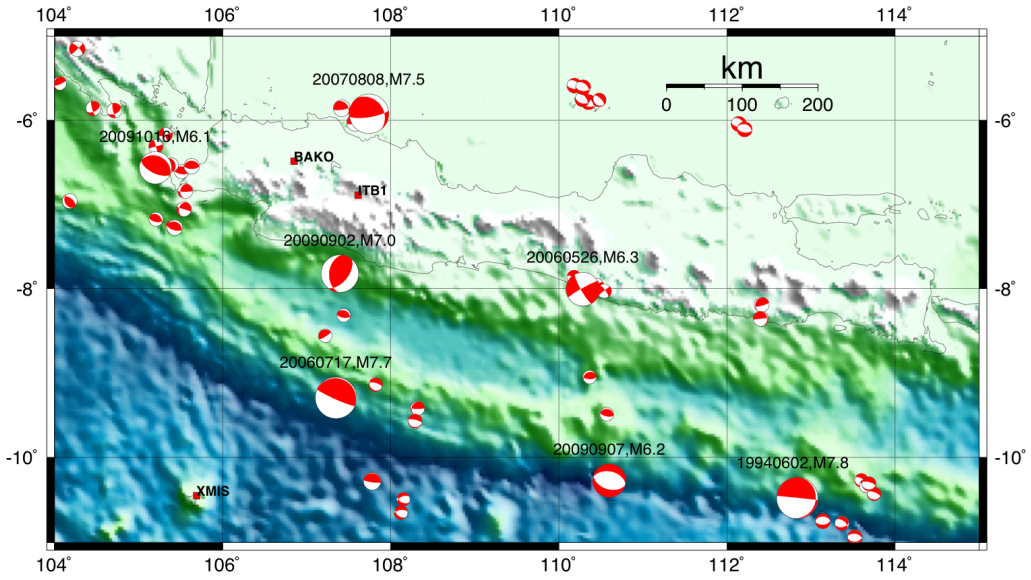

Figure 3.9. Java seismicity in 1973-Oct 2009 with M>5. CMT data are from USGS catalogue.

3.3. Tsunami Earthquakes along Java Trench

3.3.1. The 1994 M7.6~7.8 Java tsunami earthquake

The 1994 Java tsunami earthquake occurred about 200 km south coast off East Java on June 3, midnight at 01h 17m local time. This event was a shallow thrust earthquake occurring near the trench at depth 15 km (Dziewonski et al., 1995). The shaking was reported to be felt by local people in the south coast of East Java to Bali, however only 10-20% was awakened due to the shaking (Tsuji et al., 1995). Tsunami wave arrived to the coast 40-50 minutes after

the mainshock, inundated south coast of East Java to Bali. Run-up height reach 1-14 m in south coast of East Java and 0-5 m in west coast of Bali shown in Figure 3.10 (Tsuji et al., 1995; Synolakis et al., 1995), causing ~200 casualties (Synolakis et al., 1995).

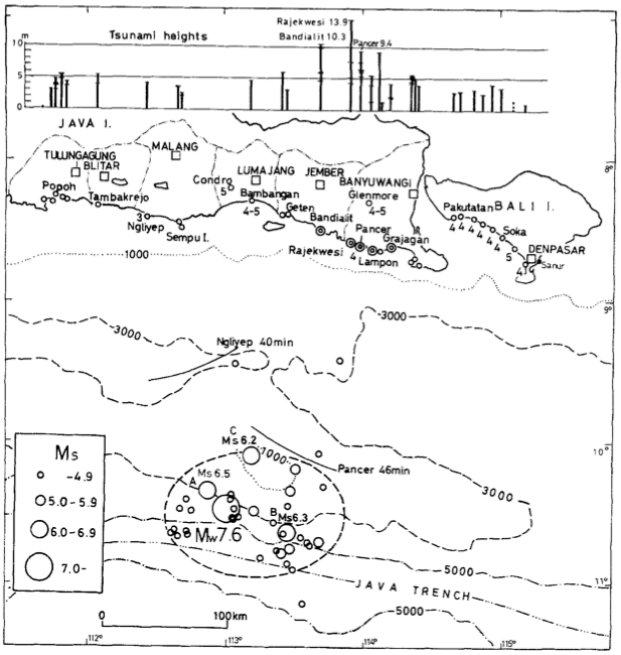

Figure 3.10. Hypocenter distribution of main shock and aftershocks of the 1994 East Java earthquake and the run-height (Tsujii et al., 1995)

Aftershocks was distributed in the shallow part of the subduction near the trench dominated with normal faulting aftershoks, about ~120km in E-W direction and diameter of ~100km in N-S direction (Figure 3.10)(Tsuji et al., 1995). Three big aftershocks were reported to also caused tsunami, smaller than the first one. Tsuji et al. (1995) suggested that the shaking was felt weaker compare to its magnitude. Based on their survey, even tough several local people have experience earthquake shaking before, but nobody expected a tsunami would come after that 1994 Java earthquake.

The 1994 Java earthquake was assigned as tsunami earthquake because of its large tsunami magnitude compare with the earthquake magnitude, and the relatively low energy radiated by the mainshock (Tsuji et al., 1995; Newman and Okal, 1998; Polet and Kanamori, 2000). Abercrombie et al. (2001) suggested that the earthquake involved slip on a locked

patch due a subducted seamount. Subduction of a large seamount would increase the normal stress on the interface that could lead to locking of the interface (e.g. Scholz and Small, 1997).

3.3.2. The 2006 M7.8 Java tsunami earthquake

On July 17, 2006, an earthquake of Mw 7.8 occurred in South of West Java, 600 km west of the 1994 event (Figure 3.11 and 3.12) as a result of shallow thrust faulting. The earthquake shaking was reported not being felt by local people along the coast, however devastated by tsunami of 3-8 m (e.g. Kato et al., 2007), with the maximum tsunami run-up heigth of 21 m in Nusakambangan island (Fritz et al., 2007). The inundation reached 200 m inland, causing 600 deaths and much destruction (Figure 3.11).

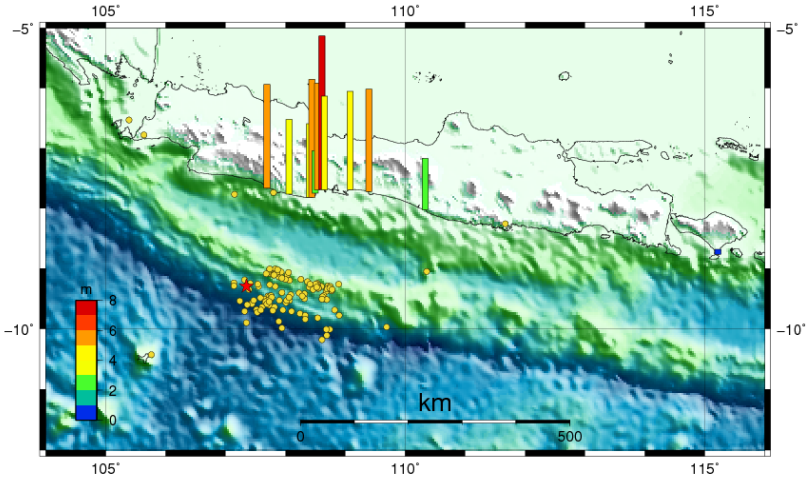

Figure 3.11. Hypocenter distribution of main shock and aftershocks of July 2006 Java Earthquake in the period within 2 days after the mainshock by USGS. Focal mechanism of the main shock by Harvard CMT solution. Observed tsunami heights by Geodesy Research Division of ITB and BMG compiled in Kato, 2007.

The timeline of the earthquake was reported as follows (BMG, 2006; Mori, 2007). The earthquake occurred at 15:19 local time. At 15:30 BMG (Geophysics and Meteorology Agency of Indonesia) announced the earthquake magnitude was Ms 6.8 and posed no danger of tsunami. At 15:16 the Pacific Tsunami Warning Center estimated magnitude of 7.2 and

issued local watch for Indonesia and Australia. At 15:46, Japan Meteorological Agency (JMA) sent a tsunami warning for Indian Ocean. At 16:05, 45 minutes after the mainshock, tsunami wave hit south coast of Java from Pangandaran in West Java to Cilacap in Central Java. This event indicated lack of knowledge and lack of warning system to the society in Indonesia.

Aftershocks occur mostly normal faulting near the trench based on USGS and CMT data. Earthquake source modeling revealed the source on the shallow portion near the trench (e.g. Ammon et al., 2006; Fujii and Satake, 2006) with about 200-250 km long and average fault slip 2.5 ~ 8 m. The radiated energy was low, and is considered due to location in a soft sediments of the accretionary prism. Unlike the 1994 Java earthquake, Bilek and Engdhal (2007) found no subducting seamounts within the rupture area of the 2006 Java earthquake.

Figure 3.12. Destruction of the 2006 Java tsunami earthquake (Photos courtesy of H.Z. Abidin of ITB)

3.3.3. The 1907 M7.6 Simuleue

Kanamori et al. (2010) has reviewed occurrence of the 1907 Sumatra earthquake based on an old seismogram. Gutenberg and Richter estimated the magnitude to be 7.6 and located this event in the outer rise area of the Java Trench. The earthquake caused people in Nias Island not able to stand due to the shaking (Newcomb and McCann, 1987). Newcomb and McCann (1987) describe the large tsunami extending almost 950 km along the Sumatra coast (Figure 3.13), which is disproportionate with its magnitude.

Based on re-analysis of the seismogram, Kanamori (2010) suggest that the 1907 event was a thrust earthquake at a depth approximately 30 km, with rupture duration of 100 s. Kanamori (2010) inferred that it is most likely that the 1907 earthquake occurred in the shallow portion of the subduction, with a magnitude range between 7.5 to 8 (Figure 3.13), and slowly rupture up-dip into the shallow sediments and generated a large tsunami. The larger tsunami compare to its magnitude made this event categorized as tsunami earthquake.

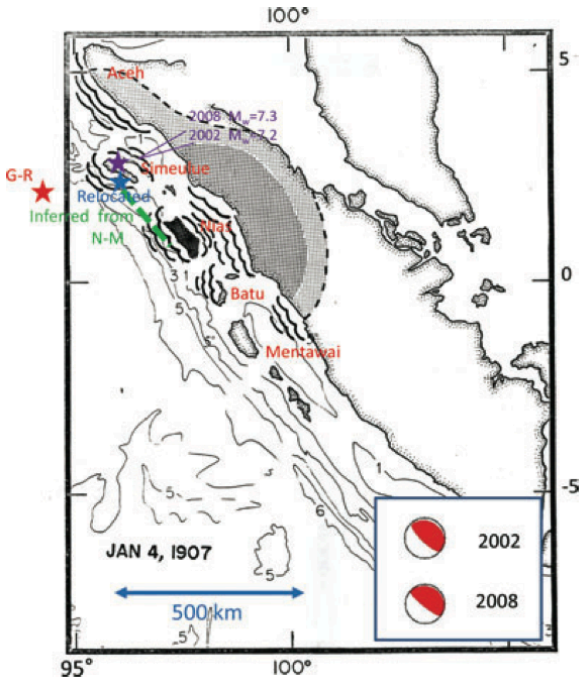

Figure 3.13. The epicenter of the 1907 overlay with maps of area affected by tsunami (Kanamori et. al., 2010; Newcomb and McCann, 1987). Red, blue, purple star indicate epicenter by Gutenber and Richter (1954), relocated epicenter by Kanamori et al. (2010) and the 2002 and 2008 earthquake, respectively.

3.3.4. The 2010 M7.8 Mentawai

This earthquake occured at the updip edge of the 2007 M8.5 Bengkulu earthquake, in a patch that has not fully ruptured since the events of 1979 M8.8 and 1833 M9 (Sieh et al., 2008; Hill, 2012). The tsunami run-up height was 6 m in average, with the maximum height of 16 m, causing 509 casualties (Hill et al., 2012). Hill et al. (2012) found small coseismic displacement of <22 cm in horizontal and <4 cm in vertical component. They inferred from the combination of GPS data and tsunami run-up height data combination that the tsunami height could be explained only if there is an extremely large fault slip at the very shallow depth.

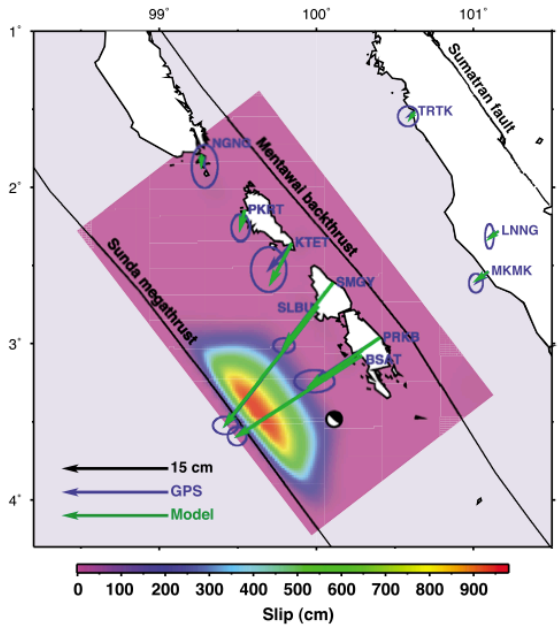

Figure 3.14. Horizontal coseismic offsets from GPS and coseismic slip distribution of the 2010 Mentawai earthquake, concentrated in the shallow portion (Hill et al., 2012).

The 2010 Mentawai earthquake occurred in an area that had been inferred as a weakly locked region from GPS observation (Chlieh et al. 2008). However in GPS inversion, boundary condition in the shallow portion is usually set to zero. So it is suggested that coupling may exist in the shallowest part. Nevertheless, the land based GPS is too far to have enough resolution to resolve the shallow portion.

This event was categorized as tsunami earthquake based on disproportionately large tsunami waves, long rupture duration about 125 s, rupture in shallow portion of the subduction, near-trench slip determined through finite-fault modeling and deficiencies in energy-to-moment and energy-to-duration-cubed ratios (Newman et al., 2011).

Recently, base on the study of coral microatolls, an earthquake similar to the 2010 event is supposed to occur around 1314 A.D. (Philibosian et al, 2012). This suggests that tsunami earthquake may repeat with an interval of around 700 years in this area.

3.3.5. Near-trench slip along the Java Trench

Along the Java trench, not only tsunami earthquakes occur near-trench, but also larger events such as the historical 1833 earthquake and the 2004 M9.3 Sumatra-Andaman earthquake (e.g. Henstock et al., 2006). Rupture to near-trench along the Java trench infer that the subduction zone off western Indonesia is capable of supporting shallow megathrust slip (e.g. Henstock et al., 2006), and also capable of generating larger tsunami than expected from its seismic magnitude.

Why many tsunami earthquakes occur along the Java Trench remains a question. Studies have shown that existence of accretionary prism in the tip of the subduction may cause the low radiated energy because of lower rigidity of soft sediments (e.g. Polet and Kanamori, 2000). Based on seismic study structure, this accretionary prism is presence along the western Java Trench (e.g. Kopp and Kukowski, 2003; Wittwer, 2011) as shown in Figure 3.15. However how the rupture can initiate remains a question (e.g. Bilek and Engdahl). In case of 1994, it is generally accepted that the rupture was due to a subducting seamount (e.g. Abercrombie et al., 2001), however subducting seamount is not found in the other area.

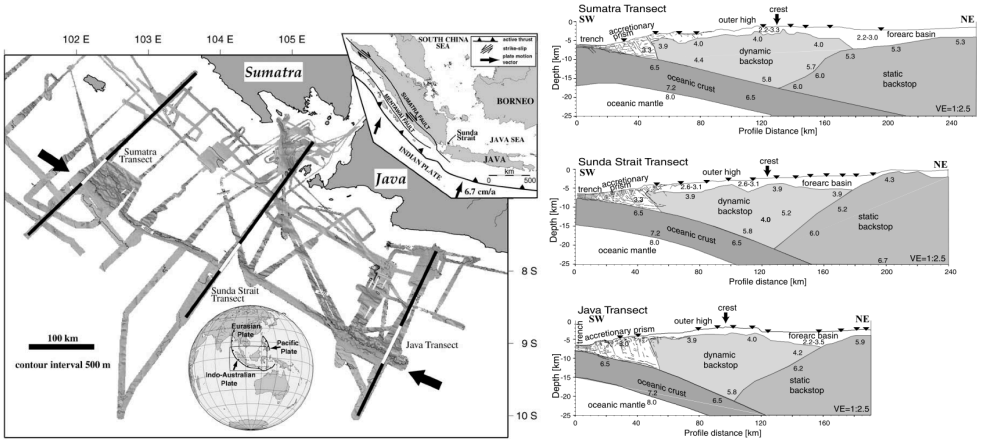

Figure 3.15. Accretionary prism in Java trench (Kopp and Kukowski, 2003)

Chapter 4

GPS Observation in West Java

4.1. GPS observation in Indonesia

Nowadays GPS has become a standard tool for monitoring crustal deformation and has been widely used to detect crustal movements to study earth geodynamics and earthquakes (e.g. Nishimura et al, 2014). GPS measurements in Indonesia started in 1989, to investigate the regional tectonic framework (e.g. Tregoning et al., 1994; Wilson et al., 1998; Prawirodirdjo et al., 2000; Bock et al., 2003; Simons et al., 1999, 2007), local deformation around major inland faults (e.g. Setyadji et al., 1997; Abidin et al., 2009; Meilano et al., 2012), as well as other ongoing processes such as land subsidence (Abidin et al., 2008; 2013).

4.1.1. GPS-GPS Project

The Geodynamics Project in Sumatra by Global Positioning System (GPS-GPS), was conducted with cooperation from Bakosurtanal (National Coordinating Agency for Surveying and Mapping) and scientists from US, Japan, and various institution and universities in Indonesia (Prawirodirdjo, et al., 2000). The GPS-GPS project was initiated after the work of Reid (1913) that measured the crustal deformation in Sumatra by triangulation. The first geodetic network revisited the triangulation points installed by Reid (1913) in campaign mode to reveal a detailed slip history along the central part of the Sumatra Fault (SF). They used 22 historical triangulation sites, and conduct 2-3 time GPS campaign survey in 1989-1993 (Prawirodirdjo, et al., 2000). By combining triangulation with GPS data, they were able to obtained long-term, near-field velocities along the northern half of the SF. They obtained the slip rates of 23-24 mm/yr with a locking depth of 20 km along the SF between 1°S and 2°N.

4.1.2. GPS across the Java Trench

The first GPS campaign in Java was conducted from 1989 to 1993 by Tregoning et al. (1994) to estimate the convergence across the Java Trench. They installed 3 GPS sites; BAKO, in West Java, XMIS in Christmas Island, and COCO in Coco Island. They conducted 6 campaign using Trimble 4000 SST receivers. They processed the GPS data using GAMIT in ITRF92 and obtained a steady time series for five years. They estimated the convergence of Christmas Island with respect to West Java (XMIS-BAKO) is 67 ± 7 mm/yr in a direction N11°E ± 4° that is orthogonal to the trench. The magnitude of convergence agrees with the rescaled NUVEL-1 relative plate motion (Argus et al., 1991) that predicts a value of 71 mm/yr between the Australia and the Eurasian plates. The direction of motion matched the direction inferred from earthquake slip vectors at the trench but is more northerly than the N20°E±3° predicted by NUVEL-1. They infer that either West Java moves with a distinct Southeast Asian plate or this region experiences plate margin deformation. They also inferred that a locked plate boundary would explain why their magnitude of convergence is slightly slower than that predicted by NUVEL-1, and why there is little seismic activity on this section of the trench.

4.1.3. GEODYSSEA Project

In 1991, the geodetic control widened to South Asia and Southeast Asia within the project of Geodynamic of South and Southeast Asia Project (GEODYSSEA) with the cooperation between Bakosurtanal, European Commission and the Association of South- East Asian Nations (Wilson et al., 1998). They installed 42 new GPS stations, to study the complex geodynamic processes and natural hazards of the region from the Southeast Asia mainland to the Philippines and northern Australia. They have provided new information about the location of active plate boundaries in and around Southeast Asia. Also, the results confirmed the existence of the Sunda Block, and provide a distinct relative motion with respect to Eurasia at a rate of about 2 cm/yr. They also inferred that slip vector azimuths of interplate earthquakes along the Java Trench consistently show a 10° westward deviation with

respect to NUVEL-1A model. This discrepancy can be resolved if the Sunda block motion is included (Wilson et al., 1998).

4.1.4. SEAMERGE Project

SEAMERGE (South-East Asia Mastering Environmental Research with Geodetic Space techniques) is a funded by the ASEAN-EU University Network program (AUNP), started from 1 January 2004 and run for two years up to 2006. SEAMERGE aimed to define the motion of Sundaland block, the deformation zones and their boundaries, and to study specific natural hazard areas in Southeast Asia such as earthquake related pre-/co-/post-seismic motions (http://www.deos.tudelft.nl/seamerges/). SEAMERGE revisited the GEODYSSEA network and also expanded the GPS networks in Southeast Asia, with total of about 100 GPS network in southeast Asia, mostly conducted in campaign mode surveyed once a year in average (Simons et al, 2007).

SEAMERGES were able to detect the 2004 M9.0 Sumatra-Andaman earthquake at GPS sites with a distance from 400 to 3000 km from the earthquake epicenter (Vigny et al., 2005). SEAMERGE latest result on the Sundaland motion and boundaries used 10 years of GPS data from 1994 to 2004 before the 2004 M9 Sumatra Andaman earthquake (Simons et al., 2007). Simons et al. (2007) is currently the newest result in defining the Sunda block Euler pole, located at (49.0°N–94.2°E), with a clockwise rotation rate of 0.34°/Myr. Sundaland moves eastward at a velocity of 6 ± 1 to 10 ± 1 mm/yr from south to north, with respect to Eurasia plate.

4.1.5. SuGAr Network

The Sumatran GPS Array (SuGAr) was established in 2002 initiated after study of paleogeodetic record found in coral microatolls of the western Sumatra (e.g. Sieh et al., 1999; Natawidjaja et al., 2000). They installed 14 GPS stations between mid-2002 to mid-2004. After the 2004 earthquake, they expand the network to 24 stations along the Sumatran plate boundary. The GPS array is still being operated until now. There has been since then many

studies related to the subduction process off Sumatra, including the interseismic, coseismic, and postseismic deformation above the Sunda megathrust off Sumatra covering the recent 2004 M9.3 Sumatra Andaman earthquake, the 2005 M8.5 Nias earthquake, the 2007 M8.7 Bengkulu earthquake, and the 2010 M7.8 Mentawai tsunami earthquake (Simoes et al., 2004; Meltzner et al., 2006; Subarya et al., 2006; Hsu, et al., 2006; Chlieh et al., 2007; Chlieh et al., 2008; Konca et al., 2008; Philibosian et al., 2012)

4.1.4. GPS Studies in Java

Previous GPS studies in Java are mostly conducted to study local deformation around major inland faults, namely Cimandiri, Lembang and Baribis faults (e.g. Setyadji et al., 1997; Abidin et al., 2009; Meilano et al., 2012), volcanoes (e.g. Janssen et al., 2002; Abidin et al., 2006), as well as land subsidence in big cities such as Jakarta, Bandung and Semarang (Abidin et al., 2008; 2013). Most GPS observations were conducted in campaign mode with yearly occupations.

GPS surveys were also conducted to investigate co-seismic and post-seismic deformation related to the May 2006 Yogyakarta (Abidin et al., 2009) and the July 2006 South Java earthquakes (Kato et al., 2007; Abidin et al., 2009). They inferred that the post-seismic horizontal deformation of the July 2006 South Java tsunami earthquake is generally less than 5 cm in the first year (2006-2007), and decreased to less than 3 cm in the second year (2007-2008) in the trenchward direction.

However, study of interplate coupling off Java has not been done prior to this study.

4.2. Indonesian Permanent GPS Station Network

The nationwide installation of Continuous GPS (cGPS) called the Indonesian Permanent GPS Station Network (IPGSN) data started at the end of 2007, (Subarya et al., 2010). IPGSN was installed and maintained by Badan Informasi Geospasial (BIG) or Geospatial Information Agency. As of 2012, IPGSN consist of 117 stations (Figure 4.1). All stations of IPGSN use the high precision L1/L2 geodetic type GPS receivers with choke ring antennas and radomes.

Example of cGPS pillar is shown in Figure 4.2. GPS data is recorded at 1Hz rate and transmitted in real time or near real time of 1-hour interval to the data processing center at BIG office in Cibinong, West Java.

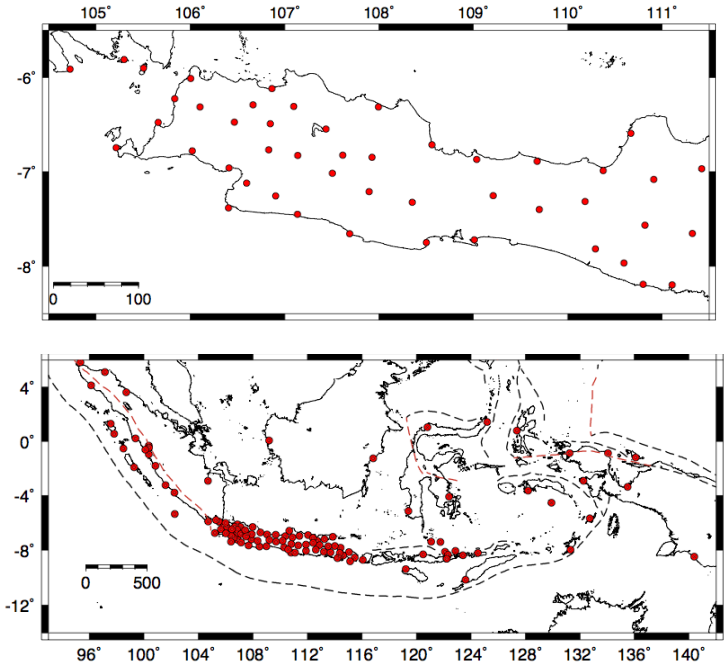

Figure 4.1. IPGSN Status in 2013 in Java (up) and Indonesia (down) (Subarya, 2013)

Figure 4.2. Example of cGPS pillar. Left. CSGT in Sagaranten. Right. CUJG in Ujung Kulon. (Subarya, 2013)

4.3. GPS Data and Processing

We use 3 years of data from 13 newly installed cGPS sites located in western Java and southern Sumatra (Figure 4.3), from 5 January 2008 to 31 December 2010. Twelve sites, namely CPMK, CLBG, CUJG, CSGT, CTVI, CPTN, CLDO, CUJK, CPSR, CTCN, CSBK, and CLGI, are part of IPGSN, and one site, namely ITB1, was established by the Geodesy Research Group of Institute of Technology Bandung (ITB).

The GPS phase data recorded at these 13 sites and 7 IGS (International GNSS Service) sites in the surrounding region; BAKO (West Java), XMIS (Christmas Island), COCO (Cocos Island), NTUS (Singapore), KUNM (China), PIMO (Philippine), and ALIC (Australia), are processed with Bernese GPS software Version 5.0 (Dach, et al., 2007) to obtain precise daily coordinates referring to the ITRF2008 reference frame. We use precise satellite orbits and earth rotation parameters provided by IGS, and ocean tide loading of the FES2004 model (Lyard et al., 2006), obtained online at http://froste.oso.chalmers.se/loading/.

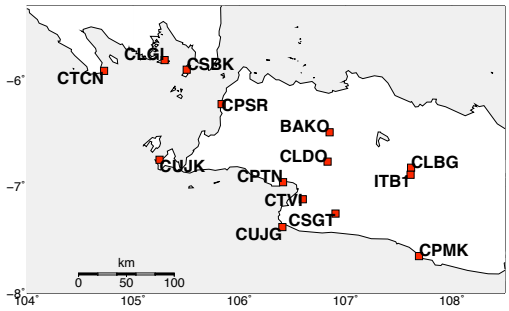

Figure 4.3. cGPS sites used in this study

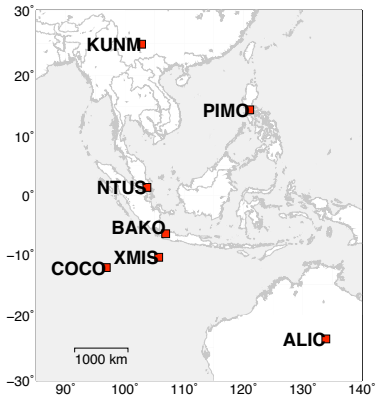

Figure 4.4. IGS sites used in this study

4.4. GPS Coordinate Time Series

The daily coordinate time series of the processed cGPS sites are shown in Figure 4.5 and 4.6 with respect to BAKO. In this time frame, a M_w7.0 earthquake occurred on 2 September 2009 off the southern coast of West Java (Figure 1.1) at the depth of 50 km, as a result of thrust faulting within the subducting Australia plate (ftp://hazards.cr.usgs.gov/maps/sigeqs/20090902/20090902.pdf). But no significant coseismic deformation is apparent in the time series.

Most of time series data show steady motion with a linear trend (Figure 4.5) except for 2 sites; CSBK and CLGI (Figure 4.6). The daily repeatability of 2.5-3.2 mm for horizontal and 9.1-12.5 mm for vertical components. CSBK and CLGI have daily repeatability was achieved for 3.9 mm and 6.9 mm for horizontal component, and 17.5 mm and 20.0 mm for vertical component, respectively.

CSBK and CLGI are located close to the Krakatau volcanic complex (Zen, 1983), and show a possible correlation with the activity of the Anak Krakatau Volcano (e.g. Dahren et al., 2012; Gardner et al. 2012; Agustan et al., 2012). In mid 2008, in coincidence with the eruption of Anak Krakatau, there is an apparent change in the time series of CSBK and CLGI, in coincidence with increase of number of volcanic earthquakes of Anak Krakatau (Figure 4.6). Also there is an apparent step in early 2010 at CLGI site, in coincidence with decreasing number of volcanic earthquake (Figure 4.6). However we are not sure if it is related to eruption of Anak Krakatau. On the other hand, there has been also neither antenna change in early 2010 (http://garner.ucsd.edu/pub/docs/site_logs/clgi.log.txt) or an earthquake event according to USGS.

Volcanological Survey of Indonesia (VSI) record two activities of Anak Krakatau of ash eruption, in April 2008 and in October 2010 (http://vsi.esdm.go.id/index.php/gunungapi/data-dasar-gunungapi/509-g-krakatau?start=1). While Global Volcanism Program recorded three eruptions of Anak Krakatau, the first from 23 October 2007 to 30 August 2008, the second

from 25 March to September 2009, and the third from 25 October 2010 to 9 March 2011 (http://www.volcano.si.edu/volcano.cfm?vn=262000)...

Because our objective is solely to study the interplate coupling of the subduction plate interface, we exclude CSBK and CLGI from further analysis.

4.5. GPS Velocities and Errors

Next, we obtain the displacement rate of each site by applying a linear trend to each coordinate time series by the least squares method. Obtained horizontal and vertical velocities in ITRF2008 are shown in Table 4.1 and Figure 4.7. The east-west component of cGPS sites ranges from 15.3 to 18.3 mm/yr eastward, the north-south component ranges from 6.2 to 19.7 mm/yr southward, and the vertical component ranges from 4.5 mm/yr subsidence to 14 mm/yr uplift.

Under the assumption of uncorrelated errors, we estimate the velocity uncertainty using the following formula (Zhang et al., 1997).

$$\sigma_{WN} = \frac{2\sqrt{3a_{WN}}}{N^{1/2}T}, N \gg 2 \qquad (4.1)$$

a_{WN} is the amplitude of random error in coordinate time series data, N is the number of observations, and T is the duration of the time series. This means that velocity uncertainty is proportional to the amplitude of coordinate error, and inversely proportional to the total number of observations and the interval time. Estimated velocity uncertainty is 0.3 to 0.9 mm/yr for horizontal components and 0.5 to 1.9 mm/yr for vertical component, at the 95% confidence level.

CPMK

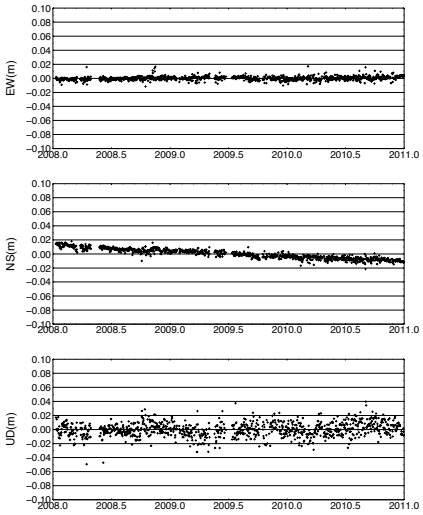

CLBG

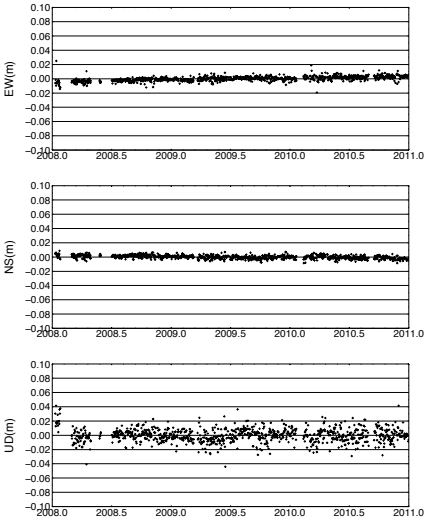

CUJG

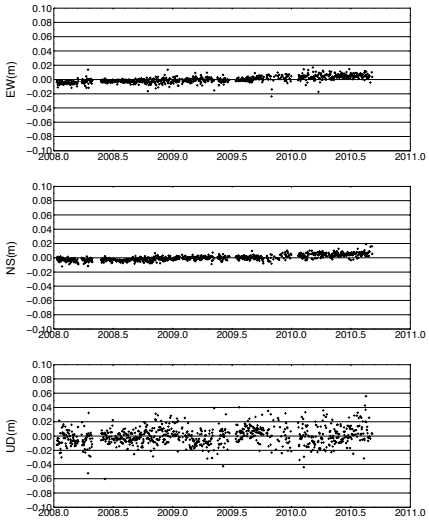

CSGT

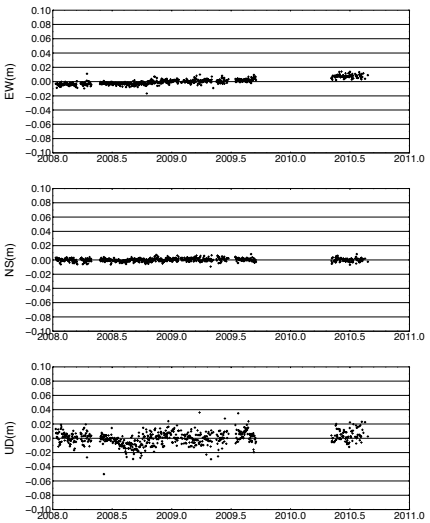

CTVI

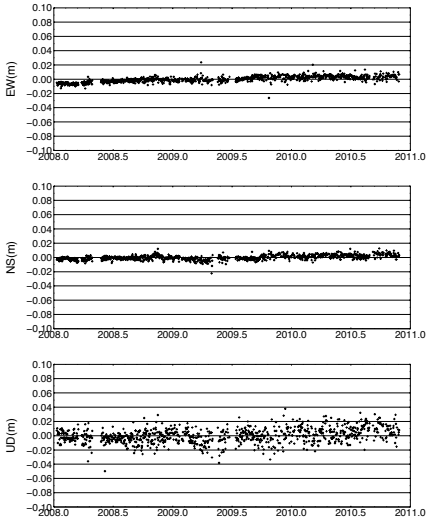

CPTN

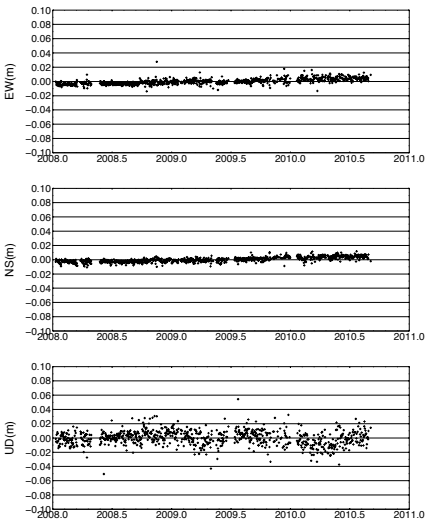

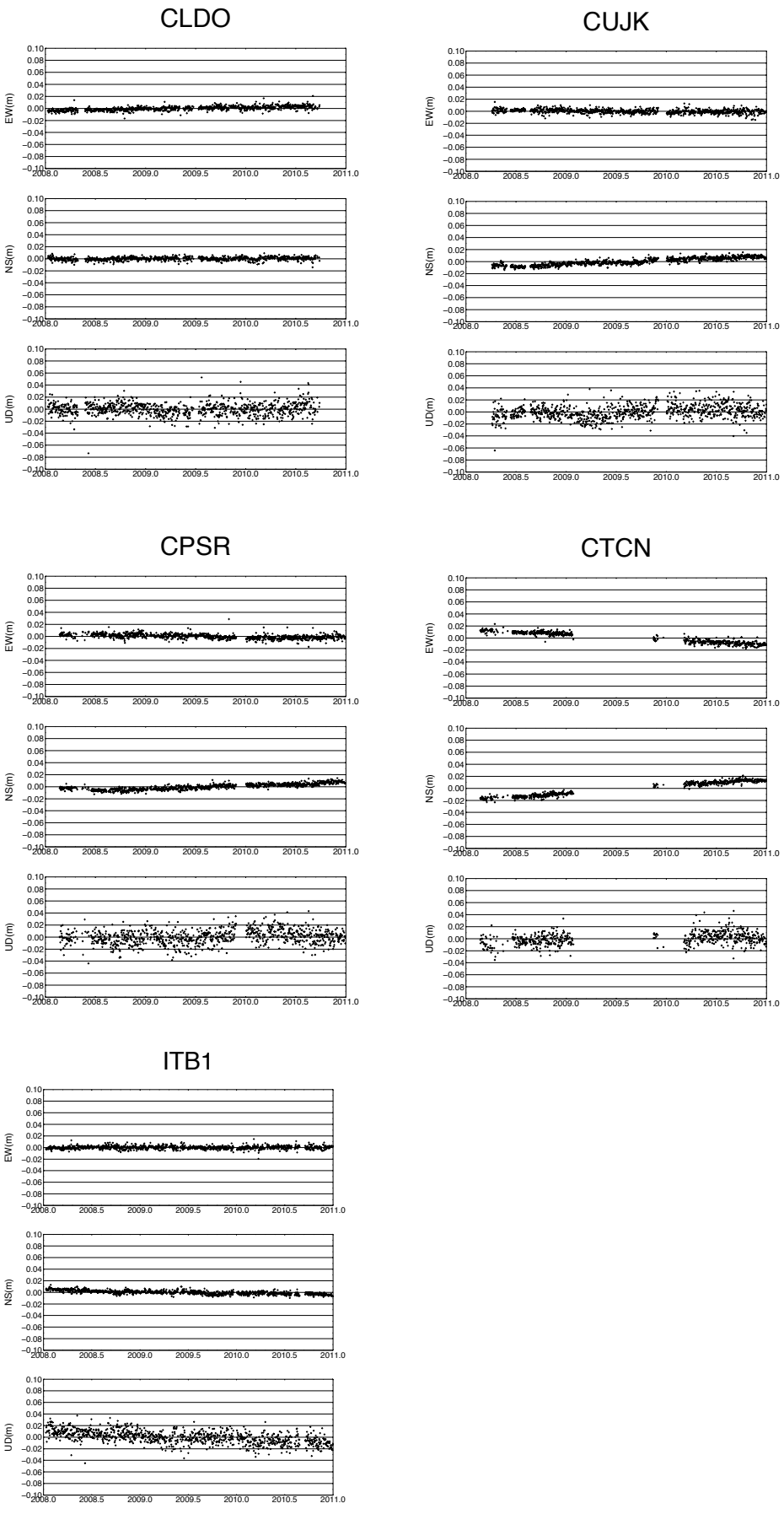

Figure 4.5. Time series of the cGPS data fix to BAKO.

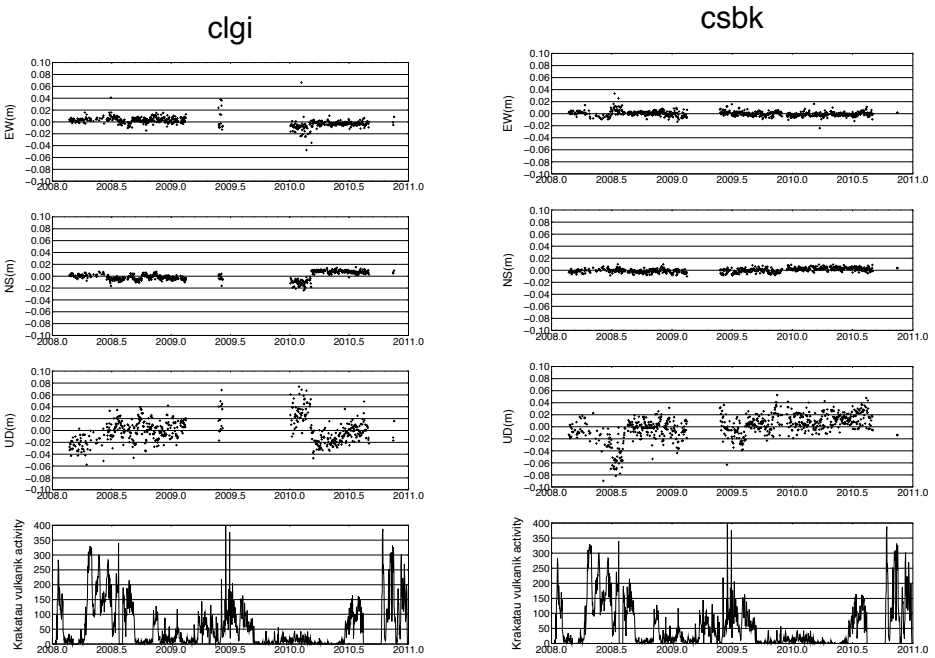

Figure 4.6. Time series of the cGPS data in CLGI and CSBK fix to BAKO, and daily earthquake frequency of Krakatau volcano in 2008-2010 (VSI).

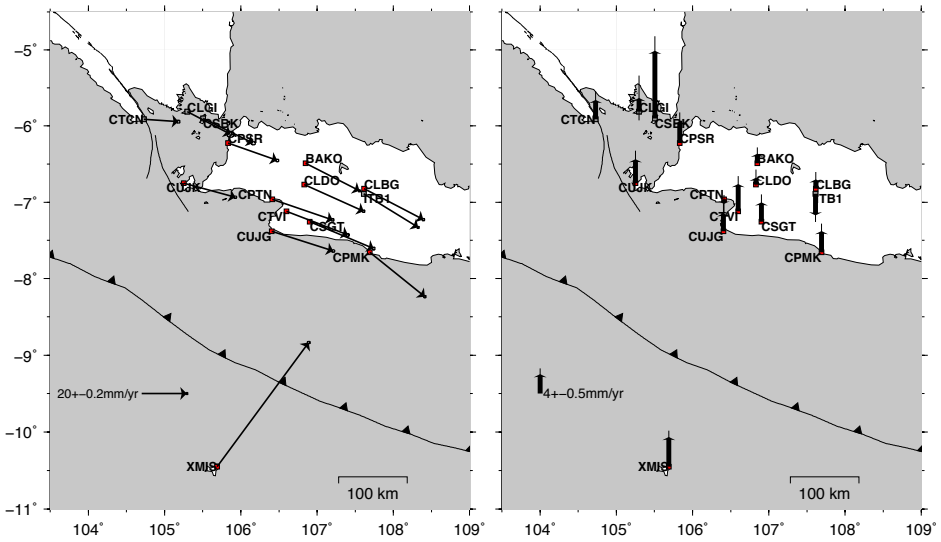

*Figure 4.7***.** Horizontal and vertical displacement rates from 3 years GPS data in 2008 to 2010 in ITRF2008.

Table 4.1. cGPS velocities in ITRF 2008 reference frame, with respect to Sundablock and with respect to BAKO site, showing east, north and vertical components with white noise uncertainty, for period January 2008 to desember 2010

Site name	Lon, °E	Lat, °N	ITRF 2008						wrt Sundablock		wrt BAKO			
			East	North	Vertical	σ(E)	σ(N)	σ(U)	East	North	East	North	Vertical	
CPMK	107.69	-7.66	24.4	-19.7	4.4	0.2	0.2	0.6	-0.7	-12.3	0.5	-7.5	1.8	IPGSN
CLBG	107.62	-6.82	26.3	-13.7	1.9	0.2	0.2	0.6	0.8	-6.3	2.3	-1.2	-0.3	IPGSN
CUJG	106.41	-7.38	27.2	-8.7	3.7	0.3	0.2	0.9	2.0	-1.8	3.9	3.8	3.0	IPGSN
CSGT	106.90	-7.26	28.3	-11.9	4.0	0.2	0.3	0.7	3.1	-4.8	4.9	0.4	3.1	IPGSN
CTVI	106.60	-7.12	27.2	-10.4	5.7	0.3	0.3	0.7	1.9	-3.5	3.5	2.0	3.9	IPGSN
CPTN	106.41	-6.96	26.8	-9.2	-1.0	0.2	0.2	0.8	1.4	-2.3	3.5	3.2	-1.4	IPGSN
CLDO	106.83	-6.77	26.4	-11.9	1.4	0.2	0.2	0.7	0.9	-4.8	2.9	0.5	0.2	IPGSN
CUJK	105.25	-6.75	22.9	-6.2	5.0	0.2	0.2	0.7	-2.6	0.2	-1.2	6.6	3.7	IPGSN
CPSR	105.83	-6.23	21.8	-7.7	4.4	0.3	0.2	0.8	-3.9	-1.0	-2.3	5.0	3.0	IPGSN
CTCN	104.73	-5.91	15.3	-1.0	4.0	0.3	0.3	0.7	-10.5	5.1	-8.6	11.9	3.5	IPGSN
CSBK	105.51	-5.90	22.3	-11.0	14.0	0.4	0.3	1.2	-3.6	-4.5	-1.2	2.1	14.5	IPGSN
CLGI	105.30	-5.81	19.2	-10.0	2.8	0.7	0.6	1.9	-6.7	-3.6	-4.1	3.1	3.1	IPGSN
ITB1	107.61	-6.89	24.1	-14.8	-4.5	0.2	0.2	0.6	-1.4	-7.5	0.1	-2.7	-7.0	CORS-ITB
BAKO	106.85	-6.49	23.9	-12.2	2.0	0.2	0.2	0.5	-1.7	-5.2	0.0	0.0	0.0	IGS
XMIS	105.69	-10.45	40.5	55.0	6.1	0.3	0.2	0.5	16.8	61.6	16.6	67.1	3.6	IGS
COCO	96.83	-12.19	45.3	52.0	1.1	0.3	0.2	0.6	22.7	55.0	21.6	64.8	1.8	IGS
NTUS	103.68	1.35	20.2	-12.9	3.1	0.2	0.2	0.6	-8.7	-7.1	-4.1	0.1	4.5	IGS
KUNM	102.80	24.88	31.9	-21.5	-7.4	0.4	0.3	1.3	-3.7	-16.0	8.0	-10.7	-1.4	IGS
PIMO	121.04	14.38	-32.4	5.4	6.7	0.4	0.2	0.8	-64.8	17.8	-55.3	19.0	3.6	IGS
ALIC	133.89	-23.67	28.3	60.0	-2.6	0.4	0.3	0.9	8.8	76.6	7.3	66.8	-17.8	IGS

4.5.1. Horizontal Component

To remove the effect of Sundablock, we convert the horizontal velocities into the Sunda block reference frame using the Euler pole estimated by Simons et al. (2007), which is the latest published Eulerpole for the Sunda block. Their estimated Euler pole of the Sunda block is located at 49.0°N–94.2°E, with a clockwise rotation rate of 0.34°/Myr. Since their solution was obtained in ITRF2000, we transform our GPS velocity from ITRF2008 to ITRF2000 using transformation parameters given by Altamimi et al. (2011)

$$\begin{pmatrix} V_x \\ V_y \\ V_z \end{pmatrix}_{ITRF00} = \begin{pmatrix} V_x \\ V_y \\ V_z \end{pmatrix}_{ITRF08} + \dot{T} + \dot{D}\begin{pmatrix} x \\ y \\ z \end{pmatrix}_{ITRF08} + \dot{R}\begin{pmatrix} x \\ y \\ z \end{pmatrix}_{ITRF08} \quad (4.2)$$

$\dot{T}$ is the translating vector,

$$\dot{T} = \left(\dot{T_x}, \dot{T_y}, \dot{T_z}\right)^T \quad (4.3)$$

$\dot{D}$ is the scale factor, and $\dot{R}$ is the matrix containing the rotation angles,

$$\dot{R} = \begin{pmatrix} 0 & -\dot{R}_z & \dot{R_y} \\ \dot{R_z} & 0 & -\dot{R}_x \\ -\dot{R}_y & \dot{R_x} & 0 \end{pmatrix} \quad (4.4)$$

Table 4.2 Transformation parameters from ITRF2008 to ITRF2000

(http://itrf.ensg.ign.fr/doc_ITRF/Transfo-ITRF2008_ITRFs.txt)

Rates	$\dot{T_x}$	$\dot{T_x}$	$\dot{T_x}$	$\dot{D}$	$\dot{T_x}$	$\dot{T_x}$	$\dot{T_x}$
Units	mm/yr	mm/yr	mm/yr	ppb/y	.001"/y	.001"/y	.001"/y
	0.1	0.1	-1.8	0.08	0.00	0.00	0.00

The motion of the Sunda block at our GPS sites are estimated 26 mm/yr to 108°E direction on average, or 25 mm/yr eastward and -5 mm/yr southward. Next we subtract the Sunda block motion from our GPS velocities in ITRF2000. Obtained velocities with respect to the Sunda block are given in Figure 4.8a and Table 4.1.

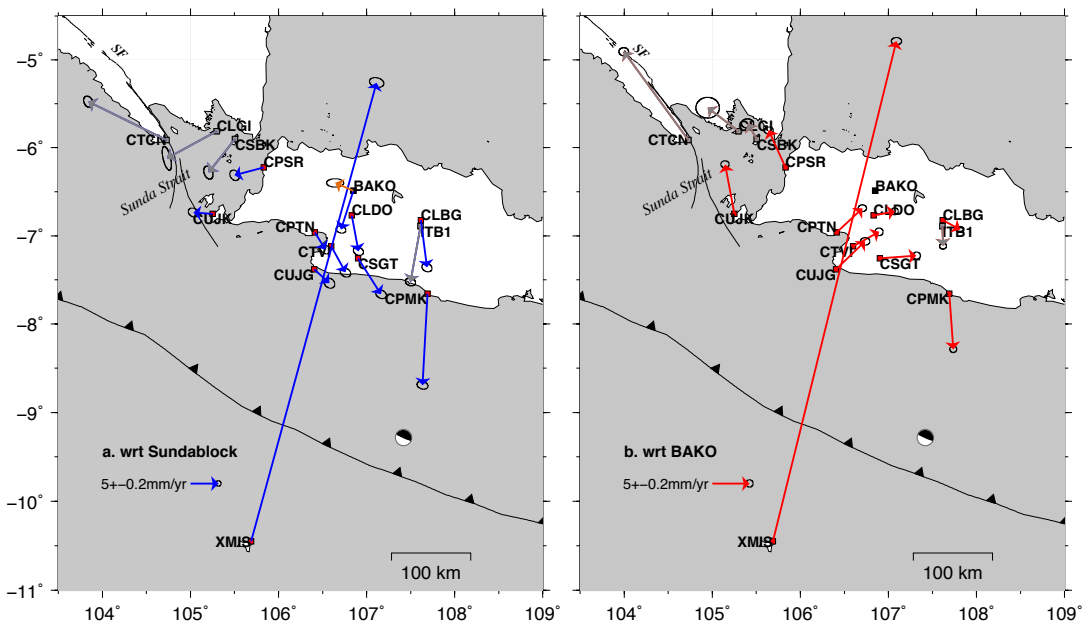

Figure 4.8. Horizontal displacement rates from 3 years GPS data in 2008 to 2010 (a) w.r.t Sundablock (b) fixed to BAKO. Gray vectors are observations that are excluded in inversion. Orange vector in (a) is the velocity of BAKO w.r.t. Sundablock estimated by Simons et al. (2007).

GPS sites near Sunda Strait shows a southwestward motion, while CUJK shows a westward motion and CTCN shows a northwestward movement (Figure 4.8a). The site CTCN shows a northwestward motion with a rate of 11.7±0.4 mm/yr suggesting an extension from CUJK that moves westward at a rate of 2.6±0.3 mm/yr. One interpretation of this northwestward motion of CTCN is the movement of the Sumatra sliver plate along the Sumatra Fault causing extension in Sunda Strait (e.g. Huchon and Le Pichon ,1984; Harjono, 1991; McCaffrey 1991; Sieh and Natawidjaja, 2000; Susilohadi et al., 2009).

Based on geology, geomorphology, and geodesy observations, there is an increase of slip rate from south to north of Sumatra Fault. Huchon and Le Pichon (1984) estimated from geological observations that the southern part of the Sumatra Fault has been displaced by about 100 km during the last 13 Ma at a slip rate of 7.7 mm/yr. Bellier et al. (1997) estimated the slip rate in the southern part of the Sumatra Fault near 5°S as 6±4 mm/yr based on offsets of geomorphological feature from SPOT images. Genrich et al. (2000) estimated slip rates

from GPS but for the northern Sumatra Fault, from 0.8°S to 5.5°N, with a slip rate of 23±5 mm/yr near 0.8°S. Assuming the slip rate decreases to the south, the magnitude of the slip rate from our GPS result in CTCN and CUJK is consistent with such information. To focus on the effect on interplate coupling alone, we exclude CLGI from further analysis.

The estimated velocity of BAKO w.r.t to Sundablock is 5.4±0.3 mm/yr at N198ºE, significantly different from the previous estimate (2.7±0.5 mm/yr at N293ºE) by Simons et al. (2007), as shown in orange color in Figure 4.9a. There are two possible causes for this discrepancy. First, the difference may be caused by a postseismic effect of the 2006 M7.8 earthquake south of Java. Postseismic deformation of a large megathrust earthquake continues for years to decades, affecting the crustal deformation pattern in the surrounding area (e.g. Feigl and Thatcher, 2006). This possibility is examined after we estimate the afterslip distribution of the 2006 event.

Another possibility is that there was a change in a rigid block motion of west Java. Such a significant change in block motion may be a rare phenomenon, but we cannot rule out the possibility since the observation period of Simons et al. (2007) is from 27 November 1994 to 25 December 2004, before the 2004 M9.0 Sumatra-Andaman earthquake, while our observation period is from 1 January 2008 to 31 December 2010.

To see if there is any velocity change at BAKO, we examined the velocity of BAKO using the solution of SOPAC, downloaded from http://sopac.ucsd.edu (Figure 4.9), for different time periods (Figure 4.10 Table 4.3). In the period of 1998-2004, same as period of Simon et al. (2007), we obtain a horizontal velocity of BAKO as 2.9 mm/yr at N290ºE with respect to Sundablock (Figure 4.10), quite similar to the velocity estimated by Simons et al. (2007). Then in the period of 2008-2010, we obtain a horizontal velocity of 3.2 mm/yr at N185ºE with respect to Sundablock (Figure 4.10).

We also examine the velocity change for every 2 years interval to see the temporal change of the velocities (Table 4.3). From Table 4.3, we can notice that before the 2006 M7.8 Java earthquake, the velocity of the N-S component of BAKO show a southward motion with

an approximate rate of ~6 mm/yr to the south. After the 2006 Java earthquake, N-S component rate increase to ~10 mm/yr to the south. Then in period of 2010-2011 and 2012-2013 N-S rate return back to ~6 mm/yr to the south, as before the 2006 Java earthquake. This strengthens our hypothesis that the postseismic effect of the 2006 Java earthquake is responsible for the velocity change in BAKO.

This indicates that the reference frame has an uncertainty or a fluctuation of a few mm/year in west Java. Because of this uncertainty, in the following inversion analysis, we did not analyze the velocity data referring to the Sunda block, but use baseline length change rate data.

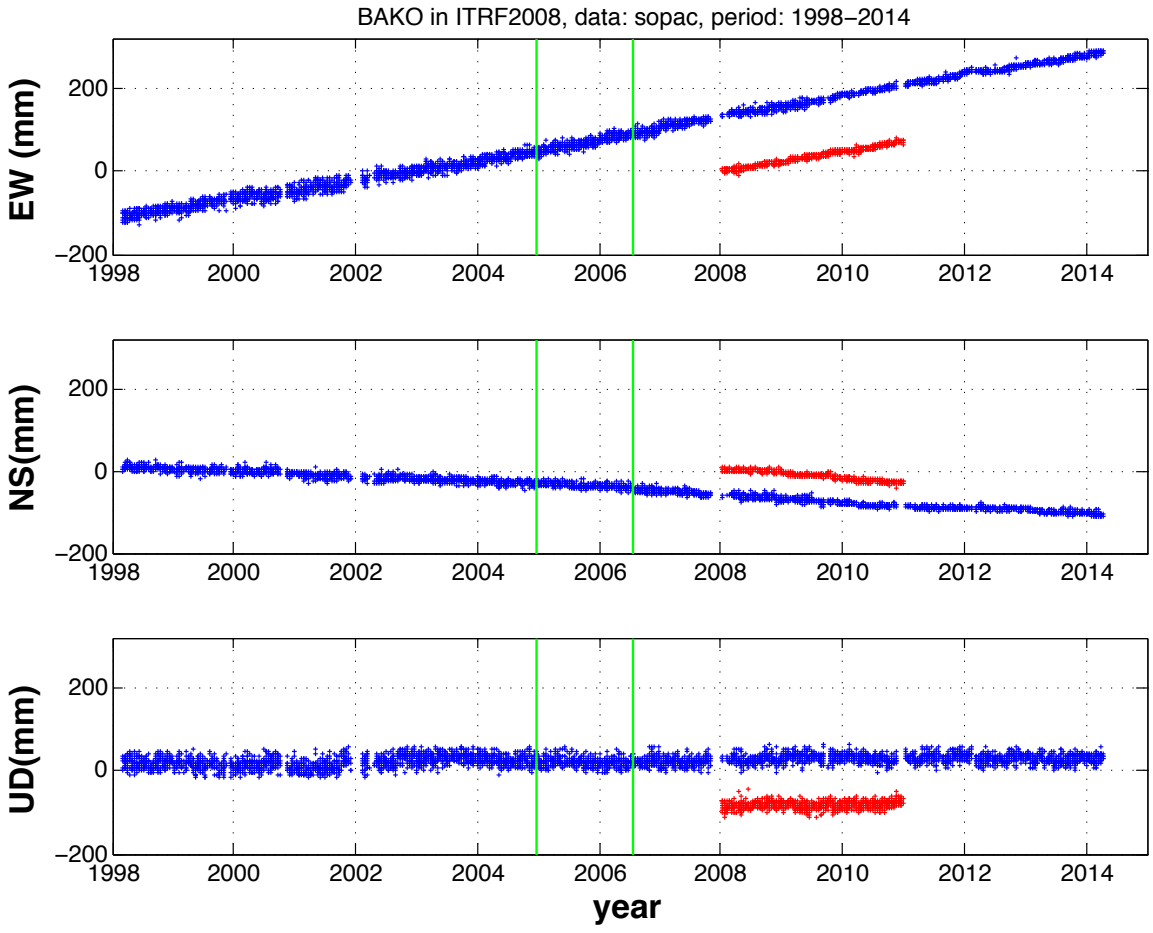

Figure 4.9. Time series of BAKO from our processing (red) and from SOPAC (blue).

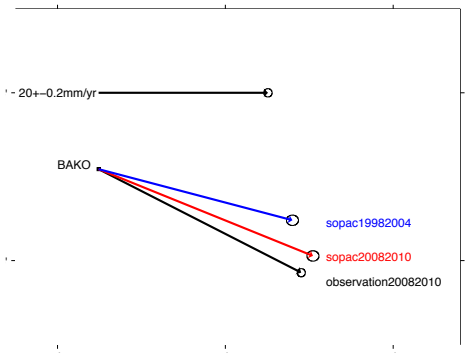

Figure 4.10. Comparison of BAKO velocity, from SOPAC timeseries in 1998-2004 (blue), from SOPAC timeseries in 2008-2010 (red), and from our processing in period of 2008-2010 (black).

Table 4.3. cGPS velocities in ITRF 2008 reference frame, derived from SOPAC time series

Period	East	North	Vertical	σ(E)	σ(N)	σ(U)	Description
Jan 1998 - 25 Dec 2005	22.9	-6.0	2.4	0.4	0.2	0.6	same as time period of Simons et al. (2007)
Jan 2010 - Dec 2011	25.3	-10.2	0.4	0.3	0.3	0.7	same as time period of this study
Jan 1998 - Dec 1999	24.2	-5.8	-4.6	0.7	0.5	1.1	
Jan 2000 - Dec 2001	20.6	-9.1	0.2	0.9	0.5	1.2	
Jan 2002 - 25 Dec 2004	23.1	-5.6	1.2	0.5	0.3	0.8	
Jan 2005 - 16 July 2006	27.5	-6.7	-4.3	0.6	0.4	1.0	
17 July 2006 - Dec 2007	30.7	-8.9	0.6	0.6	0.4	1.0	
Jan 2008 - Dec 2009	23.4	-9.8	4.3	0.4	0.3	0.8	
Jan 2010 - Dec 2011	25.2	-6.3	1.6	0.3	0.2	0.8	
Jan 2012 - Dec 2013	21.6	-6.8	-1.4	0.3	0.2	0.7	

Next, we fix velocities with respect to BAKO which is the most north site in our network, to see if there is any displacement due to the subduction. Figure 4.8b shows velocity data with respect to BAKO. These velocities (Table 4.1, Figure 4.8b) are derived by applying linear fitting to the time series that are subtracted from the time series of BAKO. In this plot, CLDO, CSGT, CPTN, CTVI, and CUJG show northward motion, indicating N-S shortening in southwest Java. These data imply the existence of interplate locking on the plate interface, which is investigated in detail in the following inversion analysis.

4.5.2. Vertical Component

In the vertical velocities shown in Figure 4.7 right and Table 4.1, all sites show uplift with a rate of 1.4 to 14 mm/yr, except ITB1 and CPTN. The vertical component of ITB1

shows a significant subsidence component with a rate of 4.5 mm/yr. We suspect this is affected by the vast land subsidence phenomena affecting some parts of Bandung Basin due to groundwater pumping. Abidin et al. (2008; 2013) found a heterogeneous subsidence distribution in the Bandung Basin with a subsidence rate of 80-230 mm/yr with GPS and InSAR data. Our ITB1 site is located within 1 km of a GPS site that was assumed to be subsidence-free in the study of Abidin et al. (2008; 2013). Thus ITB1 is likely located in a relatively stable region in the Bandung Basin. However, in our analysis, this site is not free from artificial subsidence. Thus we exclude ITB1 from further analysis to focus on the effect of interplate coupling alone.

The vertical component of CPTN shows almost no change, but it has a relative subsidence in regional uplift along the southwestern coast. Probably this is related to geothermal exploration in Cisolok where CPTN is located (e.g. GeothermEx, 2010).

4.6.3. Baseline change of horizontal component

Estimation of fault slip or slip deficit distribution on a plate interface strongly depends on the assumption of the reference site (e.g. Ito et al., 2000; Hashimoto et al., 2009). For the case of Java, the comparison of our velocity of BAKO with that of Simons et al. (2007) indicates that the current GPS velocity data may contain effects of rigid block rotation, which is independent of interplate locking. In order to avoid uncertainties regarding the reference frame, instead of analyzing velocity data with a fixed point, we use rates of baseline length changes for our analysis.

We calculate the baseline changes from the time series of 21 baselines from 10 cGPS sites: BAKO, CPMK, CLBG, CUJG, CSGT, CTVI, CPTN, CLDO, CUJK, CPSR by subtracting each daily time series in each baseline. Then we perform linear regression and calculate the uncertainty by the method of Zhang et al. (1997). From the result (Figure 4.11) we find north-south shortening in the middle of the network. The coastal shortening and uplift might reflect some amount of interseismic locking in the plate interface at its downdip limit

(e.g. Rosenau and Oncken, 2009). In contrast, the east part of the network shows north-south extension, possibly due to the postseismic effects as mentioned.

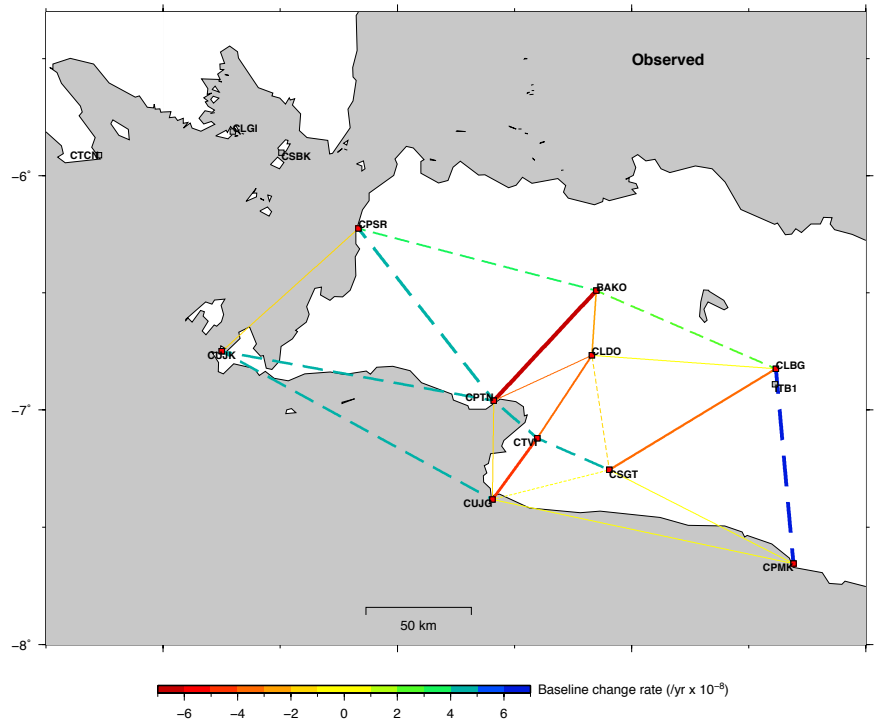

Figure 4.11. Observed baseline rates change from 3 years GPS data in 2008 to 2010. Rates are given in scale color. Solid and dash lines represent baseline shortening and extension, respectively. Gray squares are sites that are excluded in the inversion.

Chapter 5

Interplate Coupling off Western Java

5.1. Model Setup

We use the concept of interseismic deformation at subduction zones proposed by Savage (1983) to investigate the source of the observed crustal movements in western Java (Figure 5.1). That is, we interpret the observed surface deformation results from a distributed fault slip deficit or an excess on the plate boundary from steady plate subduction. In order to avoid uncertainties regarding the reference frame, we use rates of baseline length changes for our analysis, together with the absolute rate of vertical displacements in the ITRF2008 reference frame, and apply a geodetic inversion method formulated by Yabuki and Matsu'ura (1992).

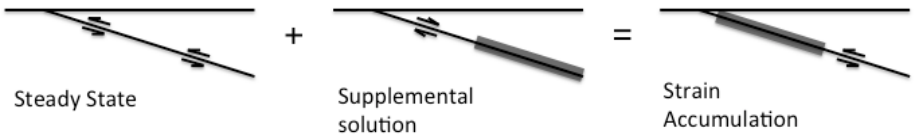

Figure 5.1. Conceptional plot of interseismic deformation at subduction zone by Savage (1983). A locked or no slip condition at an interface is indicated by thick gray line in the interface.

We assume all the surface deformation is caused by fault slip or slip deficit on the plate interface and the direction of fault slip to be parallel to the relative plate motion between the Sunda block and the Australia plate (Simons et al., 2007). Unknown parameters are the magnitude of slip deficit/excess rate on the plate interface. We use Okada's (1985) formulas to calculate the surface displacement response due to a fault dislocation on the plate interface assuming an isotropic elastic half space.

We presume a fault plane on the plate interface with a length of 500 km and a width of 225 km extending to the shallow portion (Figure 5.2 and 5.3). We divide the fault plane into 720 subfaults with a uniform size of 12.5 km x 12.5 km. We assume the dip angle of the plate

boundary based on model Slab 1.0 (Hayes et al., 2012), ranging from about 10° in the shallower part to 40° at the depth of 50 km. We assume the fault strike to be 297° based on the mechanism of the 2006 earthquake as determined by the USGS moment tensor solution. Then we assess the rake to be 284° (normal faulting with minor right-lateral strike slip) based on the plate convergence direction (N13°E) estimated from the motion of XMIS and COCO. This convergence direction is consistent with previous studies that estimated a convergence direction as N11°E to N14°E (e.g. Tregoning et al., 1994; Simons et al., 2007).

The surface displacement $\boldsymbol{u}$ in site *i* caused by a unit slip of a fault *k* on the plate interface can be expressed as:

$$\boldsymbol{u}_i(x) = \int_k \boldsymbol{G}_{ik}(x,\xi)\boldsymbol{m}_{pq}(\xi)d\xi \qquad (5.1)$$

Where $\boldsymbol{G}_{ik}$ is the Green`s tensor and $\boldsymbol{m}_{pq}$ is the moment tensor density.

We build the Green's function matrix by calculating the baseline change responses due to fault slip on the plate interface.

$$\boldsymbol{b}_i^j = \boldsymbol{G}_{ijk}\boldsymbol{a}_k + \boldsymbol{e}_i^j \qquad (5.2)$$

where $\boldsymbol{b}_i^j$ is the baseline change rate between site *i* and *j* for each baseline,

$$\boldsymbol{b}_i^j = \boldsymbol{u}_j - \boldsymbol{u}_i \qquad (5.3)$$

$\boldsymbol{G}_{ijk}$ is the Green's function representing the baseline change response due to unit displacement of a fault segment. $\boldsymbol{a}_k$ is model parameters, in this case, the slip deficit/excess at each subfault *k*. $\boldsymbol{e}_i^j$ is the observation error or the baseline change uncertainty, which is used to weight the data in the inversion.

We introduce a prior constraint that the slip distribution is spatially smooth considering that the fracture strength of actual rock is finite (Yabuki and Matsu'ura, 1992). Smoothness condition is define by

$$4k_{l,m} - k_{l,m-1} - k_{l-1,m} - k_{l+1,m} - k_{l,m+1} = 0 \qquad (5.4)$$

or

$$0 = \boldsymbol{H}\boldsymbol{a} \qquad (5.5)$$

Where $k_{l,m}$ is the number of subfaults, l in length direction and m in width direction, and **H** is the smoothing matrix to ensure that the slip distribution is spatially smooth. We set a free boundary condition along the trench, and a no-slip condition for other three boundaries of the rectangular source region.

We combine the observational equation (5.2) and the smoothness constraint (5.5) to construct a Bayes model with a hyperparameter, α^2, representing a relative weight between these two equations.

$$\boldsymbol{a} = (\boldsymbol{G}^T\boldsymbol{E}^{-1}\boldsymbol{G} + \alpha^2\boldsymbol{H})^{-1}\boldsymbol{G}^T\boldsymbol{E}^{-1}\boldsymbol{b} \quad (5.6)$$

where **E** is the variance-covariance matrix of observation error. **H** is obtained by applying a Laplacian matrix. The optimum hyperparameter is estimated based on the ABIC minimum criterion (Akaike, 1980).

$$ABIC(\alpha^2) = (N + P - M)\log s(\boldsymbol{a}) - P\log\alpha^2 + \log\|\boldsymbol{G}^T\boldsymbol{E}^{-1}\boldsymbol{G} + \alpha^2\boldsymbol{H}\| \quad (5.7)$$

with

$$s(\boldsymbol{a}) = (\boldsymbol{b} - \boldsymbol{G}\boldsymbol{a})^T\boldsymbol{E}^{-1}(\boldsymbol{b} - \boldsymbol{G}\boldsymbol{a}) + \alpha^2\boldsymbol{a}^T\boldsymbol{H}\boldsymbol{a} \quad (5.8)$$

where N is the number of observations, P is the rank of matrix **H** which in this case corresponds with the number of subfaults, and M is the number of model parameters. The covariance for the estimation of the model uncertainty is calculated by

$$C = \hat{\sigma}^2(\boldsymbol{G}^T\boldsymbol{E}^{-1}\boldsymbol{G} + \hat{\alpha}^2\boldsymbol{H})^{-1} \quad (5.9)$$

with

$$\hat{\sigma}^2 = s(\boldsymbol{a})/(N + P - M) \quad (5.10)$$

5.2. Spatial Resolution Test

To test the spatial resolution of the analysis, we conduct a checkerboard test (Figure 5.2 a-j). We divide the megathrust interface into rectangular patches and assign a synthetic slip deficit of 69 mm/yr (red), a synthetic slip excess of 70 mm/yr (blue), and no slip deficit/excess (white) as shown in Figure 5.2. We assume synthetic errors with the same values as the observation errors. We compute the theoretical uplift rates and baseline change

rates where we have observations. We invert these simulated data to estimate the distribution of slip deficit/excess and compare with the true distribution. Ten tests with different cases are shown in Figure 5.2 a-j.

The slip deficit/excess rate is reasonably resolved up to ~100 km from the coast, corresponding to the slab depth of 20-30 km, within a fault size until 62.5 km x 62.5 km (Figure 5.2 i). The model cannot resolve patches smaller than 62.5 km x 62.5 km (Figure 5.2 j). Resolution for the shallow part (depth < 20km) and the periphery of the source region is very limited although we may be able to distinguish the existence of a slip deficit in the shallow part by enlarging the fault size as shown in Figure 5.2 a, b, c, d, e, i.

In general, the resolution test shows that the appropriate spatial resolution for the middle part of the deeper section (30-70 km) is better than 62.5 km x 62.5 km, and for the shallow part (less than 30 km) is ~250 km in length and ~100 km in width.

5.3. Slip Deficit/excess distribution on the plate interface

Figure 5.3 shows the result of our estimation of the slip deficit/rate distribution based on the GPS baseline change rates and vertical components. The estimated slip deficit/excess rate ranges from -63 to 75 mm/yr, with uncertainty from 40 to 80 mm/yr. Positive and negative values (shown by red and blue colors in Figure 5.3, respectively) indicate slip deficit and slip excess, respectively. The result clearly shows a heterogeneous distribution of slip deficit/excess in both the strike and dip directions. Due to the limited number of GPS sites, the estimated error of the slip is rather large. However, we could obtain significant slip (slip magnitude larger than the estimation error) as is marked by thick black lines.

We identify two significant slip deficit patches. First, off Pangandaran, at the depth of 37 to 45 km with a slip deficit rate of 48 to 55 mm/yr. Second, between off Pelabuhan Ratu and Ujung Kulon from the shallow portion to the depth of ~43 km, with a slip deficit rate range from 48 to 73 mm/yr. These patches with significant slip deficit rates indicate the plate boundary south off Java is locked, even partially or temporarily, accumulating seismogenic stress.

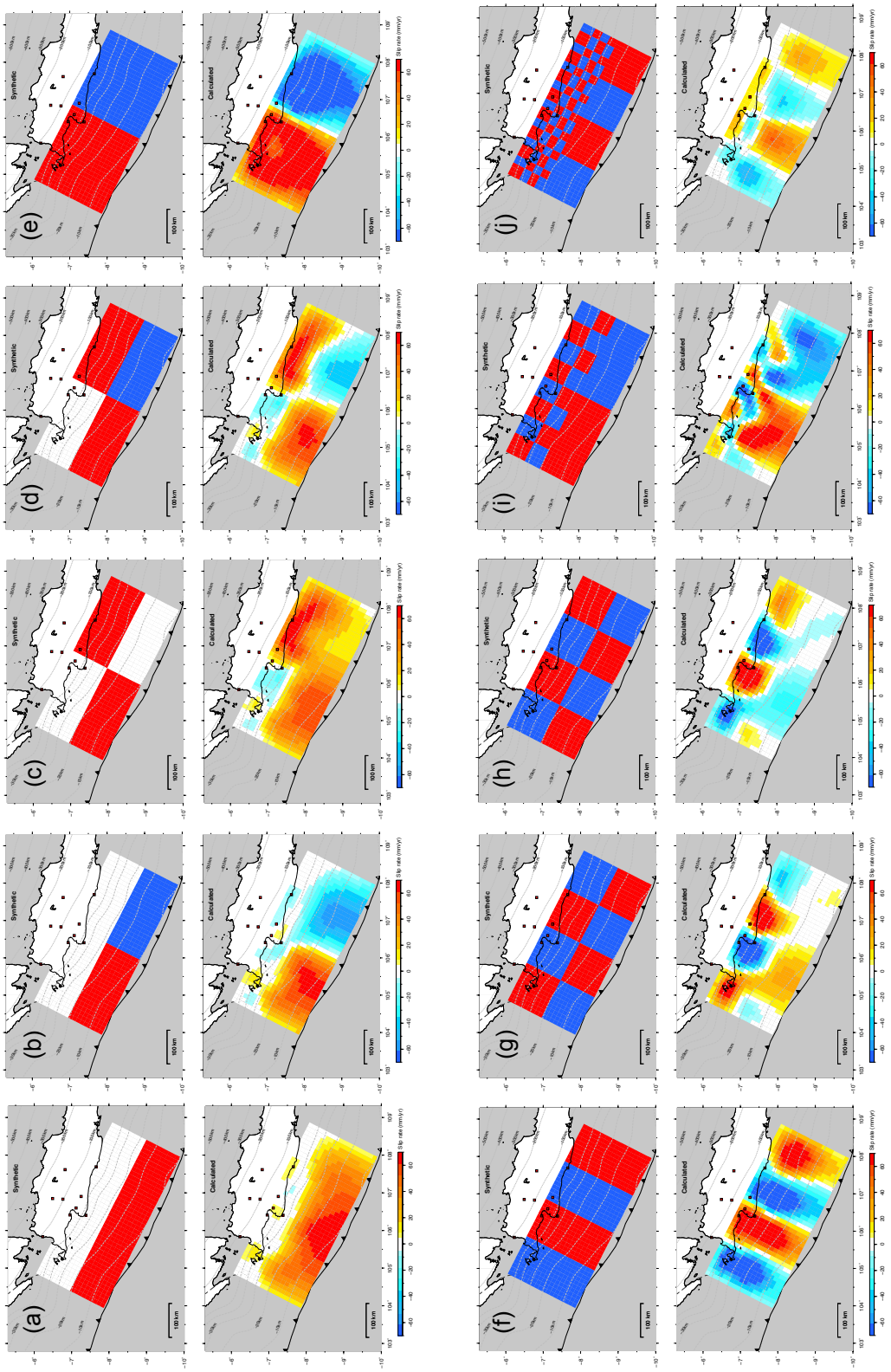

Figure 5.2.

Checkerboard test analysis for a synthetic fault rupture with different size of rectangle patches. Upper panel shows the synthetic input model, lower panel shows the results of inverting synthetic displacements from the input model. Red squares are the location of sites used in the inversion.

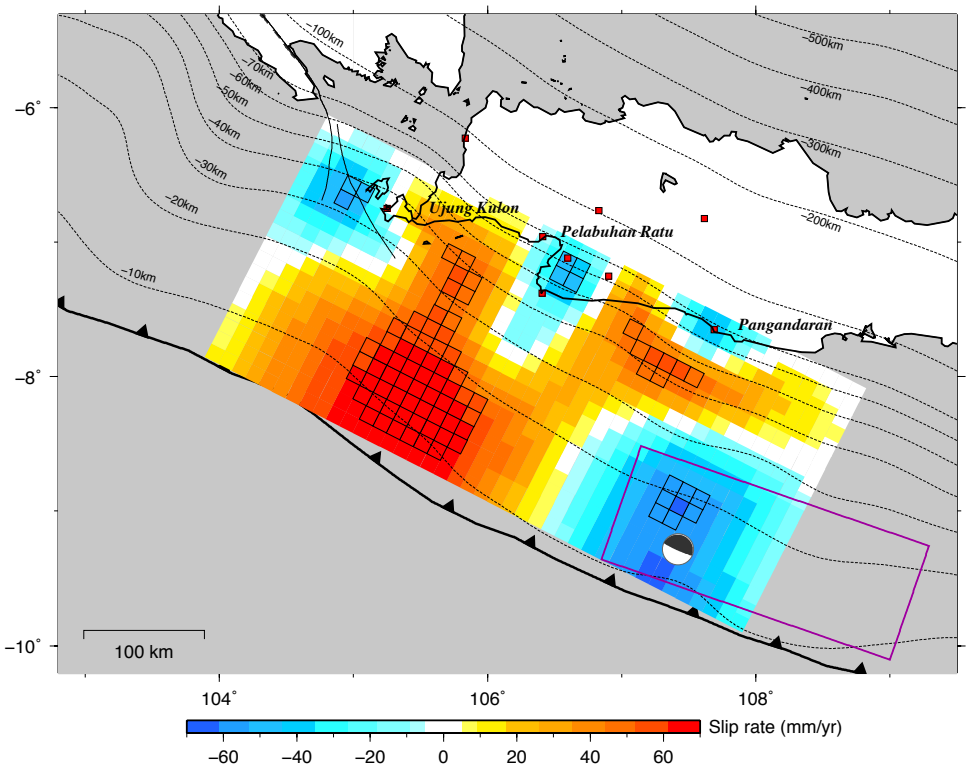

Figure 5.3. Result of interplate coupling model off the southwest coast of Java. Red squares are the location of sites used in the inversion. Dash line indicates the depth of the slab. Color scale indicates the estimated slip-deficit rate (red) and afterslip (blue). Black line rectangles are patches which estimation is larger than the error. Focal mechanism shows the focal mechanism of the 2006 M7.8 Java tsunami earthquake (NEIC catalogue). Magenta rectangle shows the coseismic rupture area redrawn from Hanifa et al. (2007).

On the other hand, there are also small patches of slip excess. First, off Pangandaran within the rupture area of the 2006 M7.8 Java earthquake, at the depth range of 15~20 km, with a slip excess rate of 57-61 mm/yr. Other slip excess patches are small ones below 30 km depth beneath Pelabuhan Ratu (44-47 mm/yr at 50-60 km depth) and west off Ujung Kulon (44-55 mm/yr at 30-35 km depth). These slip excess patches are smaller than 62 km, and may not be significant. On the other hand, there exists a large slip excess patch in the shallow portion. Although its significance is marginal based on our resolution test, it is clear that some amount of slip excess should exist to reproduce trench-ward motion at CPMK.

From the estimated fault slip deficit/excess distribution, we calculate the baseline change rate and the vertical displacement rate, as shown in Figure 5.4 and 5.5. We calculate the root-mean-square error (RMS) to check the degree of data fitting between observation and calculation, and obtain RMS of 0.7 mm/yr and 1.7 mm/yr for baseline change rate and vertical rate, respectively. From these results, although the RMS residual of 0.7 mm/yr is twice as large as the RMS observations error (0.3 mm/yr), the calculated baseline length change rate pattern reproduces the observed pattern well (Figure 5.4).

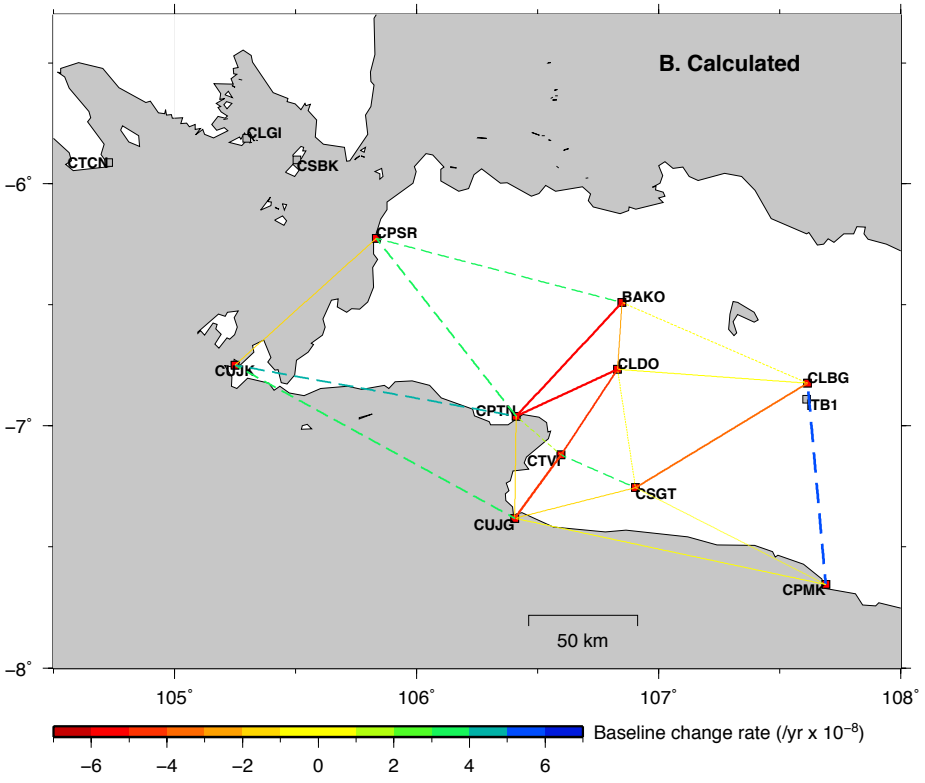

Figure 5.4. Calculated baseline rates change from inversion model. Rates are given in scale color. Solid and dash lines represent baseline shortening and extension, respectively. Gray squares are sites that are excluded in the inversion.

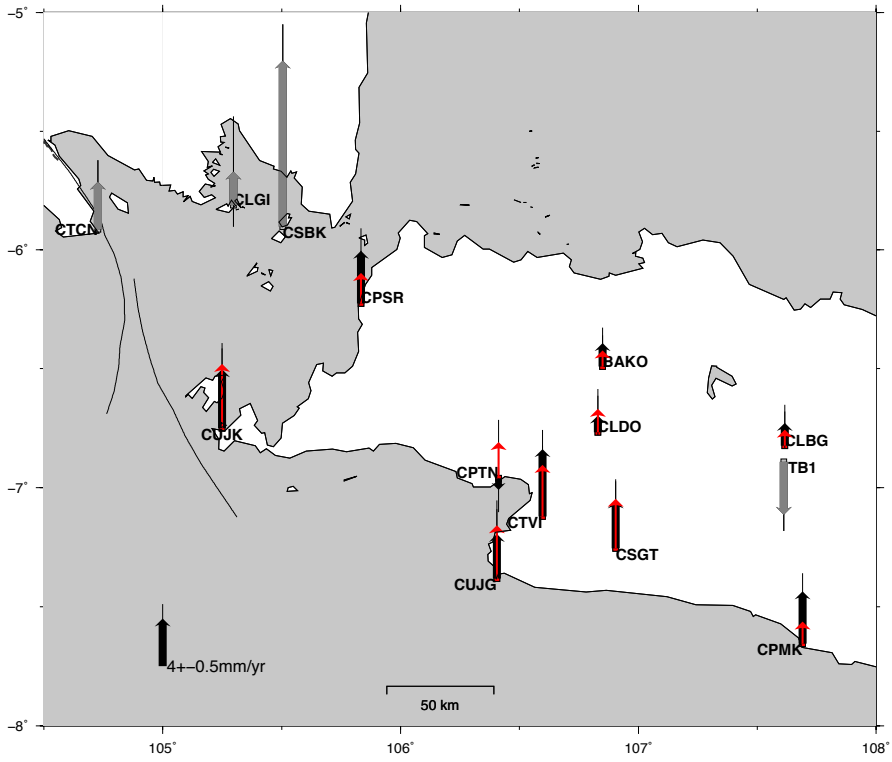

Figure 5.5. Observed (black) and calculated (red) vertical displacement. Gray vectors are the observations that are excluded in inversion

5.3.1. Slip Deficit off Ujung Kulon – Pelabuhan Ratu

We infer that the slip deficit off Ujung Kulon-Pelabuhan Ratu at the depth of 20 to 45 km is reliable, with a slip deficit rate from 48 to 56 mm/yr. The convergence rate between the Australia plate and the Sunda block is estimated to be 68 mm/yr (velocity of XMIS in the Sunda block reference frame). Considering the relative plate motion in this area, our results indicate that only a part of the plate interface may be partially locked south off western Java, with a coupling ratio in the significant patches of 70-82% in the depth range of 20 to 45 km. Though our estimation error is fairly large, it is apparent that the total seismic moment accumulation over this slip deficit region is smaller than that expected from the full interplate locking since the largest slip deficit rate is smaller than the relative plate motion. Hirai and Sagiya (2013) demonstrated that interplate locking at distributed locked patches as well as

deteriorated spatial resolution of the land-based geodetic network causes apparent partial locking. Similar situation may be responsible for this case.

As for the shallow part, Wang and Dixon (2004) pointed out that land-based GPS observations could not distinguish whether the up-dip portion is locked or creeping. In northeast Japan, for example, the dense extensive GPS network could not resolve the offshore locking status (Sagiya et al., 2011). Also in GPS studies in Sumatra that include sites in the outer island between the main island and the trench, the checkerboard-type studies illustrated low resolution in this very shallow area (e.g. Hill et al., 2012; Chlieh et al. 2008; Hsu et al., 2006). Although our model cannot resolve detailed spatial distribution of slip deficit, we are still capable of detecting signal of slip deficit within large patch size (Figure 5.2 a, b, c, d, e, i). We point out significant amount of slip deficit can exist in the shallow portion south off Java.

An integrated seismic moment accumulation rate over the slip deficit patches off Ujung Kulon-Pelabuhan Ratu amounts to 5.4 x 10^{19} Nm/yr during the period from 2008 to 2010 (Figure 5.4). This area is characterized by absence of earthquake with magnitude larger than 5 during the instrumental period of USGS catalogue. There is also no report of historical megathrust earthquake in this area. If we assume that the plate interface off south western Java has been locked at the current status for the last 300 years, during which no megathrust earthquake was reported, then the accumulated seismic moment amounts as much as 1.6 x 10^{22} Nm, equivalent to an M_w 8.7 earthquake.

Two alternative interpretations are possible for this result. If we assume that the interplate coupling is a steady feature during the last 300 years, M8.7 is a minimum estimate since the last megathrust earthquake could be earlier. Another possibility is that repeated slow slips release accumulated slip deficit without causing great earthquakes as was observed in Boso Peninsula, Japan (e.g. Sagiya, 2004) or in Guerrero, Mexico (e.g. Kostglodov et al., 2003). In order to distinguish these alternatives, we need observation data for a longer time period.

5.3.2. Slip Deficit off Pangandaran

At the depth of 37 to 45 km off Pangandaran, below the rupture area of the 2006 M7.8 earthquake, we obtain a slip deficit with a rate of 48 to 55 mm/yr. It suggests a partial locking with coupling ratio of 75-80% of the plate convergence, with integrated seismic moment in the slip deficit patch off Pangandaran of 1.3 x 10^{19} Nm/yr. One may be concerned about a possible trade off between the shallow slip excess and the deeper slip deficit. Existence of the slip deficit patch at depth is supported by the coastal uplift observed at CTVI, CSGT, CUJG, and CPMK. If the situation has continued for 300 years, the accumulated seismic moment amounts to 3.9 x 10^{21} Nm (Mw 8.3).

5.3.3. Afterslip off Pangandaran

The estimated slip excess off Pangandaran is located in the shallow portion above 30 km depth (Figure 5.3), where the detailed slip distribution can not be resolved by the on-land GPS. Based on the resolution test (Figure 5.2), we assured that there is an ongoing afterslip of the 2006 M7.8 earthquake, 4.5 years after the mainshock. The southward motion of CPMK is the supporting evidence of this inference (Figure 4.9b). The trenchward motion with decreasing slip rate in the first two years after the 2006 earthquake (Kato et al., 2007; Abidin et al., 2009) is also a supporting evidence of afterslip.

However, we cannot resolve whether the afterslip occurs inside the mainshock rupture area or in the adjacent downdip area. We should also note that this afterslip could extend further to the east because of the absence of GPS data to the east of CPMK. According to our calculation, the calculated afterslip yield a seismic moment of 2.5 x 10^{19} Nm/yr. Theoretical displacement rate at BAKO by the calculated afterslip is 0.9 mm/yr in N186ºE, about ~20% of our estimated velocity (5.4±0.3 mm/yr in N198ºE). Thus the afterslip effect on the velocity of BAKO is expected to be minor.

Chapter 6

Numerical Modeling of the 2006 Java Tsunami Earthquake

6.1. Introduction

On July 17, 2006, at 08:24 UTC or 15:24 in local time, a magnitude 7.8 earthquake occurred off the coast of Pangandaran, South of Java Island, Indonesia. The earthquake involved thrust faulting in the Java trench and excited a deadly tsunami of 3-8 meters height that inundated the southern coast of Java. This is a very rare event, especially because previous research showed that the Java Trench is aseismic subduction (Newcomb and McCann, 1987). Ammon et al. (2006), Kato et al. (2007), and Fujii and Satake (2006) concluded that this event was a tsunami earthquake as it generated more massive tsunami than expected from the seismic waves (Kanamori, 1972).

The characteristics of tsunami earthquake are summarized as follows.

1. Slow rupture process (Kanamori, 1972).
2. Long rupture duration, about 100 sec. from seismological studies. This is investigated from the 1992 Nicaragua which is the first tsunami earthquake recorded on modern broadband seismic instruments (Kanamori and Kikuchi, 1993).
3. Have similar seismic waveforms, which are different from normal (tsunamigenic) earthquakes (Kanamori, 2006).
4. Occur at the plate boundaries where the plate coupling is weak (Ruff and Kanamori, 1980).
5. Source area is located within shallow sedimentary layers (Fukao, 1979; Okal, 1988] or on the plate boundary near the trenches (Satake and Tanioka, 1999).

Tsunami earthquakes are rare events and only 11 examples of tsunami earthquake events are known so far since the late 19th century.

. 1896 Meiji Sanriku Tsunami Earthquake (Kanamori, 1972; Tanioka and Satake, 1996)
. 1946 Aleutian Tsunami Earthquake (Kanamori, 1972; Lopez and Okal, 2006)
. 1960 Peru Tsunami Earthquake (Pelayo and Wiens, 1992)
. 1963 Kuriles Tsunami Earthquake (Fukao, 1979; Okal and Newman, 2001; Pelayo and Wiens, 1992)
. 1975 Kuriles Tsunami Earthquake (Fukao, 1979, Pelayo and Wiens, 1992)
. 1992 Nicaragua Tsunami Earthquake (Kanamori and Kikuchi, 1993, Satake, 1994)
. 1992 Flores Tsunami Earthquake (Beckers and Lay, 1995)
. 1994 Java Tsunami Earthquake (Abercrombie et al., 2001; Polet and Kanamori, 2000; Polet and Thio, 2003; Sella et a;., 2002(
. 1996 Peru Tsunami Earthquake (Okal and Newman, 2001)
. 1998 Papua New Guinea Tsunami Earthquake (Satake and Tanioka, 2003)
. 2006 Java Tsunami Earthquake (Ammon et al., 2006; Fujii and Satake, 2006; Kato et al., 2007)

Very complicated plate-convergences consisting of subduction, collision, back-arc thrusting and back-arc are ongoing in and around the Indonesia. As the result of this complexity, the region is considered as one of the most tectonically active areas in the world (Latief et al., 2000). In Indonesia, at least 460 earthquakes of M>4.0 occur every year (Ibrahim et al., 1989). Based on data compiled during the period 1600-1999, 105 tsunamis have been recorded in Indonesia (Latief et al., 2000). 95 events (90%) of them were caused by earthquakes in shallow region at subduction and plate boundaries, 9 (8%) by volcano eruptions, and 1 (1%) by a landslide (Latief et al., 2000).

Oblique subduction of the India-Australian plates beneath the Sumatra has a rate of 5.6 cm/yr (Sella et al, 2002). Subduction rate off West Java where the 17 July 2006 earthquake occurred is ~6.4 cm/yr (Sella et al, 2002), and increase to further east subduction rate of ~6.9 cm/yr off East Java (Figure 6.1). The age of the oceanic floor increase from western Sumatra

to eastern Java, with younger plate of 60 Ma subduct beneath Sumatra, and older oceanic crust of 140 Ma subduct beneath Java.

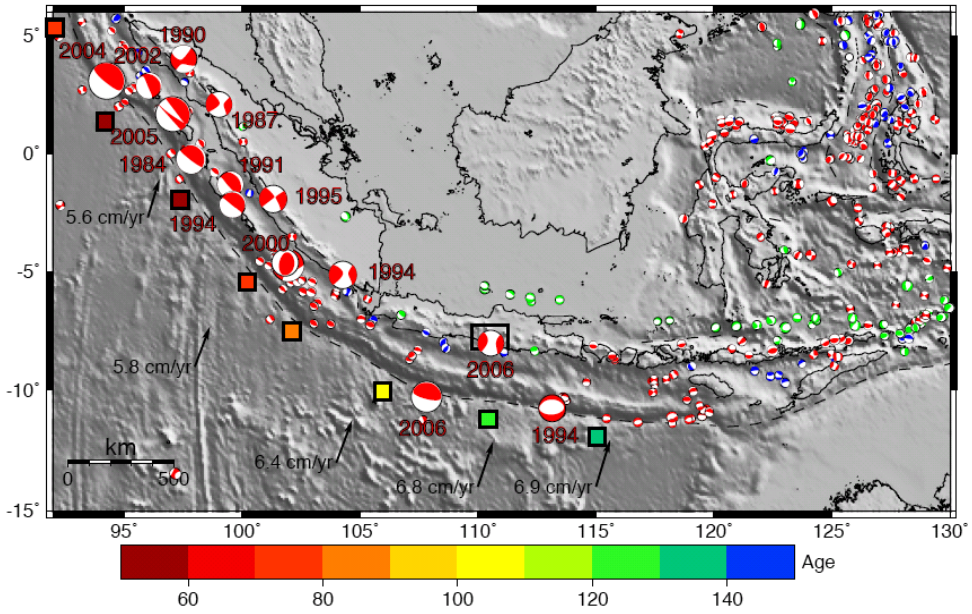

Figure 6.1. Tectonic setting and historical earthquake along Sunda trench in Indonesia. The hypocenters of the earthquakes are by USGS and focal mechanisms are by Harvard CMT solution. Convergent rates of the India-Austrian plate are by Sella et al. (2002). Ages of ocean bottom are shown as the colored squares.

Newcomb and McCann (1987) reviewed the seismic history and seismotectonics of the Sunda Arc. They concluded that there are more frequent and larger earthquakes along Sumatra, indicating a significant seismic coupling. The entire length of the plate boundary has a potential to produce great thrust earthquakes. Conversley, less frequent and smaller events occur along Java where subduction of older seafloor takes place relatively aseismically. However, there are needs for further seismological investigation along Java after 3 deadly earthquakes since 1987. The first one was the M7.7 Java tsunami earthquake on May 1994. Other two earthquakes of M6.4 and M7.8 hit Java in 2006, the Yogyakarta earthquake in May, and Pangandaran tsunami earthquake in July.

We describe the result of the 2006 Java numerical modeling using finite difference to understand the mechanism of the 2006 Java tsunami earthquake. The numerical modeling used several scenarios to find the closest fair agreement with the continuous GPS observation and observed tsunami run-up heights.

6.2. Java 2006 Tsunami Earthquake

The earthquake was centered at 9.295°S, 107.347°E, with a depth of 6 km below the mean sea level (USGS) (Figure 6.2). The source mechanism was a low angle thrust indicating the event occurred on the plate interface between the Australia and the Sunda plates along the Java trench (http://www.globalcmt.org/). The strike, dip and rake angles of the fault slip are estimated 287˚, 10˚, and 95˚, respectively. The earthquake occurred on the shallow part of the plate boundary, about 250 km north of the Java trench.

Based on the report of the Indonesia Agency for Meteorology, Climatology, and Geophysic (BMKG), the tsunami inundated the southern Java coastline by about 236 meters on average. The tsunami waves destroyed around 90 houses, 62 hotels, 5 office buildings, 56 cars, 97 motorbikes, 190 boats and 29 traditional transportations. At least 378 deaths occurred, 272 injured, and 77 are missing. The area destruction can be seen clearly by the remote sensing image. Center for Remote Imaging, Sensing and Processing of National University of Singapore had provided Satellite image of Spot in the Java tsunami area.

Tsunami run-up height was measured by Geodesy Research Group of Bandung Institute of Technology under cooperation with The University of Tokyo. BMKG also conducted the tsunami run-up height measurement separately. The run-up height was about 3 to 8 meters along the coast from Pameugpeuk to Kebumen (Table 6.1, Figure 6.2), while the tsunami maximum height measured by International Tsunami Survey Team (ITST) was 21 meter in Nusa Kambangan Islands (Fritz et al., 2007).

Kato et al. (2007) concluded this event as tsunami earthquake based on their observation of run-up height, GPS observation, and numerical modeling. Their GPS results suggested that the motion of the Java Island is due ESE, almost perpendicular to the direction of the plate

subduction, and does not show any influence of the plate convergence of the Australian plate that subducts underneath the Java Island. They inferred plate coupling at the subducting plate interface must be very weak, that is one characteristic of tsunami earthquakes potential zone.

They also mentioned that people along the coast felt weak ground shaking only, but suffered from unexpectedly high tsunami. The considerably weaker ground shaking than expected from its magnitude (Mw7.8) strongly indicates that the slip velocity on the fault would be slow enough not to radiate much seismic wave. The slow rupture velocity was estimated to be 1 km/s (Mori and Park, 2006; Ammon et al., 2006), much slower than normal earthquakes that usually show rupture speed of 2-3km/s.

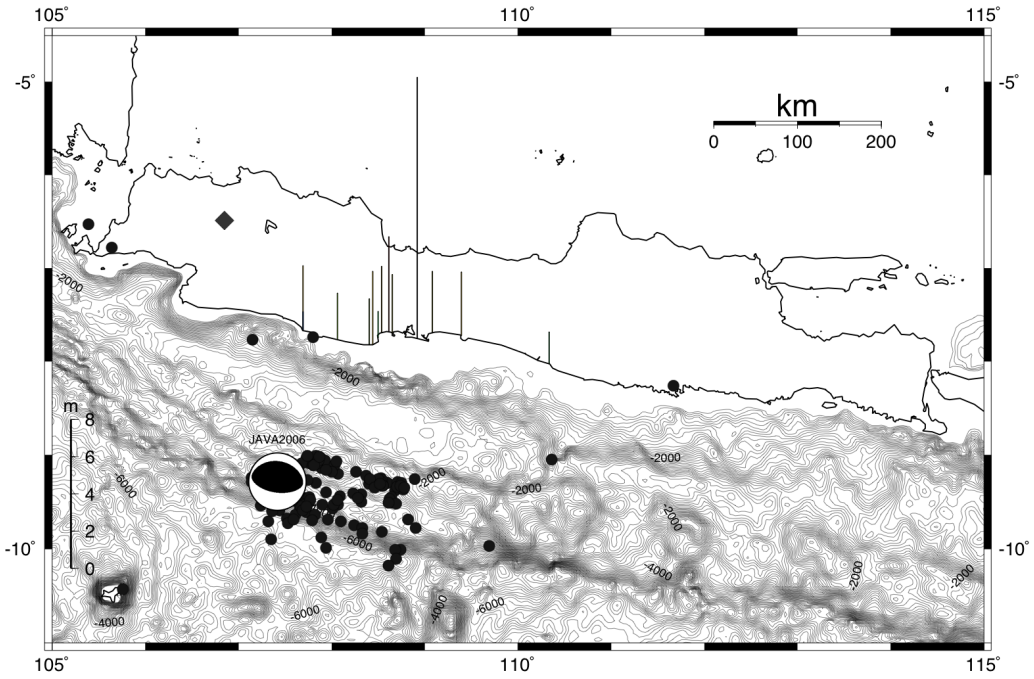

Figure 6.2. Hypocenter distribution of main shock and aftershocks of July 2006 Java Earthquake in the period within 2 days after the mainshock by USGS. Focal mechanism of the main shock by Harvard CMT solution. Observed tsunami heights by Geodesy Research Division of ITB and BMG are also shown.

Based on numerical simulation, Koshimura (2006) suggests that if the earthquake was on a low angle thrust fault, the simulated tsunami height have a maximum of 3.5 m in the west of Pangandaran area. whereas simulated height from high angle faults generates about 3 m of maximum tsunami. In both case, their tsunami simulation does not reach to east of Cilacap. Latief et al. (2006) also have simulated the tsunami numerical modeling and get tsunami height of 3-4 m along the coast from Pameungpeuk to Kebumen.

Table 6.1. Observed Run Up Tsunami Height

Point	Data Source	Long	Lat	Heights
				Observed (m)
1	ITB	107.690722	-7.668306	5.2
2	ITB	108.059917	-7.764667	3.74
3	ITB	108.402750	-7.815556	3.67
4	ITB	108.442250	-7.819500	5.9
5	ITB	108.497583	-7.746833	2.12
6	ITB	108.535944	-7.692194	5.34
7	ITB	108.612028	-7.683667	7.67
8	ITB	108.651667	-7.693778	4.69
Ngantik Kisik	BMG	109.079970	-7.689440	4.92
Ayah Kebumen	BMG	109.394100	-7.724510	5.12
Parangtritis	BMG	110.334690	-8.025970	2.57
Benoa		115.216667	-8.766667	0.243

Ammon et al. (2006) stated that the size of the 2006 Java earthquake varies significantly with seismic wave frequency band analyzed: analysis of very long-period signals of around 300-500+ seconds indicates a seismic moment of 6.7 x 10^{20} Nm (Mw = 7.8), while the surface wave magnitude is M_S (~20 s) = 7.2, the body-wave magnitude is m_b (~1 s) = 6.2, and shaking intensities (3-10 Hz) were ≤ MMIV. According to them, the rupture time of the 2006 Java Earthquake was abnormally long, continued for about 185 seconds, and propagated slowly at about 1.0-1.5 km/s. These attributes are common with other tsunami earthquakes, such as the 1994 Mw 7.8 Java earthquake, that occured about 600 km east of the 2006 event. The 1994 event had similar strong tsunami excitation with 15 m maximum run-up height and aftershock sequences dominated by normal faulting. They inferred that the 2006 Java

earthquake is likely to occure in weak material properties related to subduction sediment or the presence of fluids.

Fujii and Satake (2006) have inverted tsunami waveforms and inferred that the tsunami source was about 200 km long. In their model, most of the slip occurred on shallow part of the fault, with largest slip of about 2.5 m located about 150 km east of the epicenter. Their estimated slip distribution yields a total seismic moment of 7.0×10^{20} Nm (Mw = 7.8).

Cummins et al. (2006) have constrained the slip distribution of the 2006 Java earthquake using long-period surface waves. Their model obtained a maximum slip of 2 meters, with concentration of slip in the shallow part of the fault plan. They reconciled this slip model with GPS and tide gauge data. GPS measurements of coseismic displacement at Christmas Island, Australia and the IGS station BAKO on Java both suggest about 6 mm of horizontal displacement, which is about half that predicted from their slip model. They suggest that this inconsistency is because the usage of surface waves filtered to pass periods of 300-80 sec is insufficient to resolve the total slip. About this inconsistency, we will propose an alternative interpretation in discussion.

6.3. GPS PPP continuous observation

Continuous GPS station, the BAKO IGS station-in West Java, was being operated during the Java 2006 earthquake. We computed horizontal displacement from this continuous GPS station using Bernese GPS software version 5.0 with the PPP (Precise Point Positioning) method. The results of GPS PPP data processing at BAKO show coseismic displacement due to the 2006 Java tsunami earthquake as small as 4 mm in the southward direction (Figure 6.3).

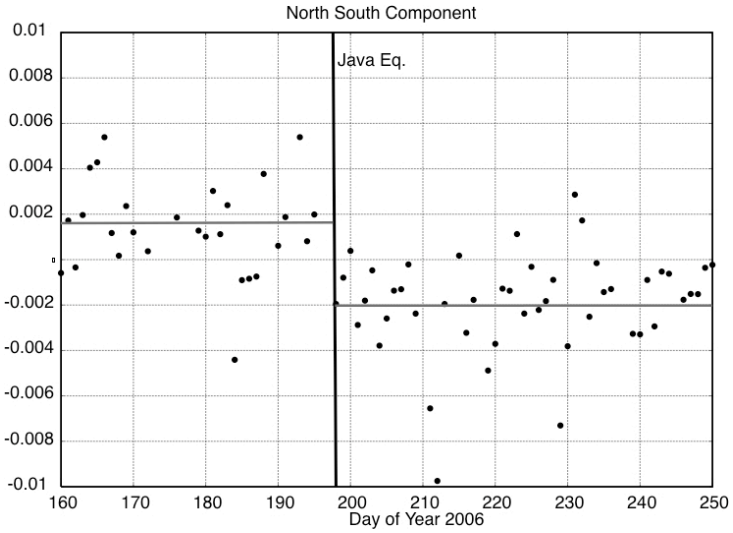

Figure 6.3. GPS PPP result of BAKO-IGS station in year 2006

6.4. Tsunami Modeling Method

We conducted model calculation of crustal deformation and tsunami propagation assuming various fault models to study earthquake source process to check if they satisfy our observations of GPS and tsunami height. We do linear and non-linear tsunami modeling of tsunami propagation using a finite difference code by Nakamura (2006). Seafloor displacement as the initial condition of tsunami propagation was computed using Okada (1985) formula.

In the simulation of tsunami propagation, we can apply the long wave (shallow water) approximation when the tsunami wavelength is much larger than the water depth and the tsunami height is negligible compared with the water depth. The wavelength of tsunami depends on the rupture length, which must be 20 times as large as the water depth to satisfy such a condition. In case of the 2006 Java tsunami, the water depth is 6 km and the rupture length is about 200 km (Ammon et al., 2006), more than 30 times larger than the water depth so that the long wave approximation is validated.

Under the long wave approximation, velocity of tsunami propagation is expressed as follows.

$$v = \sqrt{g.d} \tag{6.1}$$

where v is propagation velocity in m/sec, **g** is the gravitational acceleration (9.8 m/sec^2), and **d** is the water depth in meters. Tsunami wave propagates faster in deep sea, with a small wave height. Approaching shallower area, propagation becomes slower, then the wavelength decreases and the wave height is amplified. Relation between the water depth and the wave height is illustrated in Figure 6.4.

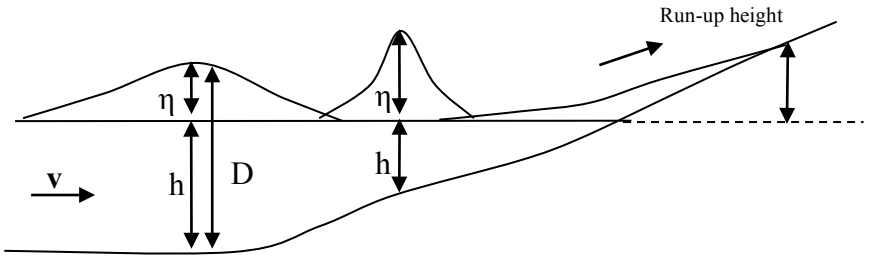

Figure 6.4. Relation between water depth and wave height (Nakamura, 2006)

For water deeper than 50 meters, we can assume that the tsunami amplitude is much smaller than the water depth, and then the linear equation under the long wave approximation can be applied (Satake, 1991)

$$du/dt = -g\nabla h \tag{6.2}$$

For water depth less than 50 meters (shallow water), non-linear effects have to be properly taken into account and the equation of tsunami propagation can be written as (Satake, 1991):

$$du/dt + (u.\nabla)u = -g\nabla h \tag{6.3}$$

$$v = \sqrt{\left(\frac{g\lambda}{2\pi}\right)\left(\tanh\left(\frac{2\pi d}{\lambda}\right)\right)} \tag{6.4}$$

From the difference in water height, the flux change is computed using the momentum equation. Then from flux change, difference in water height is calculated again using mass conservation equation, and repeated. This is the equation of motion and continuity of tsunami

wave propagation used in this study. Mass conservation equation is written as (Nakamura, 2006):

$$\frac{\partial \eta}{\partial t} + \frac{\partial M}{\partial x} + \frac{\partial N}{\partial y} = 0 \tag{6.5}$$

and the momentum equation is written as (Nakamura, 2006):

$$\frac{\partial M}{\partial t} + \frac{\partial}{\partial x}\left(\frac{M^2}{D}\right) + \frac{\partial}{\partial y}\left(\frac{MN}{D}\right) + gD\frac{\partial \eta}{\partial x} + \frac{gn^2}{D^{7/3}} M\sqrt{M^2 + N^2} = 0 \tag{6.6}$$

$$\frac{\partial N}{\partial t} + \frac{\partial}{\partial x}\left(\frac{MN}{D}\right) + \frac{\partial}{\partial y}\left(\frac{N^2}{D}\right) + gD\frac{\partial \eta}{\partial y} + \frac{gn^2}{D^{7/3}} N\sqrt{M^2 + N^2} = 0$$

η is vertical displacement of water surface above the still water level, **D** is total water depth (D= η + h), **g** is gravitational acceleration, **x** and **y** are horizontal coordinates, **t** is time, **M** and **N** are discharge fluxes in the **x-** and **y-** directions respectively, and **n** is coefficient of bottom friction.

If η /h is close to zero (wave height is very small compare to water depth), nonlinear term is negligible. The momentum equation then become:

$$\frac{\partial M}{\partial t} + gD\frac{\partial \eta}{\partial x} = 0 \tag{6.7}$$

$$\frac{\partial N}{\partial t} + gD\frac{\partial \eta}{\partial y} = 0$$

We use ETOPO2 (http://www.ngdc.noaa.gov/mgg/global/relief/ETOPO2/ ETOPO2v2-2006) for 2-minute grid bathymetric data and GEBCO

(http://www.ngdc.noaa.gov/mgg/gebco/grid/1mingrid.html) for 1-minute grid bathymetric data.

Initial condition of the tsunami propagation is given by coseismic displacement calculated with Okada (1985) formula. We tested various fault parameters compiled from the information of USGS, BMKG, Ammon et al. (2006) and Fujii and Satake (2006) as shown in Table 6.2 to check if the generated tsunami reproduces the run-up height observation. On the other hand, based on the same fault parameters, we also calculate displacement at BAKO GPS station to compare with the observation. Fault location is assumed to be the same for all the cases based on NEIC moment tensor solution of USGS which is 9.295°S, 107.347°E. Some of the model parameters tested are given in Table 6.2.

For the model 1, we tested fault parameters based on USGS-NEIC moment tensor solution, with ETOPO-2 as bathymetric data. The fault area is estimated based on aftershock distribution by USGS, with a rupture length of about 200km and the width of 40 km. The slip is computed using the definition of seismic moment:

$$M_0 = \mu DS \tag{6.8}$$

Mo is seismic moment, **μ** is rigidity, **D** is rupture area in square km, and **S** is slip in meter. We use rigidity value of 10 GPa based on Ammon et al. (2006). This small rigidity is consistent with sedimentary material within the accretionary wedge. The result showed a maximum wave height of 0.531 meters.

For the model 2, we revised the value of seismic moment. We computed the seismic moment from moment magnitude

$$\log M_0 = 1.5 M_w + 9.1 \tag{6.9}$$

We got Mw of 4.5 x 10^{20} Nm and so the slip is estimated as 5.6 meters. The result gave the maximum wave height of 2.928 meters.

The model 3 uses the parameter from Fujii and Satake (2006). They did inversion calculation of tsunami waveforms from tide gauge data to get the tsunami source. They

suggested a rupture length of 200 km, a slip of 2.5 meter, and a seismic moment of 6.0 x 10^{20} (equivalent to Mw 7.8). They assumed the rigidity of 3.0 x 10^{10} N/m^2. The result gave a maximum wave height of 1.386 meters. This result is in fair agreement with the tsunami waveforms recorded at tide gauges, but much smaller than the coastal observation.

For the next model, we used the source information by Ammon et al. (2006). They suggested a seismic moment of 6.7 x 10^{20}. The variable slip ranges 8-15 m on the fault plane, the fault width of 75 km. They assumed the rigidity of 1.0 x 10^{10} N/m^2.

Tabel 6.2. Fault models and calculation results.

Column1	Unit	Model 1	Model 2	Model 3	Model 4	Model 9	Model 11
reference		USGS modified	USGS	Fujii and Satake (2006)	Ammon et al. (2006)	Ammon et al. (2006) max slip	Ammon et al. (2006) avr slip
Mw		7.2	7.7	7.8	7.8	8.1	7.9
Mo		8.1E+19	4.5E+20	6E+20	6.7E+20	2.1E+21	1.E+21
Rigidity	Pa	1.0E+10	1.0E+10	3.0E+10	1.0E+10	1.0E+10	1.0E+10
Strike	degree	297	297	289	289	289	289
dip	degree	6	6	10	10	10	10
Rake	degree	93	93	95	95	95	95
Depth	km	6	6	6	6	8	8
Slip	m	1.01	5.63	2.50	8.38	15.00	12.00
Length	km	200	200	200	200	200	200
Width	km	40	40	40	40	70	70
Max Tsunami	m	0.531	2.928	1.386	4.596	8.665	6.2907
BAKO displacement	mm	5	30	13	40	83	25
Tsunami height RMS	m	4.6	4.6	4.5	4.3	3.2	3.4

For the model 4, we use an average slip over the entire fault plane (200km x 40km) based on Ammon et al. (2006). We computed the slip as 8.3 meters. The result gave a maximum wave height of 4.596 meters.

For the model 5, we modified the rupture width to 70 km. The result gave the maximum wave height as 5.02 meters. The chosen rupture area of 200x70 km covers all the aftershock distribution, so that we keep this rupture area in the following models.

In the model 6, we try the maximum slip of 15 m from Ammon et al.[2], and get the maximum wave height of 8.832 meters. In the model 7, we modified the fault depth to 8 km,

and used the slip of 15 meters. Model 7 produces the maximum tsunami height of 8.997m from the result of Ammon et al. (2006). It seems fault depth of 6 km does not give significant difference, but the increase of slip from 8 to 15 m causes significant difference. Model 7 reproduce the pattern of the tsunami wave shown in Figure 6.2 fairly well.

We compared the usage of 2-minute data of ETOPO with 1-minute data grid of GEBCO. The maximum parameter based on Ammon et al. (2006) is 15 meters of slip, rupture of 200x70 km, depth 8 meters generate a maximum wave of 8.665 meters with maximum height in the coastline of 5.821 meters using nonlinear equation (model 9).

In model 11, we try the average slip of 12m based on Ammon et al. (2006) with 1-minute grid bathymetry data. We gained tsunami maximum height of 6.291 meter near the coast and displacement in BAKO of 25 mm. Illustration of result is given in Figure 6.5 for model 11.

The use of 1-minute grid gives much improvement than 2-minute grid. This is fair with the result of Satake (1995).

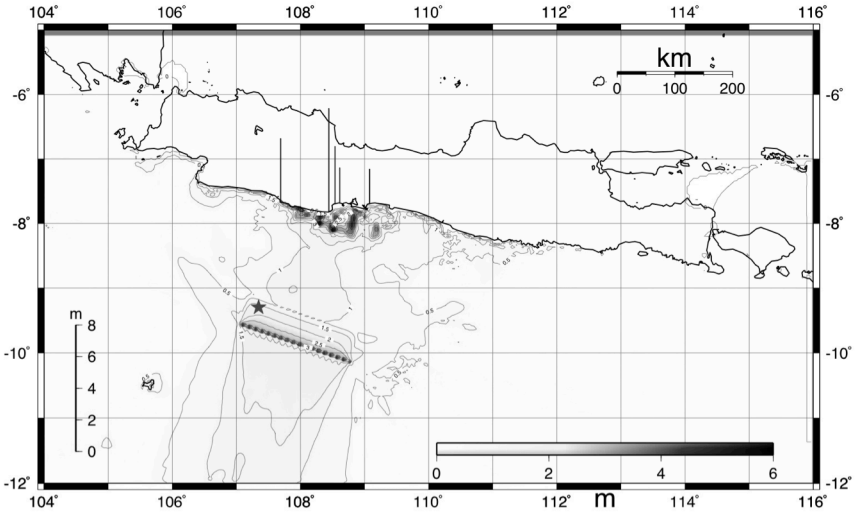

Figure 6.5. Tsunami height of model 11, our preferred model.

In summary of tsunami simulation, we conclude that the best model for the 2006 Java earthquake we obtained so far is model 11, assuming a fault area of 200km x 70km, an average fault slip of 12m, with the tsunami propagation calculated with 1-minute grid

bathymetry data. This model reproduces the coastal tsunami observation, but the GPS displacement at BAKO is calculated as 25 mm using Okada (1985) formula. This discrepancy will be interpreted in the discussion.

6.5. Discussion

The 2006 Java earthquake occurred near the Java trench where soft sediments form accretionary wedge. So a small rigidity is appropriate for the source region. Seismologically estimated fault model (model 1) satisfied the GPS data but the calculated tsunami height was too small. On the other hand, in order to reproduce the observed tsunami height, seismic moment becomes as large as 2.1×10^{21} Nm, which is equivalent to Mw 8.1 (model 9). However, if we use the Okada's formula, the same fault model results in a southward displacement of about 83 mm at BAKO station in west Java, which is far too larger than the observation data of 4 mm. Model 11 reproduces 6 m tsunami height with displacement in BAKO of 25 mm, equivalent with moment magnitude of Mw= 8.1 and seismic moment of 1.7×10^{21} Nm. Comparing the result of the models with the tsunami height and GPS displacement in BAKO station, the most suitable model is model 11, with small RMS of tsunami height compare with tsunami run up height data, with displacement of 25 mm at BAKO.

This discrepancy can be attributed to two effects. First, if the source process was accompanied by splay faulting, vertical displacement of the sea floor becomes larger and caused massive tsunami (Figure 6.6). Another possibility is an effect of structural heterogeneity.

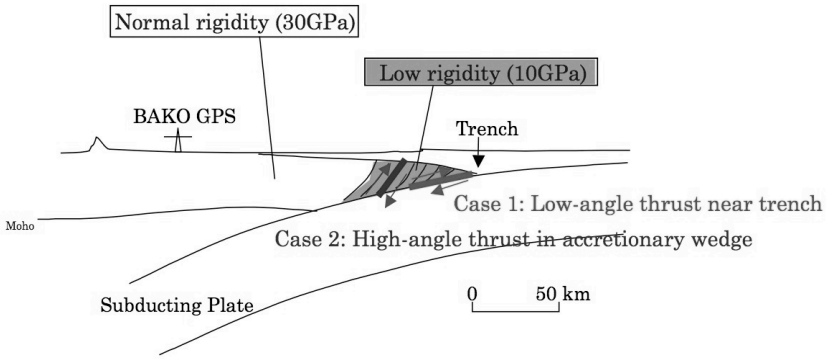

Figure 6.6. Illustration of case possibility of the 2006 Java Earthquake mechanism

The source region of the 2006 Java earthquake is near trench. A rigidity of the source region should be as low as 10 GPa (Ammon et al., 2006). On the other hand, if we look at the source region from BAKO GPS station, we do not know the rigidity of the source region, but we can only infer a mechanical effect by the seismic source, which can be represented by moment tensor density

$$u_i(x,t) = \int_{-\infty}^{t} d\tau \int_{v} \frac{\partial}{\partial \xi_q} G_{ip}(x,t;\xi,\tau) m_{pq}(\xi,\tau) d\xi \tag{6.10}$$

Here, $\mathbf{m_{pq}}$ is moment tensor density, containing rigidity of the source region, and $\mathbf{G_{ip}}$ is Green`s tensor, surface displacement response to a unit force in the p-th direction at the source, containing rigidity of the medium.

In Okada`s formula, , displacements are calculated under the semi-infinite elastic body rigidity of the surrounding medium is assumed to be the same and cancel out each other. In the case of the Java earthquake, rigidity around epicenter and at BAKO should be different. However for the calculation of a far-field static displacement at BAKO, we need to assume

the same amount of seismic moment ($1.7x10^{21}$Nm) with a normal rigidity (30GPa). As a result, we have to reduce the slip amount in accordance with the ratio between two rigidities. If we assume the ratio to be 1/3, displacement is calculated 8 mm at BAKO, which is more consistent with the GPS observation. With this assumption, the model 11 shows the best fit both the tsunami height and the horizontal displacement at BAKO GPS site.

From our discussion, it makes clear that structural heterogeneity is accounted to the modeling based on crustal deformation. It also implies an easy way to deal with a heterogeneous structure in calculating crustal deformation. With this methodology, it is also possible to estimate rigidity of the source region by adjusting the slip amount so that the same seismic moment can reproduce both the tsunami data and far-field displacement data.

Chapter 7

Discussion and Conclusion

7.1. Discussion

7.1.1. Assessment of megathrust earthquake potential

Based on the interplate coupling model discussed in Chapter 5, considering the uncertainties in the estimation of slip deficit/excess, we propose the following two scenarios about current interplate coupling as well as future earthquakes (Figure 7.1). The first scenario is that the inversion result properly reflects the current interplate coupling status and the depth range of 20-45 km is the main locked zone (Figure 7.1 a, scenario A). With the presence of interplate locking at the down-dip portion, the up-dip part may accumulate slip deficit regardless of its mechanical coupling (Wang and Dixon, 2004). In this scenario, we should also note that future earthquake ruptures from the slip-deficit patch have the potential to propagate to shallow portion near the trench as a result of conditional stability of fault friction (e.g. Scholz, 1998; Hu and Wang, 2008), such as demonstrated by the 2011 M9.0 Tohoku earthquake (e.g. Ozawa et al., 2012; Kodaira et al., 2012), and capable of producing a large tsunami.

The other slip deficit scenario is that the shallow portion of the plate interface is locked to the trench, and that the partially locked patch is a transition zone between the shallow locked zone and the deep steady slip zone (e.g. Scholz and Campos, 2012) (Figure 7.1 b, scenario B). In scenario B, earthquakes may nucleate in the shallow part, generating a tsunami earthquake, and the down-dip portion will release stress by afterslip. This may be the case of the 2006 M7.8 Java and the 2010 M7.8 Mentawai tsunami earthquake. This has been suggested also by GPS data in Mentawai, combined with tsunami run-up data, that significant coseismic slip must have occurred in a very narrow and shallow strip near the trench (Hill et al., 2012). In both scenarios, there is a high potential of rupture propagation to the shallow part of the subduction causing a large tsunami.

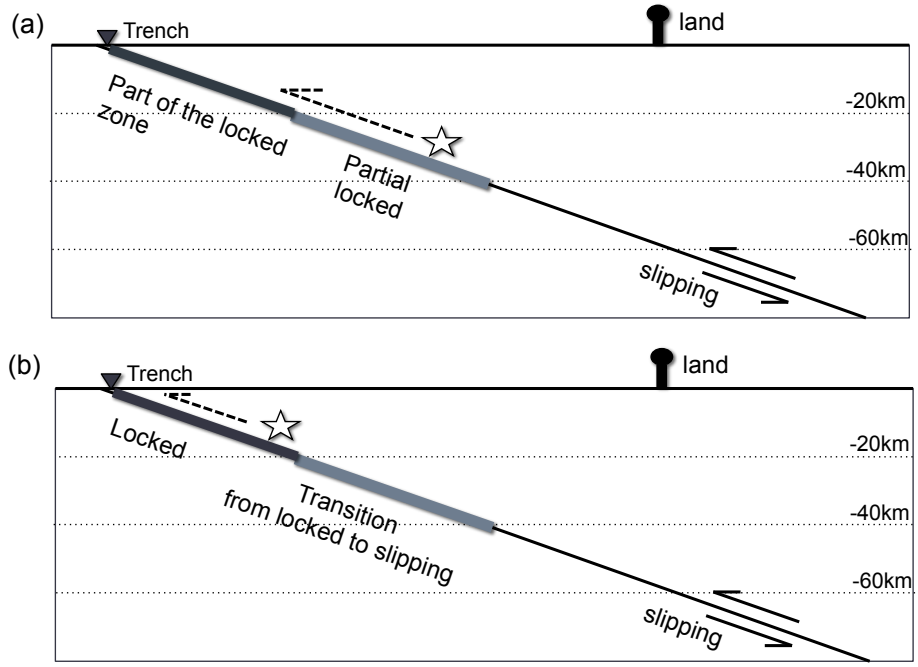

Figure 7.1. Illustration of possible scenario of interseismic deformation model off southwestern Java. (a) Scenario A: The up-dip is part of the locked zone (Wang and Dixon, 2004). In this case, future earthquake (white star) might nucleate from the slip-deficit patch and propagate to the shallow portion as the 2011 M9.0 Tohoku earthquake. (b) Scenario B: The up-dip is locked and future earthquake (white star) might nucleate in the shallow part. The slip-deficit patch is a transition between locked to slipping, and will release its stress by slow slip such as afterslip. This case is similar to the 2006 M7.8 Java and 2010 M7.8 Mentawai tsunami earthquakes.

There is no clear evidence of megathrust events with magnitude larger than 8 south off Java between ~104°E to ~108°E (Wichmann, 1918; Visser, 1922; Newcomb and McCann, 1987; Latief, et al., 2000; Okal, 2012; USGS and CMT Harvard catalogue). However it is possible that the historical records are incomplete and/or they cover only a limited time period compared to a very long recurrence interval of large earthquakes such as the 2004 M9.3 Sumatra-Andaman megathrust earthquake (e.g. Monecke et al., 2008; Meltzner et al., 2010) and the 2011 M9.0 Tohoku earthquake in Japan (e.g. Sagiya et al., 2011). The plate interface between 104°E and 108°E may be interpreted as either a seismic gap (Kelleher and McCann, 1976; McCann et al., 1979) or an aseismic zone (Newcomb and McCann, 1987). Tanioka et al. (2012), rather arbitrarily, assumed the area off Ujung Kulon-Pelabuhan Ratu as a seismic

gap and hypothesized a thrust earthquake with M8.0~8.5 that is capable of generating a tsunami with the maximum tsunami height of 2 to 7 meters. In our study, based on new cGPS data, we show a possibility that the zone between ~104° to ~108° off western coast of Java is a seismic gap with the potential of large earthquake occurrence in the slip-deficit patch.

7.1.2 Possibility for Shallow Coupling and Shallow Afterslip

In Scenario B, shallow portion is considered to be fully locked. To consider such a possibility, we conduct a forward modeling by placing a slip deficit patch and an afterslip patch in the shallow-most part above 20 km depth (Figure 7.2). We assume the slip deficit patch is fully locked (left rectangle in Figure 7.2) with an annual slip deficit equal to the rate of the Australia plate motion. The afterslip patch (right rectangle in Figure 7.2) is assumed to have a slip rate of 190 mm/yr in order to reproduce the motion at CPMK. The along-strike extent of the slip deficit patch is constrained by directions of horizontal GPS velocities on land. As a result, a shallow slip deficit patch cannot reproduce either the observed horizontal velocity or the coastal uplift (Figure 7.2). So there must be significant amount of interplate locking at the down-dip portion. Nevertheless, the result does not exclude a possibility that the shallow up dip portion is also locked.

On the other hand, the trench-ward motion at CPMK can be reproduced solely by the afterslip in the shallow portion where many aftershocks are located. The vertical component of CPMK is stable within its uncertainty. This prefers an afterslip in the shallow part since the afterslip at 15-40 km depth causes coastal subsidence as is shown in Figure 7.2.

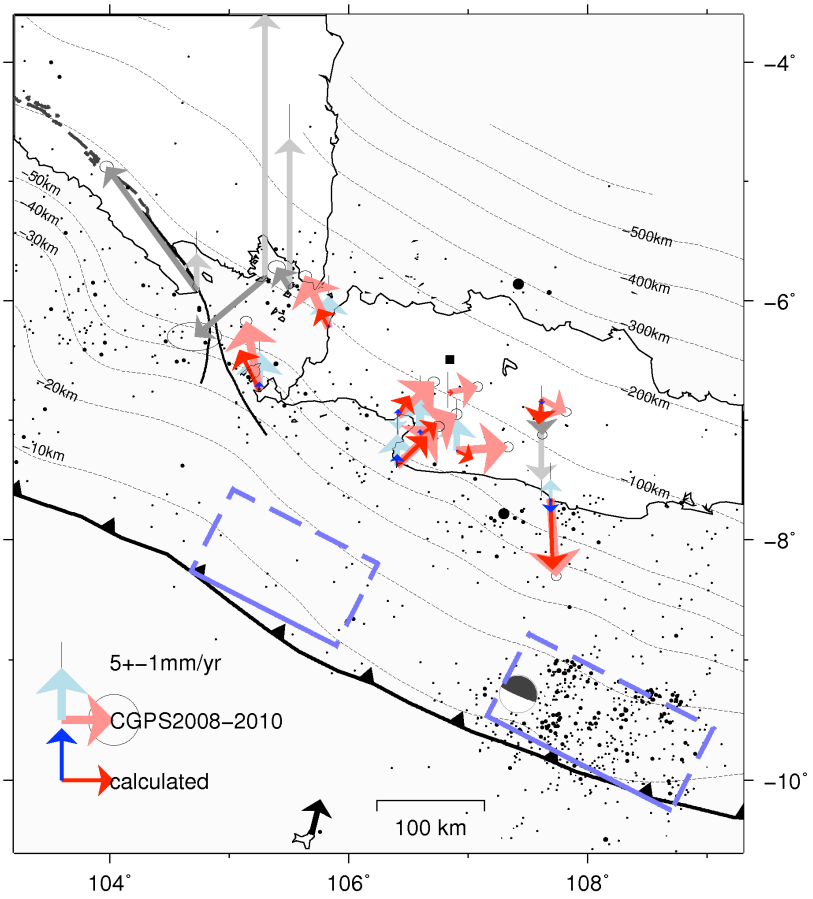

Figure 7.2. Interplate coupling model deduced from forward modeling, assuming the plate interface in the shallow part (above 20 km) is fully coupled (left rectangle) with an annual slip deficit equal to the Australia plate convergence, and an afterslip (right rectangle) with a slip rate of 190 mm/yr. Focal mechanism and black dots shows the focal mechanism of the 2006 M7.8 Java tsunami earthquake and seismicity from 1973 to 2010 (NEIC catalogue), respectively.

7.1.3 Viscoelastic relaxation associated to the 2006 earthquake

Viscoelastic behavior may also affect the postseismic relaxation (Wang et al., 2012). To check possibility of viscoelastic relaxation, we estimate the viscoelastic relaxation using an elastic layer of 65 km depth overlaying a rheological structure with a steady Maxwell viscosity of 8 x 10^{18} Pa s (Gunawan et al., 2014) using the VISCO1D program (Pollitz et al., 1997). In our calculation process, we use the coseismic fault model of Ji (2006) inferred from seismic waveform inversion. The seismic moment release of their model is 3.98e+20 Nm (Mw 7.7). Table 7.1 shows the calculated viscoelastic displacements during January 2008 to

December 2010. The result imply a small viscoelastic effect of 2006 M7.8 Java earthquake. In future studies other coseismic model should also be considered.

Table 7.1. Calculated viscoelastic displacements during January 2008 to December 2010

Site	E(mm)	N(mm)	H(mm)
BAKO	0.0	-0.7	0.4
CLBG	-0.2	-1.1	0.6
CLDO	-0.1	-0.7	0.5
CLGI	0.0	-0.2	0.1
CPMK	-0.5	-1.4	1.5
CPSR	0.0	-0.3	0.2
CPTN	-0.1	-0.5	0.4
CSBK	0.0	-0.2	0.2
CTCN	0.0	-0.1	0.1
CSGT	-0.3	-0.7	0.7
CTVI	-0.2	-0.6	0.5
CUJG	-0.3	-0.5	0.6
CUJK	-0.1	-0.1	0.2
ITB1	-0.2	-1.1	0.7

7.1.4 Disaster Mitigation in Western Java

We have proposed two scenarios for the possible interplate earthquake occurrence off south coast of western Java (Figure 7.1). In scenario A, earthquake nucleates in intermediate depth, with potential to rupture all the way to the trench, and capable to generate large tsunami. Example of this case is the 2011 M9 Tohoku-Oki earthquake. Because it initiates at intermediate depth (20-40 km) within normal rigidity, it is possible to cause strong ground motion in Java island. Strong ground motion can cause collapse of buildings and infrastructures, causing casualties, structural damage and economic loss. So to mitigate disasters caused by earthquakes, it is important to predict strong ground motion in future research. Ground motion can be predicted based on our estimated earthquake source model, because strong ground motion in related to the fault slip on the fault plane (e.g. Irikura and Miyake, 2011; Goda et. al., 2014).

In scenario B, earthquake nucleates in the shallow portion, potentially generating a tsunami earthquake. Generally, the shallow area of subduction zones near the trench is assumed freely slipping, due to the presence of unconsolidated sediments (e.g. Byrne et al., 1988). From 4 events of tsunami earthquakes along Java Trench indicates that earthquake can nucleate in shallowest portion of the subduction, generating large tsunami.

Okal (2011) has reminded to learn from lessons of tsunami earthquakes occurrence along Java Trench to mitigate future possibility of such a similar events. Indonesia has "failed" in providing adequate tsunami warning in the occurrence of the 2006 Java Tsunami Earthquake and also the 2010 Mentawai Earthquake (e.g. Okal 2011).

There will be enough time for local people along the coastline to evacuate if the earthquake information is delivered in a timely manner. An adequate early tsunami warning system should be improved. GPS can play an important to supplement seismic data since it can provide coseismic displacement in real time (e.g. Ohta et al., 2012). Also tsunami education and awareness campaign should be improved to local people along the coast.

7.1.5. Further Studies

This study demonstrates the importance of GPS measurements in assessing seismic and tsunami hazards in the Java trench. For better understanding of interplate coupling, more sites should be installed and monitoring should be continued. Longer time series are indispensable to distinguish whether the plate boundary south of west Java is aseismic or a seismic gap. It is also worthwhile to consider introducing GPS/Acoustic measurements (Spiess et al., 1998, Fujimoto, 2006, Fujita et al., 2006) to improve spatial resolution for the offshore area.

In data analysis, the viscoelastic behavior of the mantle may influence the estimation of the down-dip limit of interplate locking, and consequently the width of the locked zone (Wang, 2007; Wang et al., 2012). Viscoelastic behavior may also affect the postseismic relaxation (Wang et al., 2012).

Recorded historical earthquake in Java is too short or incomplete. So paleoseismology and paleotsunami study is important. From deposits left by tsunamis, times and reccurrence

intervals of past tsunamis can be estimated, as well as water depth and velocity of past inundations (e.g. Rhodes et al., 2006). There are ongoing paleotsunami researches in Java by team group from USGS, The Indonesian Institute of Science (LIPI) and Gajah Mada University (UGM) (e.g. Yudhita, et al., 2009). They found paleotsunami deposit in Cikembulan, an area in Pangandaran, West Java. They analyze three destructive tsunamis in last 400 years. They infer from preliminary analysis that one sediment layer might be caused by tsunami of 1600 AD. There is currently no report on paleotsunami finding in the coast along Pangandaran to Ujung Kulon.

Historical earthquakes in Indonesia are mostly originally from report from the Dutch, who colonialized Indonesia since the 17th century. Research on historical documents from local people is also important to compile more information on historical earthquake..

7.2. Conclusion

We have analyzed 3 years data from 13 sites of the Indonesian Permanent GPS Station Network from 8 January 2008 to 31 December 2010. Surface displacement obtained from GPS data show a landward motion and coastal uplift in western Java near Pelabuhan Ratu to Ujung Kulon, while in the eastern part of the network near Pangandaran it shows a seaward motion.

We interpret the main source of the observed velocity resulting from contribution of:

(1) Slip deficit on the main thrust zone off Ujung Kulon-Pelabuhan Ratu to depth 45 km, with a rate about 70-88% of the plate convergence of the Indo-Australia plate. It is also possible that the shallow up-dip portion is also locked.

(2) Slip deficit on the main thrust zone off Pangandaran in depth range of 37-45 km, with a rate about 75-80% of the plate convergence of the Indo-Australia plate.

(3) Afterslip of the 2006 M7.8 Java Tsunami Earthquake that is still continuing 4.5 years after the earthquake within the rupture area of the earthquake where many aftershocks of the 2006 Java Tsunami Earthquake are located.

The absence of a megathrust earthquake for at least 300 years in this region implies a minimum accumulated seismic moment as much as 1.6×10^{22} Nm (~Mw 8.7) off Ujung Kulon-Pelabuhan Ratu, and 3.9×10^{21} Nm (~Mw 8.3) off Pangandaran, unless the slip is released by slow slip. We propose two possible scenarios for future earthquake.

(1) Scenario A: Earthquake nucleates from the slip-deficit patch at the intermediate depth, then propagates to the shallower portion of the plate boundary producing a large tsunami as the 2011 M9.0 Tohoku earthquake.

(2) Scenario B: Earthquake nucleates in the shallow part, generating a tsunami earthquake, and the downdip portion will release stress by afterslip, as in the case of the 2006 M7.8 Java and 2010 M7.8 Mentawai tsunami earthquakes.

In either case, there is a high potential of rupture propagation to the shallow part of the plate interface and generation of a large tsunami.

Bibliography

Abercrombie, R.E., Antolik, M., Felzer, K. & Ekström, G. (2001). The 1994 Java tsunami earthquake: Slip over a subducting seamount. J. Geophys. Res. 106(B4), 6595–6607.

Abidin, H. Z., Andreas, H., Gamal, M., Suganda, O. K., Meilano, I., Hendrasto, M., ... & Kimata, F. (2006). Ground deformation of Papandayan volcano before, during, and after the 2002 eruption as detected by GPS surveys. GPS Solutions, 10(2), 75-84.

Abidin, H.Z., Andreas, H., Gamal, M., Wirakusumah, A.D., Darmawan, D., Deguchi, T. & Maruyama, Y. (2008). Land subsidence characteristics of the Bandung Basin, Indonesia, as estimated from GPS and InSAR. J. Appl. Geod. 2(3), 167–177, doi:10.1515/JAG.2008.019.

Abidin, H.Z., Andreas, H., Kato, T., Ito, T., Meilano, I., Kimata, F., Natawidjaya, D.H. & Harjono, H. (2009). Crustal deformation studies in Java (Indonesia) using GPS. J. Earthq. Tsunami 3(2), 77-88.

Abidin, H.Z., Gumilar I., Andreas H., Murdohardono D. & Fukuda Y. (2013). On causes and impacts of land subsidence in Bandung Basin, Indonesia. Environ. Earth Sci. 68, 1545-1553, doi: 10.1007/s12665-012-1848-z.

Agustan, Kimata, F., Pamitro, Y.E., & Abidin, H.Z. (2012). Understanding the 2007–2008 eruption of Anak Krakatau Volcano by combining remote sensing technique and seismic data. Int. J. Appl. Earth Obs. Geoinf.14(1), 73-82.

Akaike, H. (1980). Likelihood and the Bayes procedure. In: Bernardo, J. M., et al. (Eds), Bayesian Statistics. University Press, Valencia, Spain, pp. 143-166.

Altamimi, Z., Collilieux, X. & Métivier, L. (2011). ITRF2008: an improved solution of the international terrestrial reference frame. J. Geod, 85, 457-473, doi:10.1007/s00190-011-0444-4.

Ammon, C.J., Kanamori, H., Lay, T. & Velasco, A.A. (2006). The 17 July 2006 Java tsunami earthquake. Geophys. Res. Lett. 33, L24308, doi:10.1029/2006GL028005.

Argus, D. F., & Gordon, R. G. (1991). No‐net‐rotation model of current plate velocities incorporating plate motion model NUVEL‐1. Geophys. Res. Lett., 18(11), 2039-2042.

Bammelen, V. R. (1949). The Geology of Indonesia. Vol. I A. The Hague, Netherlands.

Barbot, S., & Fialko, Y. (2010). A unified continuum representation of post-seismic relaxation mechanisms: semi-analytic models of afterslip, poroelastic rebound and viscoelastic flow. Geophysical Journal International, 182(3), 1124-1140.

Beckers, J., & Lay, T. (1995). Very broadband seismic analysis of the 1992 Flores, Indonesia, earthquake (Mw= 7.9). Journal of Geophysical Research: Solid Earth (1978–2012), 100(B9), 18179-18193.

Bellier, O., Sébrier, M., Pramumijoyo, S., Beaudouin, T., Harjono, H., Bahar, I. & Forni, &zO. (1997). Paleoseismicity and seismic hazard along the Great Sumatran Fault (Indonesia). J. Geodyn. 24, 169-183.

Bilek, S.L. & Engdahl, E.R. (2007). Rupture characterization and aftershock relocations for the 1994 and 2006 tsunami earthquakes in the Java subduction zone. Geophys. Res. Lett. 34, L20311, doi:10.1029/2007GL031357.

Bock, Y., Prawirodirdjo, L., Genrich, J.F., Stevens, C.W., McCaffrey, R., Subarya, C., Puntodewo, S.S.O. & Calais, E. (2003). Crustal motion in Indonesia from Global Positioning System measurements. J. Geophys. Res. 108(B8), 2367, doi:10.1029/2001JB000324.

Bürgmann, R., Kogan, M. G., Levin, V. E., Scholz, C. H., King, R. W., & Steblov, G. M. (2001). Rapid aseismic moment release following the 5 December, 1997 Kronotsky, Kamchatka, earthquake. Geophys. Res. Lett., 28(7), 1331-1334.

Byrne, D. E., Davis, D. M., & Sykes, L. R. (1988). Loci and maximum size of thrust earthquakes and the mechanics of the shallow region of subduction zones. Tectonics, 7(4), 833-857.

Chlieh, M., Avouac, J. P., Hjorleifsdottir, V., Song, T. R. A., Ji, C., Sieh, K., ... & Galetzka, J. (2007). Coseismic slip and afterslip of the great Mw 9.15 Sumatra–Andaman earthquake of 2004. Bulletin of the Seismological Society of America, 97(1A), S152-S173.

Chlieh, M., Avouac, J.P., Sieh, K., Natawidjaja, D.H. & Galetzka, J. (2008). Heterogeneous coupling of the Sumatran megathrust constrained by geodetic and paleogeodetic measurements. J. Geophys. Res. 113, B05305, doi:10.1029/2007JB004981.

Cummins, P. R., Jia, M., Mleczko, R., Burbidge, D., Thio, H. K., & Polet, J. (2006). Modelling the slip of the 17 July, Java earthquake using seismic, GPS, and tide gauge data. In AGU Fall Meeting Abstracts (Vol. 1, p. 08).

Dach, R., Hugentobler, U., Fridez, P. & Meindl, M. (2007). Bernese GPS software Version 5.0. User Manual. Astronomical Institute, University of Bern.

Dahren, B., Troll, V.R., Andersson, U.B., Chadwick, J.P., Gardner, M.F., Jaxybulatov, K. & Koulakov, I. (2012). Magma plumbing beneath Anak Krakatau volcano, Indonesia: evidence for multiple magma storage regions. Contrib. Mineral. Petrol.163(4), 631-651.

DeMets, C., Gordon, R.G. & Argus, D.F. (2010). Geologycally current plate motions. Geophys. J. Int. 181, 1-80, doi: 10.1111/j.1365-246X.2009.04491.x

Douglas, A., Beavan, J., Wallace, L., & Townend, J. (2005). Slow slip on the northern Hikurangi subduction interface, New Zealand. Geophys. Res. Lett., 32(16).

Dragert, H., Wang, K., & James, T. S. (2001). A silent slip event on the deeper Cascadia subduction interface. Science, 292(5521), 1525-1528.

Dziewonski, A. M., Ekström, G., & Salganik, M. P. (1995). Centroid-moment tensor solutions for April–June 1994. Phys. Earth Planet. Int., 88(2), 69-78.

Dziewonski, A. M., Chou T.-A., and Woodhouse, J. H. (1981) Determination of earthquake source parameters from waveform data for studies of global and regional seismicity, J. Geophys. Res., 86, 2825-2852. doi:10.1029/JB086iB04p02825.

Feigl, K.L. & Thatcher, W. (2006). Geodetic observations of post-seismic transients in the context of the earthquake deformation cycle. Comptes Rendus Geosci. 338, 14-15, 1012-1028, doi:10.1016/j.crte.2006.06.006.

Fialko, Y. (2004). Evidence of fluid-filled upper crust from observations of postseismic deformation due to the 1992 Mw7. 3 Landers earthquake. Journal of Geophysical Research: Solid Earth (1978–2012), 109(B8)

Fritz, H. M., Kongko, W., Moore, A., McAdoo, B., Goff, J., Harbitz, C., ... & Synolakis, C. (2007). Extreme runup from the 17 July 2006 Java tsunami. Geophysical Research Letters, 34(12).

Fujii, Y. & Satake, K.(2006). Source of the July 2006 West Java tsunami estimated from tide gauge records. Geophys. Res. Lett. 33, L24317, doi:10.1029/2006GL028049.

Fujimoto H. (2006). Ocean Bottom Crustal Movement Observation Using GPS/Acoustic System by Universities in Japan. J. Geod. Soc. Jpn. 52, 265-272.

Fujita M, Ishikawa, T., Mochizuki, M., Sato, M., Toyama, S., Katayama, M., Kawai, K., Matsumoto, Y., Yabuki, T., Asada, A. & Colombo, O.L. (2006). GPS/Acoustic seafloor geodetic observation: method of data analysis and its application. Earth Planets Space 58, 265-275.

Fukao, Y. (1979). Tsunami earthquakes and subduction processes near deep‐sea trenches. Journal of Geophysical Research: Solid Earth (1978–2012), 84(B5), 2303-2314.

Gardner M. F., Troll, V. R., Gamble, J. A., Gertisser, R., Hart, G. L., Ellam, R. M., Harris, C. & Wolff, J. A. (2012). Crustal Differentiation Processes at Krakatau Volcano, Indonesia. J. Petrology, 1, 34, doi:10.1093/petrology/egs066.

Genrich, J. F., Bock, Y., McCaffrey, R., Prawirodirdjo, L., Stevens, C. W., Puntodewo, S. S. O., Subarya, C. & Wdowinski, S. (2000). Distribution of slip at the northern Sumatran fault system. J. Geophys. Res. 105, B12, 28327–28341, doi:10.1029/2000JB900158.

GeothermEx, Inc. (2010). An Assessment of Geothermal Resource Risks in Indonesia. The World Bank/Public-Provate Infrastructure Advisory Facility.

Goda K., Susumu Kurahashi, Hadi Ghofrani, Gail M. Atkinson & Kojiro Irikura. (2014) Nonlinear Response Potential of Real versus Simulated Ground Motions for the 11th March 2011 Great East Japan Earthquake. Earthquake Spectra In-Press.

Gunawan, E., Sagiya, T., Ito, T., Kimata, F., Tabei, T., Ohta, Y., ... & Sugiyanto, D. (2014). A comprehensive model of postseismic deformation of the 2004 Sumatra–Andaman earthquake deduced from GPS observations in northern Sumatra. Journal of Asian Earth Sciences, 88, 218-229

Gutenberg, B., & Richter, C. F. (1954). Seismicity of the Earth and its Associate Phenomena. Princton Un. Press, Princton, 310pp.

Hall, R., Clements, B., & Smyth, H. R. (2009) Sundaland: basement character, structure and plate tectonic development. Proceedings, Indonesian Petroleum Association, IPA09-G-134

Hanifa, N. R., Meilano, I., Sagiya, T., Kimata, F. & Abidin, H. Z. (2007). Numerical modeling of the 2006 Java tsunami earthquake. Adv. Geosc. Solid Earth 13, 231-248.

Harjono H., Diament, M., Dubois, J. & Larue, M. (1991). Seismicity of the Sunda strait: evidence for crustal extension and volcanological implications. Tectonics 10, 17–30.

Hashimoto, C., Noda, A., & Matsu, M. (2012). The Mw 9.0 northeast Japan earthquake: total rupture of a basement asperity. Geophysical Journal International, 189(1), 1-5.

Hashimoto, C., Noda, A., Sagiya, T. & Matsu`ura, M. (2009). Interplate seismogenic zones along the Kuril–Japan trench inferred from GPS data inversion. Nat. Geosci. 2, doi:10.1038/NGEO421.

Hayes, G. P., D. J. Wald, & Johnson, R. L. (2012). Slab1.0: A three-dimensional model of global subduction zone geometries. J. Geophys. Res., 117, B01302, doi:10.1029/2011JB008524.

Heki, K., Miyazaki, S. I., & Tsuji, H. (1997). Silent fault slip following an interplate thrust earthquake at the Japan Trench.

Henstock, T. J., McNeill, L. C., & Tappin, D. R. (2006). Seafloor morphology of the Sumatran subduction zone: Surface rupture during megathrust earthquakes?. Geology, 34(6), 485-488.

Hill, E.M., Borrero, J.C., Huang, Z., Qiu, Q., Banerjee, P., Natawidjaja, D.H., Elosegui, P., Fritz, H.M., Suwargadi, B.W., Pranantyo, I.R., Li, L., Macpherson, K.A., Skanavis, V.,

Synolakis, C.E. & Sieh, K. (2012). The 2010 Mw 7.8 Mentawai earthquake: Very shallow source of a rare tsunami earthquake determined from tsunami field survey and near‐field GPS data. J. Geoph. Res. Solid Earth117, B06402, doi:10.1029/2012JB009159.

Hirai, T. & Sagiya, T. (2013). Biased geodetic inference on asperity distribution on a subducted plate interface: a quantitative study. Earth Planets Space 65, 313-321.

Hirose, H., Hirahara, K., Kimata, F., Fujii, N., & Miyazaki, S. I. (1999). A slow thrust slip event following the two 1996 Hyuganada earthquakes beneath the Bungo Channel, southwest Japan. Geophys. Res. Lett., 26(21), 3237-3240.

Hsu, Y. J., Simons, M., Avouac, J. P., Galetzka, J., Sieh, K., Chlieh, M., ... & Bock, Y. (2006). Frictional afterslip following the 2005 Nias-Simeulue earthquake, Sumatra. Science, 312(5782), 1921-1926.

Hsu, Y. J., Simons, M., Avouac, J.P., Galetzka, J., Sieh, K., Chlieh, M., Natawidjaja, D., Prawirodirdjo, L. & Bock, Y. (2006). Frictional afterslip following the 2005 Nias-Simeulue earthquake, Sumatra. Science 312, 1921-1926, doi: 10.1126/science.1126960.

Hu, Y & Wang, K. (2008). Coseismic strengthening of the shallow portion of the subduction fault and its effects on wedge taper. J. Geophys. Res. 113, B12411, doi:10.1029/2008JB005724.

Huchon, P. & Le Pichon, X. (1984). Sunda Strait and Central Sumatra fault. Geology 12, 11, 668-672, doi: 10.1130/0091-7613(1984)12<668:SSACSF>2.0.CO;2.

Hyndman, R. D. (2007). The seismogenic zone of subduction thrust faults. The seismogenic zone of subduction thrust faults, 15-40.

Ibrahim, G., Untoro, M., & Hendrawan, A., R. (1989). Earthquake statistics in Indonesia. Technical Report. Bandung Institut of Technology, Indonesia.

Irikura, K., & Miyake, H. (2011). Recipe for predicting strong ground motion from crustal earthquake scenarios. Pure and Applied Geophysics, 168(1-2), 85-104.

Ito, T., Yoshioka, S. & Miyazaki, S. (2000). Interplate coupling in northeast Japan deduced from inversion analysis of GPS data. Earth Planet. Sci. Lett. 176, 117-130, http://dx.doi.org/10.1016/S0012-821X(99)00316-7.

Janssen, V., Roberts, C., Rizos, C., & Abidin, H. Z. (2002). Low-cost GPS-based volcano deformation monitoring at Mt. Papandayan, Indonesia. J. Volc. and Geotherm. Res., 115(1), 139-151.

Ji,C. (2006). Preliminary Result of the 2006 July 17 M7.7 - SOUTH OF JAVA, INDONESIA Earthquake, http://neic.usgs.gov/neis/eq_depot/2006/eq_060717_qgaf/neic_qgaf_ff.html

Kanamori, H. (2006). Attribute of tsunami earthquake. Lecture presentation in Nagoya University.

Kanamori, H. (1972). Mechanism of tsunami earthquakes. Phys. Earth Planet. Inter. 6, 346–359.

Kanamori, H., & Kikuchi, M. (1993). The 1992 Nicaragua earthquake: a slow tsunami earthquake associated with subducted sediments. Nature, 361(6414), 714-716.

Kanamori, H., Rivera, L., Lee & W.H.K. (2010). Historical seismograms for unravelling a mysterious earthquake: The 1907 Sumatra Earthquake. Geophys. J. Int. 183(1), 358-374, doi: 10.1111/j.1365-246X.2010.04731.x.

Kato, T., Ito, T., Abidin, H.Z. & Agustan. (2007). Preliminary report on crustal deformation surveys and tsunami measurements due to the July 17, 2006 South off Java Island Earthquake and Tsunami, Indonesia. Earth Planets Space, 59, 9, 1055-1059.

Kelleher, J. A. & McCann, W. (1976). Buoyant zones, Great earthquakes and unstable boundaries of subduction. J. Geophys. Res. 81, 4885-4908.

Kodaira, S., No, T., Nakamura, Y., Fujiwara, T., Kaiho, Y., Miura, S., Takahashi, N., Kaneda, Y. & Taira, A. (2012). Coseismic fault rupture at the trench axis during the 2011 Tohoku-oki earthquake. Nat. Geosci. 5, 646-650, doi:10.1038/ngeo1547.

Konca, A. O., Avouac, J. P., Sladen, A., Meltzner, A. J., Sieh, K., Fang, P., ... & Helmberger, D. V. (2008). Partial rupture of a locked patch of the Sumatra megathrust during the 2007 earthquake sequence. Nature, 456(7222), 631-635.

Kopp, H., & Kukowski, N. (2003). Backstop geometry and accretionary mechanics of the Sunda margin. Tectonics, 22(6).

Koshimura et al., 2006. http://www.tsunami.civil.tohoku.ac.jp/hokusai2/disaster/06_Java/July17_Java.html

Kostoglodov, V., Singh, S.K., Santiago, J.A., Franco, S.I., Larson, K.M., Lowry, A.R. & Bilham, R. (2003). A large silent earthquake in the Guerrero seismic gap, Mexico. Geophys. Res. Lett. 30(15), 1807, doi:10.1029/2003GL017219.

H. Latief, A. Riadi, & Zulkarnaen, A., R. (2006) www.ocean-partners.org/documents/News/2006_West_Java_tsunami.pdf

Latief, H., Puspito, N. & Imamura, F. (2000). Tsunami catalogue and zones in Indonesia. J. Nat. Disaster Sci. 22(1), 25-43.

Lay, T., & Bilek, S. (2007). Anomalous earthquake ruptures at shallow depths on subduction zone megathrusts. The Seismogenic Zone of Subduction Thrust Faults, 476-511.

Lay, T., & Kanamori, H. (1981). An asperity model of large earthquake sequences. Earthquake prediction, 579-592.

Lay, T., Ammon, C.J., Kanamori, H., Yamazaki, Y., Cheung, K.F. & Hutko, A.R. (2011). The 25 October 2010 Mentawai tsunami earthquake (Mw 7.8) and the tsunami hazard presented by shallow megathrust ruptures. Geophys. Res. Lett. 38, L06302, doi: 10.1029/2010GL046552.

Lay, T., Kanamori, H., & Ruff, L. (1982). The asperity model and the nature of large subduction zone earthquakes, in Earthquake Prediction Research, 1, Terra Scientific Publishing Co., Tokyo, Japan, 3- 71.

Lay, T., Kanamori, H., Ammon, C. J., Koper, K. D., Hutko, A. R., Ye, L., ... & Rushing, T. M. (2012). Depth‐varying rupture properties of subduction zone megathrust faults. J. Geophys. Res.: Solid Earth (1978–2012), 117(B4).

Leonard, L. J., Hyndman, R. D., & Mazzotti, S. (2004). Coseismic subsidence in the 1700 great Cascadia earthquake: Coastal estimates versus elastic dislocation models. Geological Society of America Bulletin, 116(5-6), 655-670.

López, A. M., & Okal, E. A. (2006). A seismological reassessment of the source of the 1946 Aleutian 'tsunami'earthquake. Geophys. J. Int., 165(3), 835-849.

Lowry, A. R., Larson, K. M., Kostoglodov, V., & Bilham, R. (2001). Transient fault slip in Guerrero, southern Mexico. Geophys. Res. Lett., 28(19), 3753-3756.

Lyard, F., Lefevre, F., Letellier, T. & Francis, O. (2006). Modelling the global ocean tides: modern insights from FES2004. Ocean Dyn. 56, 394-415, doi: 10.1007/s10236-006-0086-x.

McCaffrey, R. (1991). Slip vectors and stretching of the Sumatran fore arc. Geology, 19, 881–884.

McCaffrey, R. (2008). Global frequency of magnitude 9 earthquakes. Geology, 36(3), 263-266.

McCaffrey, R., Wallace, L. M., & Beavan, J. (2008). Slow slip and frictional transition at low temperature at the Hikurangi subduction zone. Nature Geoscience, 1(5), 316-320.

McCann, W.R., Nishenko, S.P., Sykes, L.R. & Krause, J. (1979). Seismic gaps and plate tectonics: Seismic potential for major boundaries. Pure Appl. Geophys. 117, 1082-1147.

Meilano, I., Abidin, H.Z., Andreas, H., Gumilar, I., Sarsito, D., Hanifa, N.R., Rino, Harjono, H., Kato, T., Kimata, F. & Fukuda, Y. (2012). Slip Rate Estimation of the Lembang Fault West Java from Geodetic Observation. J. Disaster Res. 7(1), 12-18.

Meltzner, A. J., Sieh, K., Abrams, M., Agnew, D. C., Hudnut, K. W., Avouac, J. P., & Natawidjaja, D. H. (2006). Uplift and subsidence associated with the great Aceh‐Andaman earthquake of 2004. J. Geophys. Res.: Solid Earth (1978–2012), 111(B2).

Meltzner, A.J., Sieh, K.,Chiang, H.W., Shen, C.C., Suwargadi, B.W., Natawidjaja, D.H., Philibosian, B.E., Briggs, R.W. & Galetzka, J. (2010). Coral evidence for earthquake

recurrence and an A.D. 1390–1455 cluster at the south end of the 2004 Aceh–Andaman rupture. J. Geophys. Res. 115, B10402, doi:10.1029/2010JB007499.

Monecke, K., Finger, W., Klarer, D., Kongko, W., McAdoo, B.G., Moore, A.L. & Sudrajat, S.U. (2008). A 1.000-year sediment record of tsunami recurrence in northern Sumatra. Nature 455, 1232-1234, doi: 10.1038/nature07374.

Moore, J. C., & Saffer, D. (2001). Updip limit of the seismogenic zone beneath the accretionary prism of southwest Japan: An effect of diagenetic to low-grade metamorphic processes and increasing effective stress. Geology, 29(2), 183-186.

Moreno, M., Melnick, D., Rosenau, M., Baez, J., Klotz, J., Oncken, O., ... & Hase, H. (2012). Toward understanding tectonic control on the M8.8 2010 Maule Chile earthquake. Earth Planet. Sci. Lett., 321, 152-165.

Mori, J., & Park, S. (2006). Rupture Propagation of the July 17, 2006 Java Earthquake from Back Projection of Hi-Net Data. In AGU Fall Meeting Abstracts (Vol. 1, p. 0126).

Mori, J., Mooney, W. D., Kurniawan, S., Anaya, A. I., & Widiyantoro, S. (2007). The 17 July 2006 tsunami earthquake in west Java, Indonesia. Seismological Res. Lett., 78(2), 201-207.

Nakamura, M. 2006. Numerical modelling of tsunami. Lecture presentation in Nagoya University.

Natawidjaja, D. H., Sieh, K., Ward, S. N., Cheng, H., Edwards, R. L., Galetzka, J., & Suwargadi, B. W. (2004). Paleogeodetic records of seismic and aseismic subduction from central Sumatran microatolls, Indonesia. J. Geophys. Res.: Solid Earth (1978–2012), 109(B4).

Newcomb, K.R. & McCann, W.R. (1987). Seismic History and Seismotectonics of the Sunda Arc. J. Geophys. Res. 92 (B1), 421-439.

Newman, A. V., & Okal, E. A. (1998). Teleseismic estimates of radiated seismic energy: The E/M 0 discriminant for tsunami earthquakes. J. Geophys. Res.: Solid Earth (1978–2012), 103(B11), 26885-26898.

Newman, A. V., Hayes, G., Wei, Y., & Convers, J. (2011). The 25 October 2010 Mentawai tsunami earthquake, from real‐time discriminants, finite‐fault rupture, and tsunami excitation. Geophys. Res. Lett., 38(5).

Newman, A.V., Hayes, G., Wei, Y. & Convers, J. (2011). The 25 October 2010 Mentawai tsunami earthquake, from real-time discriminants, finite-fault rupture, and tsunami excitation. Geophys. Res. Lett. 38, L05302, doi:10.1029/2010GL046498.

Nishimura, T., Hirasawa, T., Miyazaki, S. I., Sagiya, T., Tada, T., Miura, S., & Tanaka, K. (2004). Temporal change of interplate coupling in northeastern Japan during 1995–2002 estimated from continuous GPS observations. Geophys. J. Int., 157(2), 901-916.

Nishimura, T., Sato, M., & Sagiya, T. (2014). Global Positioning System (GPS) and GPS-Acoustic Observations: Insight into Slip Along the Subduction Zones Around Japan. Ann. Rev. Earth Planet. Sci., 42:653–74.

Ohta, Y., Kobayashi, T., Tsushima, H., Miura, S., Hino, R., Takasu, T., ... & Umino, N. (2012). Quasi real□time fault model estimation for near□field tsunami forecasting based on RTK□GPS analysis: Application to the 2011 Tohoku□Oki earthquake (Mw 9.0). J. Geophys. Res.: Solid Earth (1978–2012), 117(B2).

Okada, Y. (1985). Surface deformation due to shear and tensile faults in a half-space. Bull. Seism. Soc. Am. 75, 1135-1154.

Okal, E. A. (1988). Seismic parameters controlling far-field tsunami amplitudes: A review. Natural Hazards, 1(1), 67-96.

Okal, E. A., & Newman, A. V. (2001). Tsunami earthquakes: The quest for a regional signal. Physics of the Earth and Planetary Interiors, 124(1), 45-70.

Okal, E. A., Borrero, J. C., & Chagué-Goff, C. (2011). Tsunamigenic predecessors to the 2009 Samoa earthquake. Earth-Science Reviews, 107(1), 128-140.

Okal, E.A. (2012). The south of Java earthquake of 1921 September 11: a negative search for a large interplate thrust event at the Java Trench. Geophys. J. Int. 190, 1657-1672, doi: 10.1111/j.1365-246X.2012.05570.x.

Outerbridge, K. C., Dixon, T. H., Schwartz, S. Y., Walter, J. I., Protti, M., Gonzalez, V., ... & Rabbel, W. (2010). A tremor and slip event on the Cocos‐Caribbean subduction zone as measured by a global positioning system (GPS) and seismic network on the Nicoya Peninsula, Costa Rica. Journal of Geophysical Research: Solid Earth (1978–2012), 115(B10).

Ozawa, S., Nishimura, T., Munekane, H., Suito, H., Kobayashi, T., Tobita, M. & Imakiire, T. (2012). Preceding, coseismic, and postseismic slips of the 2011 Tohoku earthquake, Japan. J. Geophys. Res., 117, B07404, doi:10.1029/2011JB009120.

Ozawa, S. (2014). Shortening of recurrence interval of Boso slow slip events in Japan. Geophysical Research Letters, 41(8), 2762-2768.

Pelayo, A. M., & Wiens, D. A. (1992). Tsunami earthquakes: Slow thrust‐faulting events in the accretionary wedge. Journal of Geophysical Research: Solid Earth (1978–2012), 97(B11), 15321-15337.

Philibosian, B., Sieh, K., Natawidjaja, D. H., Chiang, H. W., Shen, C. C., Suwargadi, B. W., ... & Edwards, R. L. (2012). An ancient shallow slip event on the Mentawai segment of the Sunda megathrust, Sumatra. Journal of Geophysical Research: Solid Earth (1978–2012), 117(B5).

Polet, J. & Kanamori, H. (2000). Shallow subduction zone earthquakes and their tsunamigenic potential. Geophys. J. Int. 142, 684-702.

Polet, J., & Thio, H. K. (2003). The 1994 Java tsunami earthquake and its “normal” aftershocks. Geophysical research letters, 30(9).

Pollitz, F. F. (1997). Gravitational viscoelastic postseismic relaxation on a layered spherical Earth. Journal of Geophysical Research: Solid Earth (1978–2012), 102(B8), 17921-17941

Pollitz, F. F., Peltzer, G., & Bürgmann, R. (2000). Mobility of continental mantle: Evidence from postseismic geodetic observations following the 1992 Landers earthquake. Journal of Geophysical Research: Solid Earth (1978–2012), 105(B4), 8035-8054.

Prawirodirdjo, L., Bock, Y., Genrich, J. F., Puntodewo, S. S. O., Rais, J., Subarya, C., & Sutisna, S. (2000). One century of tectonic deformation along the Sumatran fault from triangulation and Global Positioning System surveys. Journal of Geophysical Research: Solid Earth (1978–2012), 105(B12), 28343-28361.

Reid, H. F. (1913). Sudden earth-movements in Sumatra in 1892. Bulletin of the Seismological Society of America, 3(2), 72-79.

Rhodes, B., Tuttle, M., Horton, B., Doner, L., Kelsey, H., Nelson, A., & Cisternas, M. (2006). Paleotsunami research. Eos, Transactions American Geophysical Union, 87(21), 205-209.

Rosenau, M. & Oncken, O. (2009). Fore-arc deformation controls frequency-size distribution of megathrust earthquakes in subduction zones. J. Geophys. Res. 114, B10311, doi:10.1029/2009JB006359.

Ruff, L., & Kanamori, H. (1980). Seismicity and the subduction process. Physics of the Earth and Planetary Interiors, 23(3), 240-252.

Sagiya, T. (2004). Interplate coupling in the Kanto District, Central Japan, and the Boso Peninsula Silent Earthquake in May 1996. Pure Appl. Geophys. 161, 2327-2342, doi. 10.1007/s00024-00402566-6.

Sagiya, T., Kanamori, H., Yagi, Y., Yamada, M. & Mori, J. (2011). Rebuilding Seismology. Nature 473, 146-148, doi: 10.1038/473146a.

Satake, K. (1991). Recent studies on tsunamis. Zisin second series. 44 special issue, 99-112.

Satake, K. (1994). Mechanism of the 1992 Nicaragua tsunami earthquake. Geophysical Research Letters, 21(23), 2519-2522.

Satake, K., & Tanioka, Y. (1999). Sources of tsunami and tsunamigenic earthquakes in subduction zones. In Seismogenic and Tsunamigenic Processes in Shallow Subduction Zones (pp. 467-483). Birkhäuser Basel.

Satake, K., & Tanioka, Y. (2003). The July 1998 Papua New Guinea earthquake: Mechanism and quantification of unusual tsunami generation. pure and applied geophysics, 160(10-11), 2087-2118.

Satake, K., Baba, T., Hirata, K., Iwasaki, S. I., Kato, T., Koshimura, S., ... & Terada, Y. (2005). Tsunami source of the 2004 off the Kii Peninsula earthquakes inferred from offshore tsunami and coastal tide gauges. Earth, Planets, and Space, 57(3), 173-178.

Savage, J.C. (1983). A dislocation model of strain accumulation and release at a subduction zone. J. Geophys. Res. 88(B6), 4984-1996.

Scholz, C. H., & Small, C. (1997). The effect of seamount subduction on seismic coupling. Geology, 25(6), 487-490.

Scholz, C.H. (1998). Earthquakes and friction laws. Nature 391, 37-42, doi:10.1038/34097.

Scholz, C.H. & Campos, J. (2012). The seismic coupling of subduction zones revisited. J. Geophys. Res. 117, B05310, doi:10.1029/2011JB009003.

Schwartz, S. Y., & Rokosky, J. M. (2007). Slow slip events and seismic tremor at circum‐Pacific subduction zones. Reviews of Geophysics, 45(3).

Sella, G. F., Dixon, T. H., & Mao, A. (2002). REVEL: A model for recent plate velocities from space geodesy. Journal of Geophysical Research: Solid Earth (1978–2012), 107(B4), ETG-11.

Setyadji, B., Murata, I., Kahar, J., Suparka, S. & Tanaka, T. (1997). Analysis of GPS measurement in West-Java, Indonesia. Ann. Disas. Prev. Res. Inst. Kyoto Univ. 40, B-1, 27-33.

Sieh, K. & Natawidjaja, D. (2000). Neotectonics of the Sumatran fault, Indonesia. J. Geophys. Res. 105(28), 295–28, 326.

Sieh, K., Natawidjaja, D. H., Meltzner, A. J., Shen, C. C., Cheng, H., Li, K. S., ... & Edwards, R. L. (2008). Earthquake supercycles inferred from sea-level changes recorded in the corals of west Sumatra. Science, 322(5908), 1674-1678.

Sieh, K., Ward, S. N., Natawidjaja, D., & Suwargadi, B. W. (1999). Crustal deformation at the Sumatran subduction zone revealed by coral rings. Geophysical Research Letters, 26(20), 3141-3144.

Simoes, M., Avouac, J. P., Cattin, R., & Henry, P. (2004). The Sumatra subduction zone: A case for a locked fault zone extending into the mantle. Journal of Geophysical Research: Solid Earth (1978–2012), 109(B10).

Simons, W.J.F., Ambrosius, B.A.C., Noomen, R., Angermann, D., Wilson, P., Becker, M., Reinhart, E., Walpersdorf, A. & Vigny, C. (1999). Observing plate motions in South East Asia: geodetic results of the GEODYSSEA project. Geophys. Res. Lett. 26, 2081–2084.

Simons, W.J.F., Socquet, A., Vigny, C., Ambrosius, B.A.C., Abu, S.H., Promthong, C., Subarya, C., Sarsito, D.A., Matheussen, S., Morgan, P. & Spakman, W. (2007). A decade of GPS in Southeast Asia: Resolving Sundaland motion and boundaries. J. Geophys. Res. 112, B06420, doi:10.1029/2005JB003868.

Simons, M., Minson, S. E., Sladen, A., Ortega, F., Jiang, J., Owen, S. E., ... & Webb, F. H. (2011). The 2011 magnitude 9.0 Tohoku-Oki earthquake: Mosaicking the megathrust from seconds to centuries. science, 332(6036), 1421-1425.

Singh, S.C., Hananto, N., Mukti, M., Permana, H., Djajadihardja, Y., Harjono, H. (2011). Seismic images of the megathrust rupture during the 25 October 2010 Pagai earthquake, SW Sumatra: Frontal rupture and large tsunami. Geophys. Res. Lett. 38, L16313, doi: 10.1029/2011GL048935.

Spiess, F.N., Chadwell, C.D., Hildebrand, J.A., Young, L.E., Purcell Jr., G.H. & Dragert, H. (1998). Precise GPS/Acoustic positioning of seafloor reference points for tectonic studies. Phys. Earth Planet. Inter. 108, 101-112.

Subarya, C., Chlieh, M., Prawirodirdjo, L., Avouac, J. P., Bock, Y., Sieh, K., ... & McCaffrey, R. (2006). Plate-boundary deformation associated with the great Sumatra–Andaman earthquake. Nature, 440(7080), 46-51.

Subarya C., Abidin, H.Z., Koncoro, W. & Efendi, J. (2010). GPS analysis strategies to minimize the error contribution to geodetic GPS determination. Paper presented at FIG Congress 2010, TS-3C, GNSS CORS Networks, Positioning Infrastructure, Analysis and Applications. Sydney, Australia, April 11-16.

Subarya, C. (2013). Sistem Referensi Geospasial Indonesia. Prosiding at Workshop Sistem Referensi Geospasial Nasional ke-3. In Indonesian.

Susilohadi, S., Gaedicke, C. & Djajadihardja, Y. (2009). Structures and sedimentary deposition in the Sunda Strait, Indonesia. Tectonophys.467(1), 55-71.

Synolakis, C., Imamura, F., Tsuji, Y., Matsutomi, H., Tinti, S., Cook, B., ... & Usman, M. (1995). Damage, conditions of East Java tsunami of 1994 analyzed. EOS, Transactions American Geophysical Union, 76(26), 257-257.

Tanioka Y., Latief, H., Suhendar, H., Gusman, A.R. & Koshimura, S. (2012). Tsunami Hazard Mitigation at Pelabuhan Ratu, Indonesia. J. Disaster Res. 7(1).

Tanioka, Y., & Satake, K. (1996). Tsunami generation by horizontal displacement of ocean bottom. Geophysical Research Letters, 23(8), 861-864.

Tregoning, P., Brunner, F.K., Bock, Y., Puntodewo, S.S.O., McCaffrey, R., Genrich, J.F., Calais, E., Rais, J. & Subarya, C. (1994). First geodetic measurement of convergence across the Java Trench. Geophys. Res. Lett. 21(19), 2135-2138.

Tsuji, Y., Imamura, F., Matsutomi, H., Synolakis, C. E., Nanang, P. T., Harada, S., ... & Cook, B. (1995). Field survey of the East Java earthquake and tsunami of June 3, 1994. Pure and Applied Geophysics, 144(3-4), 839-854.

Vigny, C., Simons, W. J., Abu, S., Bamphenyu, R., Satirapod, C., Choosakul, N., ... & Ambrosius, B. A. C. (2005). Insight into the 2004 Sumatra–Andaman earthquake from GPS measurements in southeast Asia. Nature, 436(7048), 201-206.

Visser, S.W. (1922). Inland and submarine epicenters of Sumatra and Java earthquakes. Koninklijk Magnetisch en Meteorologisch Observatorium te Batavia, Verhandelingen, 9, 14 pp.

Wang, K. (2007). Elastic and viscoelastic models of crustal deformation in subduction earthquake cycles. In: Dixon, T.H., Moore, J.C. (Eds), The seismogenic zone of subduction thrust faults, pp. 540-575.

Wang, K. & Dixon, T. (2004). “Coupling” Semantics and science in earthquake research. Eos, Transactions American Geophysical Union85(18), 180-180.

Wang, K., Hu, Y. & He, J. (2012). Deformation cycles of subduction earthquakes in a viscoelastic Earth. Nature484, 7394, 327-332.

Wichmann, A. (1918). The earthquakes of the Indian Archipelago to the 1857.Verhandelingen der Koninklijke Akademie can Wetenschappen te Amsterdam (Tweede Sectie), Deel XX, 4, in Germany.

Wilson, P., Rais, J., Reigber, C., Reinhart, E., Ambrosius, B. A. C., Le Pichon, X., ... & Boonphakdee, C. (1998). Study provides data on active plate tectonics in Southeast Asia region. Eos, Transactions American Geophysical Union, 79(45), 545-549.

Wittwer, A. (2011). Investigating the crustal and upper mantle structure of the central java subduction zone with marene wide-angle seismic and gravity data. Doctoral dissertation at University of Kiel.

Yabuki, T. & Matsu`ura, M. (1992). Geodetic data inversion using a Bayesian information criterion for spatial distribution of fault slip, Geophys. J. Int., 109, 363-375.

Yudhita, C., Amijaya, D. H., Yulianto, E. (2009). Identification of paleotsunami deposit in Cikembulan Area, Pangandaran, West Java, based on Granulometry Analysis. Prociding Abstract in Annual Meeting of Indonesian Geologist (PIT-IAGI).

Zen, M.T. (1983). Krakatau and the tectonic importance of Strait Sunda. Buletin Jurusan Geologi, 12

Zhang, J., Bock, Y., Johnson, H., Fang, P., Wiliiams, S., Genrich, J., Wdowinski, S. & Behr, J. (1997). Southern California permanent GPS geodetic array: Error Analysis of daily position estimates and site velocities. J. Geophys. Res. 102(B8), 18,035-18,055.